Universidade Vigo

Marco Antonio Marcos Millán DOCTORAL DISSERTATION

Development of nanofluids for thermal energy storage based on phase change materials 2021

DOCTORAL DISSERTATION

Development of nanofluids for thermal energy storage based on phase change materials

Marco Antonio Marcos Millán

2021

International Mention

Universidade Vigo

EIDO
Escola Internacional
de Doutoramento

Universidade Vigo

International Doctoral School

Marco Antonio Marcos Millán

DOCTORAL DISSERTATION

Development of nanofluids for thermal energy storage based on phase change materials

Supervised by:

Luis Lugo Latas

David Cabaleiro Álvarez

2021

International Mention

Universidade de Vigo
Departamento de Física Aplicada

Dr. LUIS LUGO LATAS, Profesor Titular de la Universidade de Vigo y Dr. DAVID CABALEIRO ÁLVAREZ, Investigador Postdoctoral de la Universidade de Vigo,

INFORMAN:

Que la presente memoria titulada *"Development of nanofluids for thermal energy storage based on phase change materials"* ha sido realizada por el Ingeniero de Minas D. MARCO ANTONIO MARCOS MILLÁN bajo nuestra dirección y constituye su Tesis para optar al grado de Doctor con Mención Internacional.

Que el trabajo que se presenta ha sido desarrollado en el marco de los siguientes proyectos de investigación: *"Diseño y desarrollo de nanofluidos para la producción y el almacenamiento de energía (ENE2014-55489-C2-1/2-R)"* (2014-2017) y *"Desarrollo de nanofluidos híbridos, nanolubricantes y materiales de cambio de fase nano-mejorados para la transferencia, almacenamiento y producción de energía (ENE2017-86425-C2-1/2-R)"* (2017-2021) concedidos por el Ministerio de Economía y Competitividad y el Programa Europeo FEDER además de la Acción COST *"Nanouptake –Overcoming Barriers to Nanofluids MarketUptake (CA15119)"* (2016-2021) financiada dentro del Horizonte 2020 de la Unión Europea.

Y para que así conste a los efectos oportunos, firman el presente informe en Vigo, 21 de enero de 2021.

Los directores:

Dr. Luis Lugo Latas

Dr. David Cabaleiro Álvarez

A mis padres, mi mujer y mis hijas.

Acknowledgements

Para el desarrollo de esta Tesis Doctoral ha sido necesaria la colaboración desinteresada de muchas personas y entidades, sin las que no sería posible llevarla a cabo. Por ello, quiero agradecer en primer lugar a mis directores Dr. Luis Lugo Latas y Dr. David Cabaleiro Álvarez, la dedicación y el apoyo que me han dado desde el primer día, poniendo siempre a mi alcance muchas facilidades fruto de su esfuerzo, así como de ser la base de mi aprendizaje en esta etapa.

Al Ministerio de Economía, Industria y Competitividad del Gobierno de España y al programa FEDER de Unión Europea por la financiación recibida bajo los proyectos ENE2014-55489-C2-2-R e ENE2017-86425-C2-1-R. A la COST Action de Unión Europea "CA15119: Overcoming Barriers to Nanofluids Market Uptake" por darme la oportunidad de financiar gran parte de las estancias, en las que he podido conocer y colaborar con algunos de los mayores expertos en la materia en la que se desarrolla la Tesis.

A todos los coautores de los trabajos presentados en esta Tesis, porque ha sido un placer desarrollar un trabajo colaborativo del que he podido aprender tanto.

A Laura Fedele y Sergio Bobbo, así como a Mauro, Marco y demás miembros del Istituto per le Tecnologie della Costruzione CNR-ITC, por recibirme siempre con los brazos abiertos haciendo que me sintiera siempre como en casa y por todo lo que he aprendido en las estancias realizadas en Padova, Italia. Sempre nel mio cuore.

A Gaweł Żyła y a su equipo de la Rzeszów University of Technology por darme la oportunidad de trabajar con ellos, por su gran recibimiento, atención y por todos los conocimientos que me ha aportado la estancia en Rzeszów, Polonia.

A los compañeros del grupo de investigación FA2 de la Universidad de Vigo, por compartir conmigo el día a día, así como esos momentos fuera de la Universidad, y hacer que este trabajo se haya convertido en una experiencia que voy a recordar siempre con una sonrisa. Por ello, no quiero dejar de citar a Javier, Bea, Iván, Marifé, Carmen, Carolina, Ángel, José, Uxía o Martín.

Gracias también a aquellas personas que pasan por mi vida casi sin saber cuántas cosas buenas aportan a ella, a mis amigos, compadres, cuñados, sobrinos y demás familia.

A mis padres, gracias ahora y siempre, por creer en mí y por enseñarme con cariño a ser lo que soy, transmitiéndome unos valores que espero saber transmitir a mis hijas. Y gracias a mis hermanos por ser también mi referencia y un modelo a seguir.

A mi mujer Ana, y a mis hijas Ana y Kiara porque sois la mayor motivación que tengo en la vida y lo que más quiero.

A todos, muchas gracias.

Abstract

In recent decades, the growing international concern for environmental problems and other issues directly or indirectly related to energy consumption has motivated a great interest in improving the efficiency of thermal installations. In this sense, energy storage is expected to play a key role in the coming years. The two main objectives of this Doctoral Thesis were to develop different nano-enhanced phase change materials, NePCMs, and characterize them on the basis of those thermophysical properties that are considered most representative for thermal energy storage. Novel NePCMs were designed by dispersing different nanomaterials, *viz.* commercial Baytubes® multi-walled carbon nanotubes (c-MWCNT) and MWCNTs synthesized within the framework of this PhD Thesis (s-MWCNT), Iolitec functionalized graphene (fGnP) nanoplatelets, and PVP-coated Ag nanoparticles (PVP-Ag). NePCM preparition has been carried out using a two-step method for samples designed using carbon-based nanoadditives, and in one-step for those designed with silver metal nanoparticles. Special attention has been given to study the morphology and/or purity of base fluids and nanoparticles as well as the temporal and thermal stability of NePCMs by using different physico-chemical techniques. Thus, five different nanofluids sets were designed at nanoparticle mass concentrations ranging from 0.025 to 1.1% in different types of poly(ethylene glycol)s, *i.e.* c-MWCNT/PEG200, c-MWCNT/PEG300, s-MWCNT/PEG400, fGnP/PEG400 and PVP-Ag/PEG400, which makes a total of twenty-four dispersions.

Regarding the thermal and physical characterization, solid-liquid phase change transitions were determined for fGnP/PEG400 and PVP-Ag/PEG400 systems using a DSC Q2000 differential scanning calorimeter. The same device, working with a quasi-isothermal temperature-modulated differential scanning calorimetry (TMDSC) method, was used to obtain the isobaric heat capacity for several PEG400-based systems. The study of the influence of nanoparticles on the thermal conductivity was carried out by means of a KD2 Pro Thermal Properties Analyzer, working with the transient hot wire technique, for the fGnP and s-MWCNT dispersions based on PEG400, while studies on PVP-Ag/PEG400 samples were conducted using a Hot Disk Thermal Constants, which relies on transient plane source technique. Results show that thermal conductivity improves with the nanoparticle concentration for all investigated NePCM systems. Experimental data were also compared with the correlated or predicted values by using different theoretical models such as those of Maxwell, Hamilton-Crosser, Nan, Murshed or Xue. Density measurements were performed for fGnP/PEG400, s-MWCNT/PEG400 and PVP-Ag/PEG400 systems using a DMA501 densimeter based on the well-known vibrating U-tube technique. Dynamic viscosity was studied as a function of temperature and nanoparticle concentration for all designed NePCMs. Experiments were carried out by means of a SVM 3000

rotational Stabinger viscometer-densimeter in the case of fGnP/PEG400 samples, using a Physica MCR 101 rotational rheometer for c-MWCNT/PEG200, c-MWCNT/PEG300 and s-MWCNT/PEG400 systems and utilizing an AR-G2 Magnetic Rotational Bearing Rheometer for PVP-Ag/PEG400 samples. Experimental data on dynamic viscosity were also compared with the values provided by means of Einstein, Batchelor, Brinkman, Krieger-Dougherty, Maron-Pierce or Brenner-Condiff models. Oscillatory rheology experiments were also conducted for c-MWCNT/PEG200 and c-MWCNT/PEG300 sets. In addition, surface tension at the air-sample surface was experimental investigated for pure PEG400 and PVP-Ag/PEG400 NePCMs using a DSA30 droplet shape analyzer.

Resumen

En las últimas décadas, la creciente preocupación internacional por los problemas ambientales y diferentes aspectos relacionados directa o indirectamente con el consumo de energía han motivado un gran interés por mejorar la eficiencia de las instalaciones térmicas. En este sentido, se espera que el almacenamiento de energía juegue un papel clave en los próximos años. Los dos principales objetivos de esta Tesis Doctoral han sido desarrollar diferentes materiales nano-mejorados de cambio de fase, NePCMs, y caracterizarlos en base a aquellas propiedades termofísicas que se consideran más representativas para el almacenamiento de energía térmica. Los nuevos NePCMs se han diseñado mediante la dispersión de diferentes nanomateriales, esto es, nanotubos de carbono de pared múltiple tanto comerciales Baytubes® (c-MWCNT) como sintetizados en el marco de esta tesis doctoral (s-MWCNT), nanoplaquetas de grafeno funcionalizado Iolitec (fGnP), y nanopartículas de Ag recubiertas de PVP (PVP-Ag). La preparación de NePCMs se ha realizado mediante el método de dos pasos para las muestras diseñadas con nanoaditivos en base carbono, y mediante un método de un solo paso para aquellas diseñadas con nanopartículas metálicas de plata. Se ha prestado especial atención al estudio de la morfología y/o pureza de los fluidos base y nanopartículas, así como la estabilidad temporal y térmica de los NePCMs mediante el uso de diferentes técnicas físico-químicas. Así, se han diseñado cinco conjuntos de nanofluidos diferentes en concentraciones en masa de nanopartículas que van desde 0.025 a 1.1% en diferentes tipos de polietilenglicoles, es decir, c-MWCNT/PEG200, c-MWCNT/PEG300, s-MWCNT/PEG400, fGnP/PEG400 y PVP-Ag/PEG400, lo que hace un total de veinticuatro dispersiones.

En cuanto a la caracterización térmofísica, se determinaron las transiciones de cambio de fase sólido-líquido para los sistemas fGnP/PEG400 y PVP-Ag/PEG400 utilizando un calorímetro diferencial de barrido DSC Q2000. Ese mismo dispositivo, trabajando en modo de temperatura modulada cuasi-isotérmica (TMDSC), se utilizó también para obtener la capacidad calorífica isobárica de aquellos sistemas basados en PEG400. El estudio de la influencia de las nanopartículas en la conductividad térmica se realizó mediante un Analizador de Propiedades Térmicas KD2 Pro, que opera con la técnica de hilo caliente transitorio, para las dispersiones fGnP y s-MWCNT basadas en PEG400, mientras que los estudios en PVP-Ag/PEG400 se realizaron utilizando un Hot Disk Thermal Constants, que trabaja con la técnica de fuente plana transitoria. Los resultados muestran que la conductividad térmica mejora con la concentración de nanopartículas para todos los sistemas de NePCM investigados. Las conductividades térmicas experimentales también se compararon con correlaciones o predicciones realizadas mediante el uso de diferentes modelos como los de Maxwell, Hamilton-Crosser, Nan, Murshed o Xue. Se realizaron mediciones de densidad para los sistemas fGnP/PEG400, s-MWCNT/PEG400 y PVP-Ag/PEG400 utilizando un densímetro DMA501 basado en la conocida técnica de tubo en U

vibratorio. La viscosidad dinámica se estudió en función de la temperatura y la concentración de nanopartículas para todos los NePCMs diseñados. Los experimentos se realizaron mediante un viscosímetro-densímetro Stabinger rotacional SVM 3000 para las muestras fGnP/PEG400, utilizando un reómetro rotacional Physica MCR 101 para c-MWCNT/PEG200, c-MWCNT/PEG300 y s-MWCNT/PEG400 y utilizando un reómetro de cojinete giratorio magnético AR-G2 para muestras PVP-Ag/PEG400. Los datos experimentales de viscosidad dinámica también se compararon con los valores proporcionados por los modelos de Einstein, Batchelor, Brinkman, Krieger-Dougherty, Maron-Pierce o Brenner-Condiff. Asimismo, se realizaron experimentos de reología oscilatoria para los conjuntos de dispersions c-MWCNT/PEG200 y c-MWCNT/PEG300. Además, se investigó experimentalmente la tensión superficial para PEG400 puro y los NePCMs basados en PVP-Ag/PEG400, utilizando un analizador de gotas DSA30.

Index

Chapter 1

Introduction

1 Introduction

1.1 Background

According to the Global Energy & CO_2 Status Report 2019 [1], energy consumption worldwide grew by 2.3% in 2018, nearly twice the average increasing rate since 2010. Among other causes, this growth is due to increased heating and cooling needs in some parts of the world. This has led to a rising demand for all fuels, with fossil fuels meeting nearly 70% of the growth for the second year running from 2017. The global situation has resulted in a noticeable number of environmental problems [2,3]. The increasing global concern in such environmental issues and other harms derived from energy consumption have motivated a higher interest in improving the efficiency of thermal facilities. In this sense, the advantage of energy storage, *i.e.* the accumulation of energy when available in excess or at a low cost to later use that energy during periods of scarcity or demand, is assumed to play a key role in the next years. These technologies improve the flexibility of thermal installations by correcting unforeseen imbalances between supply and consumption and improve their efficiency by optimizing their use [4]. For decades, time and effort have been devoted to the study and research on the relationship between energy consumption and economic expansion [5], in addition to the relationship between economic development and environmental pollution [6,7]. The G7 economies and China are the most influential countries in relation to economic and political status [8], but it is difficult to agree on what or how policy recommendations can be universally applied to all countries. Among other aspects, this is due to the fact that energy consumption is considered to be a parameter linked to the influence of a particular sector on economic growth and environmental degradation in a country or region [9].

On the other hand, a revision of the literature shows that an important part of world's energy consumption belongs to the use made within buildings, since it represents 40% of total demand and accounts for up to 30% of annual greenhouse gas emissions [10]. The “World Energy Investment 2019” has been recently published by the International Energy Agency (IEA), indicating that investment in energy is mainly concentrated in the electricity sector, renewable energies and the construction of networks, with the cost of renewable energy as a strategic objective [11]. Many countries have put energy efficiency among their priorities, since energy saving is the most effective way to reduce dependence on fossil fuels, minimizing CO_2 emissions, which also results in economic benefits. Hence, a set of binding targets has been drawn up, in order to achieve a reduction in energy consumption of at least 32.5% by 2030, in accordance with a "business-as-usual" scenario [12,13]. Among other current global energy policy initiatives towards sustainability, the International Renewable Energy Association (IRENA 2018), has

modelled a scenario of continuous GDP (gross domestic product) growth compatible with a global warming of 2 K based on a rapid switch to renewables. According to such a scenario, an average of 350 GW is required to be installed per year until 2050 [14].

Over the last two decades, European Union (EU) has pursued a proactive climate and energy policy integrating a significant amount of renewables into energy systems. Among other common strategies to protect the environment, the 2030 Agenda for Sustainable Development has recently emerged. This action plan was born from the commitment of the all United Nations members, and its main objective is to guarantee the protection of people, the planet and prosperity [15]. The 2030 Agenda initially considered a European Union's goal to mitigate CO_2 emissions with a reduction target of 80-95% by 2050, in comparison to 1990 levels. However, the Intergovernmental Panel on Climate Change (IPCC) Special Report on Global Warming of 1.5 K [16] evidenced that such threshold was not enough and even much stronger policies and deeper energy transformations were still necessary. Thus, in line with Paris temperature goal Agreement [17,18], European Union has committed net zero greenhouse gas emissions for EU countries as a whole by 2050. As part of the green deal to enshrine the 2050 climate-neutrality, the EU Commission has recently proposed the first European Climate Law [19]. Worldwide agreements place special emphasis on the intensification of energy consumption in air conditioning and thermal comfort facilities due to their great energy demand in both the residential and non-residential sector [20].

Exploring the possible pathways for addressing the necessary transition to sustainable energy systems requires of a multidisciplinary approach [21]. As pointed out at the beginning of this section, advanced storage technologies are among the most promising technologies that can improve the competitiveness to renewable generation and provide the required flexibility in the energy system [22]. On the other hand, thermal energy storage (TES) is a key enabling technology that allows stocking thermal energy that can be further used for heating and cooling applications or power generation, for example [23]. TES systems based on the use of latent heat are linked inherently to the processes of phase change during which the heat is alternately charged into the system and discharged from it [24]. In particular, this Ph.D. Thesis deals with one particular type of thermal energy storage, those approaches that involve a phase change. Latent heat storage is especially interesting since it provides high densities of storage with small differences in temperature. Materials with appropriate features to absorb and release latent heat are known as phase change materials (PCMs) and have good potential for thermal energy storage applications [25].

1.2 Thermal Energy Storage (TES) Processes

As pointed, thermal energy storage (TES) technologies may cover the mismatches between production and consumption and allow optimizing the number of operation hours. This could maximize the performance of conventional and renewable facilities, reducing the consumption of fossil fuels and their undesirable effects.

There are three basic types of thermal energy storage:

- *Sensible heat storage* (SHS) approaches only use the intrinsic heat capacity of a material and the temperature change during the charging or discharging process, according to the equation:

$$Q = \int_{T_i}^{T_f} mC_p dT \quad (1)$$

where, Q is the thermal energy transfered by the material, dT is the temperature change, T_i and T_f are initial and final temperature, m is the mass of the substance, and C_p is the isobaric specific heat capacity of the material.

- *Latent heat storage* (LHS) relies on the thermal energy absorbed or released when a substance undergoes a phase change, either from solid to liquid, from solid to solid, from liquid to gas or vice versa. The latent adjective has its origin in the Latin "latens", which means hidden, since during the phase change there is no change in temperature of the material (equation 2), hence it is said that the phase change is latent or hidden.

$$Q = m \cdot \Delta h \quad (2)$$

where, Q is the the thermal energy transfered by the material, m is the mass of the material, and Δh is the latent heat capacity.

- *Chemical and thermo-chemical energy storage* is based on that thermal energy that is exchanged during a reversible chemical reaction due to the breakage and reform of molecular bonds in one or more compounds. Thus, thermochemical storage is connected to the internal energy that exists in a material due to the chemical bonds that occur between its chemical components.

1.3 Thermal Energy Storage (TES) Materials

Among the media that can be used to store thermal energy, phase change materials (PCMs) are increasingly used as passive systems to temperature control and management in energy efficiency initiatives such as cooling or air conditioning facilities. PCMs are technologically

interesting as they possess the capacity of storing energy in the form of latent heat in the phase change so that when cooled they can release that energy, therefore, they are useful tools to manage thermal energy more efficiently, and are increasingly important in a wide range of applications including automotive [26-32], solar harvesting [33-37], spacecraft [38-43], or heating, ventilations and air conditioning facilities [44-49].

PCM-based systems store 5–14 times more energy per unit volume than those reservoirs making only use of the sensible heat of materials such as water, masonry, or rock. A large number of PCMs are known to melt at temperatures that can be interesting for a wide range of applications. However, for their utilization as latent heat storage media such materials must exhibit certain desirable thermophysical, chemical, and economic characteristics [50]. Thus, before developing a thermal storage system based on PCMs, the thermophysical properties and other features of such materials must be thoughtfully evaluated according to the following desirable requirements [51,52].

- Thermophysical properties:
  1. Phase change temperature within the operational temperature range.
  2. High latent heat with the aim of minimizing installation volume.
  3. High specific heat, which contributes to TES throughout sensible thermal energy.
  4. High thermal conductivity in both phase liquid and solid, which ensures rapid capture and release of thermal energy.
  5. High density.
  6. No or little sub-cooling during freezing to reduce the temperature range that needs to be cover so that the TES system works reversibly.
  7. Low vapour pressure.
  8. Small volume changes during the phase transition.
- Chemical properties:
  9. Prolonged chemical stability.
  10. Compatible with capsule material.
  11. Non-toxic, non-flammable, and non-explosive.
- Kinetic properties:
  12. Sufficient crystallization rate.
  13. No sub-cooling.
- Economic properties:
  14. Abundantly available.
  15. Inexpensive.
  16. Commercially viable.

PCMs can be classified according to different criteria such as the type of exchanged heat (sensible, latent or thermochemical), the involved phase change (solid-solid, solid-liquid, liquid-gas or solid-gas), based on their composition, or attending to the potential application, taking into account the phase change characteristics (latent heat and temperature, for instance). One of the classifications that gathers in an organized way most of those parameters is that shown in Figure 1. This classification has been addapted from those by different authors such as Abhat [53] and Ma [54]:

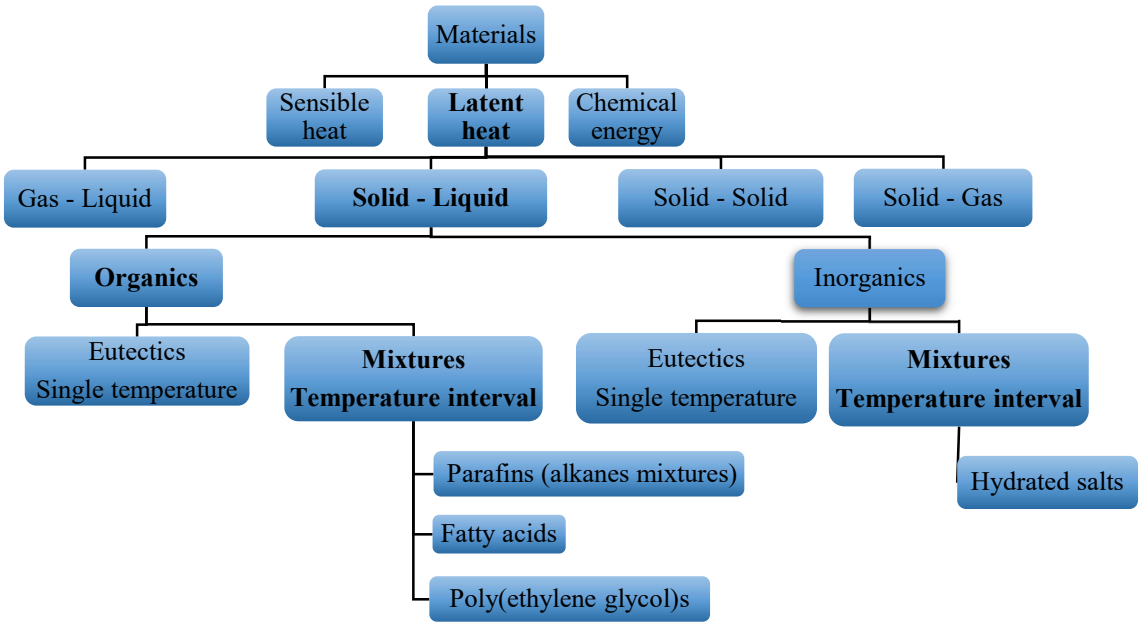

Figure 1. Classification of solid–liquid PCMs adapted from [53,54].

In recent decades, different organic and inorganic compounds (or mixtures of them) have been proposed as potential solid-liquid PCMs, the most promising transition from both technological and economic point of views [55]. A contrast based on the thermal properties of the two main groups of PCMs (organics and inorganics) evidences that the main disadvantages of organic PCMs are the lower thermal conductivities and lower energy storage capacities per unit volume, when compared with inorganic PCMs. In counterpart, organic PCMs exhibit some key factors, which confer them important advantages in view of possible industrial application, like affordable prices or almost no sub-cooling effects. This sub-cooling phenomenon implies that certain materials need to be cooled down to temperatures below their melting point so that solidification or crystallization process begins. Additionally, organic PCMs undergo solid-liquid phase transitions in certain temperature ranges that are interesting for practical applications and cannot be covered by inorganic PCMs. Among organic phase change materials, paraffins, sugars alcohols, fatty acids and different polymers such as poly(ethylene glycol)s fulfil most of the requirements for practical implementation in thermal energy storage systems, but like many other

conventional heat transfer fluids, exhibit relatively low thermal conductivity and diffusivity, especially when compared to solid materials [56]. This feature can be a limitation for the applicability of these latent heat materials, since a low thermal conductivity may hinder the heat transfer prolonging the processes of capture and release of stored energy [57]. In particular, poly(ethylene glycol)s, PEG, are ethylene oxide oligomers with linear formula $H(OCH_2CH_2)_nOH$. These synthetic polymers exhibit large latent heats at melting temperatures that can be adjusted through the molecular mass and are potentially attractive for multiple thermal applications, including cooling or heating facilities. Additionally, PEGs present non-toxicity, low vapour pressures and competitive prices.

Regarding mentioned the melting point (temperature and enthalpy), Mehling and Cabeza [58] provided another classification, which is shown in Figure 2.

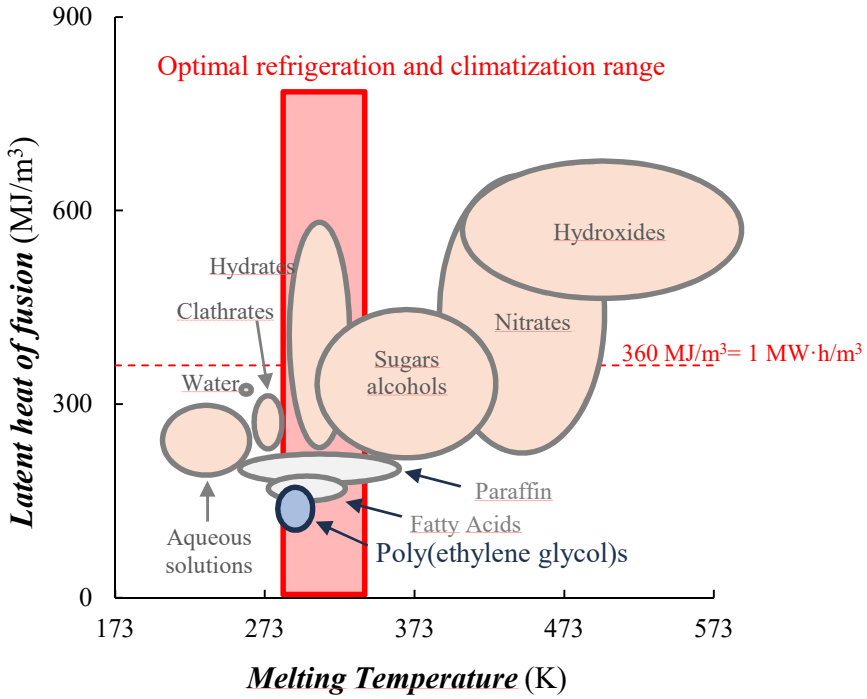

Figure 2. Types of materials that can be used as PCM according to their typical range of melting temperature and enthalpy of fusion [58].

As mentioned, latent materials have certain disadvantages that may prevent in some way their immediate practical industrial implementation. Those drawbacks are connected with their thermal properties (in particular with their relatively low thermal conductivity and/or large sub-cooling). Therefore, the sub-cooling effect is a parameter to improve since the stored energy is released at a lower temperature or in a wider temperature range than necessary [59]. In order to reduce the

time between solid-liquid and liquid-solid transitions, that is, to shorten the time it takes for the PCM to load and unload stored thermal energy, it is necessary to improve the thermal conductivity of PCM. In this sense, the dispersions of solid nanoparticles of high thermal conductivity in liquids (also called nanofluids) have taken wide attention from the research community. Thus, researchers stated positive impact of these new materials in thermal performance due to their improved thermal properties such as thermal conductivity, specific heat or density, etc. [60]. In fact, with the aim of improving the capabilities of PCMs to transfer thermal energy, the dispersion of nanometric-size materials and high thermal conductivity has acquired special relevance in recent years, giving rise to what is commonly known as nano-PCMs or nano-enhanced phase change materials, NePCMs [61,62]. Nanoparticles are considered to be those for which at least one dimension is less than 100 nm and they exhibit particular thermal properties. As the size decreases, the proportion of surface to volume increases and this causes an enhancement in the heat transfer capacity of the nanoparticles [63]. Nanostructured materials can be classified into different types based on their size, morphology, physical and chemical properties or their chemistry nature. Thus, different metallic nanoparticles [64-66], metal oxides nanoparticles [67-75], carbon-based nanoadditives [76-82], and hybrid nanomaterials [72,74-76,83-85], have been considered as thermal conductivity enhancers to improve the thermal properties of base materials. Carbon nanostructures, such as multiwalled carbon nanotubes (MWCNT) or graphene nanoplatelets (GnP), have not only high thermal conductivities but also extraordinary mechanical and electrochemical properties, as well as corrosion resistance [86]. On the other hand, metallic nanoparticles such as gold (Au), silver (Ag) or copper (Cu), are very interesting materials in the fields of physics or chemistry, due to their electrical, thermal, or optical properties. Their high resistance to corrosion helps with a good behaviour, for example, in most models of heat exchangers, such as those used in solar energy [87]. The dispersion of nanoadditives in PCMs can also help to reduce their sub-cooling effect improving the heat transfer performance of thermal energy storage systems based on latent heat materials.

1.4 Analyzed properties

The study of the thermophysical properties is a fundamental step in the development of advanced NePCMs, necessary to assess the improvements in the thermal capabilities obtained by the dispersion of nanometric-size particles. The thermophysical properties considered more representative to discern or to evaluate the benefits of the dispersion of nanoparticles are the following:

- Solid-liquid phase change characteristics (latent heat, melting temperature and recrystallization temperature)

- Isobaric heat capacity
- Thermal conductivity
- Density and volumetric behaviour
- Dynamic viscosity
- Surface tension

As already discussed, in recent years many investigations have been carried out on how to improve the thermal conductivity of PCMs by introducing high-conductivity metallic and non-metallic nanoparticles [88]. In order to evaluate the improvements obtained by the dispersion of nanoadditives in the base phase change materials, the thermophysical profile of both NePCMs and the base PCMs was experimentally determined. In particular, we will focus on those properties that are directly connected with thermal storage and heat transfer.

In a TES system that relies on the latent heat of a solid-liquid transition, energy is stored throughout the melting process and is released during the solidification process of the PCM/NePCM. Solid-liquid phase change characteristics like temperatures and enthalpies of fusion were experimentally obtained from heat flux-temperature curves measured using a differential scanning calorimetry (DSC), while isobaric heat capacity determinations were performed using that same device but working with a quasi-isothermal temperature-modulated differential scanning calorimetry (TMDSC) method. These thermal results provided fundamental information about the physical and chemical processes occurring in the designed materials during solid-liquid phase change. As it was mentioned, during the phase change cooling process, sub-cooling would appear, since the temperature of the sample may need to reach a temperature value lower than the melting point for the crystallization begins. In other words, sub-cooling is the temperature difference between the melting point (in the phase change from solid to liquid) and the freezing point (in the phase change from liquid to solid). The smaller this temperature difference, the better the thermal performance of a phase change material.

On the other hand, the heat capacity of a material is an important factor for many applications, including phase change material (PCM) selection for thermal energy storage. Aside from storing energy via the latent heat of a phase transition, significant sensible heat can be stored using the material heat capacity outside the transition temperature region. Furthermore, accurate heat capacity values are required to model and thereby optimize PCM heat storage systems.

The thermal conductivity of a material is the measure of its ability to transfer heat by conduction. This property, which usually is temperature-dependent, is normally higher in the case of solids than in liquids since in liquids intermolecular space is much larger and molecular movement is more random (which makes the transport of thermal energy less effective than in

the case of solids). The dispersion of nanoparticles with high thermal conductivity in base fluids aims to improve the thermophysical properties of these fluids, which may translate into significant energy savings. The well-established transient hot-wire (THWM) and Hot Disk Transient Plane Source (TPS) methods have been widely used to measure the thermal conductivity of different heat transfer fluids, including NePCMs. These techniques enable investigating thermal conductivity by rapid, accurate and non-destructive tests. Standard devices based on these techniques consist of a metallic probe (that works as heat source and temperature sensor), which is immersed in the tested material. As electrical energy circulates throughout the electrical wire, the temperature of the cable increases, which, in turn, heats the surrounding fluid. After the time in which power is applied to the probe, the temperature evolution is monitored by the same wire. Assuming that the sample is at rest and heat transfer is purely conductive, the rate at which heat dissipates and, consequently, the thermal conductivity can be assessed from that temperature-time dependence. Thus, for a given power and time of the electrical supply, the higher the thermal conductivity, the lower the rise in temperature recorded by the experimental device. This is due to the fact that a high thermal conductivity of the surrounding fluid allows a better diffusion (dissipation) of the heat created by Joule effect in the source/probe.

Information regarding density and volumetric behaviour are also important when designing thermal devices or facilities. Thus, accurate density values are necessary to quantify volumetric changes with temperature. Densities of base fluids and NePCMs were measured using an experimental device based on the resonance frequency that results from the oscillation of a cell filled with a known volume of sample. The operation principle of this technique is based on the laws that govern the simple harmonic movement, an oscillating U-tube whose resonance frequency varies depending on its mass and its spring constant [89]. The objective is to measure the natural period of oscillation of the vibrating tube, in which the fluid to be characterized is previously introduced. This period is a function of the mass of the tube and the mass of the liquid inside, which allows density determination.

Although the dispersion of nano-sized particles with high thermal conductivity improves the thermal conductivity of the fluid, the presence of such nanoadditives also entails an increase in dynamic viscosity, which is unfavourable for heat transfer and fluid flow [90,91]. Rheology is the science that studies the relationship between imposed stresses and resulting deformations. By means of flow rheological analyses it is possible to determine the shear viscosity as a function of shear rate and therefore investigate the Newtonian or non-Newtonian behaviour of the PCMs and NePCMs, which can differ depending on several aspects, such as the range of shear rate, concentration of nanoparticles, or the base fluid-nanoparticle combinations. Additionally, oscillatory rheological tests can also provide an insight in the viscoelastic properties of the

samples. As it is usually preferred in the case of colloidal dispersions, cone-plate geometries were selected in the framework of this PhD thesis to investigate the shear viscosity and the viscoelastic behaviour of Nano-enhanced Phase Change Materials.

The necessity of downsizing heat transfer equipment in different thermal applications has resulted in an increasing interest in microfluidics and surface patterning strategies. In those systems surface tension, ST, plays a major role due to its direct relation with other surfaced properties such as wettability, friction and adhesion. However, despite the implication of nanofluid surface tension in many heat transfer applications, the investigation of this property is still at an early stage in comparison with other physical properties such as thermal conductivity or viscosity [92]. In the framework of this Thesis, NePCMs-air surface tension has been characterized from shape profile analyses (using the Young Laplace Equation) of sample drops when pending in air-controlled atmosphere.

The main objective of this PhD Thesis has been to propose, design and characterize new stable nano-enhanced phase change materials, NePCMs, with improved thermal properties to be used in energy storage systems. To reach this goal, the thermophysical properties of phase change materials based on poly(ethylene glycol)s with different molecular masses were tuned by dispersing different nanomaterials with high thermal conductivity, namely graphene nanoplatelets, multi-walled carbon nanotubes (specifically synthetized to this PhD Thesis or commercial) or PVP-capped silver nanoparticles.

Chapter 2

Objectives and background

2.1 Background
2.2 Objectives

2 Objectives and background

2.1 Background

The object of this PhD Thesis has been to improve the thermophysical properties of phase change materials, poly(ethylene glycol)s with different molecular masses, by the dispersion of different nanomaterials such as graphene nanoplatelets, multi-walled carbon nanotubes or silver nanoparticles, to propose advanced materials with potential uses in cold thermal storage.

It is necessary to highlight that this PhD Thesis has been developed within the framework of the Research Projects "Design and development of nanofluids for the production and storage of energy (ENE2014-55489-C2-1/2-R)" and "Development of hybrid nanofluids, nanolubricants and nano-enhanced Phase Change Materials for the transfer, storage and production of energy (ENE2017-86425-C2-1/2-R)" granted within the Spanish National Research Program "Innovación Desarrollo e Investigación Orientada a los Retos de la Sociedad". These Projects have been coordinated between the Thermophysical Properties Laboratory (NaFoMat Group, University of Santiago de Compostela) and FA2 group (University of Vigo). The connections established between both research teams have contributed to broaden the characterization of the NePCMs designed in this PhD Thesis. In particular, it has been possible to incorporate to the investigation some experimental techniques and procedures available in the laboratories of NaFoMat Group.

In addition, I have developed part of this work during research stays in two international institutions, the Rzeszow University of Technology (Poland) and the Istituto per le Tecnologie della Costruzione of the Italian National Research Council (ITC-CNR, Padova). The great opportunity to work with techniques or methodologies different from those available in the laboratories of the FA2 group has undoubtedly enriched the quality of this PhD Thesis.

Part of the training as a researcher and the collaborations or stays in other European research centres, has been carried out under the action Nanouptake – Overcoming Barriers to Nanofluids Market Uptake (COST Action CA15119). This action aims to create a European and world-wide network of leading R+D+i institutions, and of key industries, to develop and foster the use of nanofluids and NePCMs as advanced heat transfer/thermal storage materials to increase the efficiency of heat exchange and storage systems. Nanouptake has contributed to achieve the European Horizon 2020 Energy and Climate objectives (Societal Challenges 3: *"Secure, efficient and clean energy"*; and 6: *"Climate action, environment, resource efficiency and raw materials"*) by developing new materials up to higher Technological Readiness Levels (TRL) and overcoming commercial application barriers.

2.2 Objectives

This PhD Thesis has aimed to propose, develop and characterize new phase change materials with improved thermal properties for their use in energy storage systems. To reach this goal, the following objectives have been proposed:

1. *To design new stable nano-enhanced phase change materials, NePCMs, by dispersing carbon-based or metallic nanoparticles with high thermal conductivity in different organic solid-liquid phase change materials.*

   The design of the nanofluids will be developed based on different poly(ethylene glycol)s in which carbon-based or metallic nanoparticles are dispersed. Firstly, the commercial nanoparticles and base fluids will be characterized in terms of size, morphology or purity to validate the information provided by the manufacturers. The dispersions will be subjected to mechanical stirring and ultrasonication by means of an ultrasound bath or high-power ultrasound probe, in order to achieve homogeneity and stability. Then, the temporal stability will be investigated throughout the temporal evolution of the hydrodynamic nanoparticle size by means of dynamic light scattering technique.

2. *To determine experimentally solid-liquid phase change characteristics of formulated NePCMs, by analysing the effect that the dispersion of the nanomaterials has on the latent heats of fusion and sub-cooling effect.*

   The study of the solid-liquid phase transitions of the poly(ethylene glycol)s used as based materials and NePCMs will be carried out in order to determine their melting and freezing points as well as latent heat. It will be investigated the behaviour of the materials when undergoing solid-liquid phase change. Moreover, the reliability of NePCMs by ruling out possible undesirable variations in phase change characteristics throughout different heating–cooling cycles will be analysed.

3. *To study the improvements in the thermal conductivity of new NePCMs in relation to base phase change materials, investigating modifications in this transport property with the dispersion of high thermal conductivity nanoparticles.*

   The measure of the thermal conductivity of both the NePCMs and the base fluids by using transient plane source and transient hot wire methods, in order to analyse the dependences with temperature and concentration of nanoadditives will be performed.

4. *To study the rheological behaviour of new designed NePCMs and base fluids in order to obtain their dynamic viscosity from non-linear viscoelastic experiments and linear viscoelastic oscillatory tests.*

The study of the effect that nanoparticle loading has on dynamic viscosity by means of a rotational rheometer equipped with a cone-plate geometry or a rotational viscosimeter working with a modified Couette principle in a wide range of temperatures, will be developed. Moreover, the linear-viscoelastic region and investigate the viscoelastic behaviour of MWCNT dispersions in different PEGs with molecular masses between 200 and 400 $g \cdot mol^{-1}$ will be identified.

5. *To determine isobaric heat capacity and volumetric properties of the new NePCMs as well as the base materials.*

   The experimental determination of the temperature and concentration effects on the isobaric heat capacities of the base fluid, nanopowders and NePCMs, by means the quasi-isothermal temperature-modulated differential scanning calorimetry method with a differential scanning calorimeter will be carried out. The density determination of the fluids will be conducted in a wide range of temperatures using a device working with the well-known oscillating U- tube technique.

6. *To check the reliability of different theoretical or semi-empirical approaches to study the behaviour of the studied thermophysical properties.*

   Several theoretical and semi-empirical models will be used to describe/predict the behaviour of the new designed NePCMs from a thermophysical point of view. The morphology of the nanoparticle, shape of the interfacial solid-liquid layer, temperature or nanoadditive concentration will be taken into account among others parameters.

7. *To establish a comparison between new NePCMs and the base phase change materials regarding their energy storage and heat transfer capabilities.*

   The thermophysical properties of the new NePCMs will be compared with the behaviour of the corresponding base fluids and other PCMs from the literature. The improvement that could be achieved by incorporating the new materials in applications such as cold thermal storage will be evaluated.

Chapter 3

Results and general discussion

3.1 Influence of molecular mass of PEG on rheological behaviour of MWCNT-based nanofluids for thermal energy storage

3.2 MWCNT in PEG-400 nanofluids for thermal applications: A chemical, physical and thermal approach

3.3 PEG 400-based phase change materials nano-enhanced with functionalized graphene nanoplatelets

3.4 NePCM based on silver dispersions in poly (ethylene glycol) as a stable solution for thermal storage

3 Results and general discussion

This Doctoral Thesis has been developed under a compendium of articles in which the design, characterization and analysis of the thermophysical properties of new nano-enhanced fluids have been carried out. Poly(ethylene glycol)s with molecular masses ranging from 200 to 400 g·mol^{-1} (labeled by their suppliers as PEG200, PEG300 and PEG400) were used as base materials in the preparation of the new NePCMs. Four nanopowders were selected as thermal enhancers, namely multi-walled carbon nanotubes (commercial Baytubes® c-MWCNT, and synthesized in this work s-MWCNT), Iolitec-functionalized graphene nanoplatelets (fGnP), and PVP-capped Ag nanoparticles (PVP-Ag),. Thus, five different nanofluids sets with a total of twenty-four dispersions were designed at nanoparticle mass concentrations from 0.025 to 1.1 % in the different types of poly(ethylene glycol). Table 1 summarizes relevant information of the studied nanofluids sets as well as investigated properties. A general discussion of the work carried out to propose, develop and characterize the NePCMs and an analysis of the main global contributions of this PhD Thesis are presented as follows.

Table 1. Designed NePCMs sets and investigated thermal and physical properties.

NePCM sets	Nanoadditives			Base fluid†	Studied properties‡
	type and provenance	morphology and size	concentration		
c-MWCNT/PEG200	Multi-walled Carbon Nanotubes (c-MWCNTs) Bayer Material Science AG (Germany)	Filament-like morphology Length: ~10-20 μm Diameter: ~20-30nm	0, 0.025, 0.050, 0.10, 0.20, 0.50 and 0.70 wt%	PEG200 (Merk-Sigma Aldrich) M_w= 259.8 g·mol^{-1} M_w/M_n= 1.05	RB
c-MWCNT/PEG300				PEG300 (Merk-Sigma Aldrich) M_w= 362.1 g·mol^{-1} M_w/M_n= 1.04	RB
s-MWCNT/PEG400	Multi-walled Carbon Nanotubes (s-MWCNTs) synthesized for this PhD Thesis	Filament-like morphology Length: ~80 nm Diameter: ~7 nm	0.010, 0.050, 0.10, 0.30, 0.50, 0.75 and 1.0 wt%	PEG400 (Merk-Sigma Aldrich) M_w= 451.7 g·mol^{-1} M_w/M_n= 1.02	C_p, k, α, ρ, RB, α_p, η
fGnP/PEG400	Functionalized graphene nanoplatelets (fGnP) Iolitec GmbH (Germany)	Sheet-like morphology Thickness: 11–15 nm.	0, 0.025, 0.050, 0.10, 0.20, 0.50 and 0.70 wt%	PEG400 (Panreac AppliChem) M_w= 417.4 g·mol^{-1} M_w/M_n= 1.02	S-L phase change C_p, k, α, ρ, α_p, η
PVP-Ag/PEG400	PVP-capped Ag/PEG400 NANOGAP Sub-NM-Powder S.A. (A Coruña, Spain)	Quasi-spherical Diameter: 22 ± 7 nm	0, 0.10, 0.50 and 1.1 wt%	PEG400 (Merk-Sigma Aldrich) M_w= 532.9 g·mol^{-1} M_w/M_n= 1.02	S-L phase change C_p, k, α, ρ, RB, η, σ

† Poly(ethylene glycol) average mass molar mass (M_w) and polydispersity index (M_w/M_n).
‡ Studied thermal and physical properties: solid-liquid phase characteristics (S-L phase change), isobaric heat capacity (C_p), thermal conductivity (k), thermal diffusivity (α), density (ρ), isobaric thermal expansivity (α_p), dynamic viscosity (η), rheological behaviour (RB), and surface tension (σ).

As discussed in the introduction, several design parameters such as the size, morphology and functionalization of the nanoparticles or the purity and molecular mass of the base fluids may play a key role in the thermal and physical properties of the final dispersions. Thus, as initial step, nanopowders and base fluids have been characterized by means of different techniques such as scanning electron microscopy (SEM), transmission electron microscopy (TEM), scanning transmission electron microscopy (S-TEM), energy dispersive spectroscopy (EDS), Raman Spectroscopy, mercury intrusion porosimetry or electrospray ionization mass spectrometry (ESI-MS). Regarding carbon-based nanomaterials, as gathered in Table 1, commercial multi-walled carbon nanotubes (c-MWCNT) showed average lengths ~10–20 μm and diameters ~20–30 nm (TEM and SEM), while s-MWCNTs synthesized in the framework of this PhD Thesis presented average diameters ~7 nm and lengths ~80 nm (TEM), graphene nanoplatelets exhibited a sheet-like morphology with average thicknesses ~11–15 nm (according to SEM analyses). Raman spectra performed for MWCNT samples showed the D- and G-bands characteristic of carbon-based materials. In the case of s-MWCNT, the G-band intensity is significantly higher than D-band, which corroborates the satisfactory quality of the obtained nano-carbon material. In addition, bands at 180 cm^{-1} and 260 cm^{-1} also indicate the presence of the admixtures of single-layered carbon nanotubes. EDS microanalyses evidenced the expected presence of carbon and oxygen in the fGnP nanopowder with some marginal contents of other elements, which may be traces of the reagents used in the synthesis of the nanomaterial. As for PVP-capped Ag samples, nanoparticles were quasi-spherical with diameters ~22±7 nm (S-TEM). Regarding the poly(ethylene glycol)s used as base materials to prepare the NePCMs, ESI mass spectrometry was used to confirm the purity of the materials as well as to determine the molecular masses and polydispersity indexes, which were in the range of 1.02-1.05 (indicating that selected polymers were quasi-monodisperse).

The temporal and thermal stabilities of prepared NePCMs were investigated by dynamic light scattering (DLS) and thermogravimetric analyses (TGA), respectively. DLS technique was used to investigate the temporal evolution of the hydrodynamic size of PVP-capped Ag nanoparticles and s-MWCNT diluted dispersions (0.01 wt.%) in PEG400 under shaken and static conditions. Results showed an increase in the average apparent hydrodynamic size of dispersed s-MWCNT particles in the case of the sample keep under static conditions, which may correspond to a possible agglomeration of s-MWCNTs under storage conditions. However, after manually shaken the samples, average apparent DLS sizes were around ~150 nm, which may indicate that agglomeration of s-MWCNT can be ruled out by the simple circulation of NePCMs when flowing in thermal devices or installations. In the case of PVP-Ag/PEG400 system, samples showed average sizes ~50 nm throughout the analyzed 26-day period (under either static or shaken conditions), which proves the good stability of designed NePCMs. On the other hand, TGA

thermograms proved that the thermal stability of poly(ethylene glycol)s is not significantly affected by the addition of nanoparticles, with slight shifts in onset decomposition temperature (the maximum modification in T_{onset} between base fluids and NePCMs was from ~536 K to ~519 for c-MWCNT/PEG200 samples).

After characterizing the nanoparticles and the base fluid, the thermophysical properties and rheological behavior of the new NePCM were studied. Solid-liquid phase change characteristics of base fluids and NePCM were determined employing the differential scanning calorimeter DSC Q2000 (TA Instruments, New Castle, DE, USA) working with a refrigerated cooling system RSC90 under nitrogen atmosphere (mole fraction purity higher than 0.9999). DSC thermograms at different scanning rates, 1-5 $K \cdot min^{-1}$, were obtained for the base fluid, fGnP/PEG400 and PVP-Ag/PEG400 nanofluids in a temperature range from 188 to 313 K. In the case of fGnP/PEG400 nano-enhanced phase change materials, the dispersion of nanoparticles reduced crystallization temperature (up to 4 K when compared the 0.50 wt.% concentration with neat PEG400) and shorten the interval in which melting occurs (by 2.5 K also in the case of 0.5 wt.% loading). The addition of PVP-capped Ag nanoparticles slightly reduced the sub-cooling phenomenon of PEG400. Thus, a maximum improvement of 7.1% was found when compared the highest concentration (1.1 wt.%) with the PEG400 used as base material. No significant reduction in latent heat capacity of the poly(ethylene glycol)s was observed after dispersing the nanoadditives.

This same differential scanning calorimeter was also utilized to obtain the isobaric heat capacity (C_p), working with a quasi-isothermal Temperature-Modulated Differential Scanning Calorimetry (TMDSC) method. Isobaric heat capacity was experimentally determined, in a wide range of temperatures for PEG400 and fGnP nanoparticles and NePCM PEG400-based. As also reported in the literature for different water- or glycol-based nanofluids, isobaric heat capacity reduces with nanoparticle loading. In this case, maximum reductions (regarding the corresponding base fluid) of 3%, 0.34% and 0.9% were calculated or experimentally measured for s-MWCNT(1wt.%)/PEG400, fGnP(0.5wt.%)/PEG400 and PVP-Ag(1.1wt.%)/PEG400 samples, respectively.

Thermal conductivities (k) of PEG400-based NePCMs were carried out in the temperature range from 283–333 K (for fGnP/PEG400 samples), 288–343 K (for s-MWCNT/PEG400) and 283–313 K (for PVP-Ag/PEG400). In the case of fGnP and s-MWCNT systems, measurements were carried out with a KD2-Pro Thermal Properties Analyser (Decagon Devices, Inc., Pullman,WA, USA) based on transient hot-wire (THW) technique, while a Hot Disk Thermal Constants Analyzer (Hot Disk AB, Göteborg, Sweden), which works with the transient plane source (TPS) technique, was utilized for PVP-capped Ag nanoparticles in PEG400. Thermal conductivity improves with the addition of nanoparticles for all investigated NePCM systems,

reaching maximum enhancements of 23%, 12.7% and 3.9% for GnP(0.5wt.%)/PEG400, s-MWCNT(1.0wt.%)/PEG400 and PVP-capped Ag(1.1wt.%)/PEG400 samples, respectively. Experimental effective thermal conductivities were compared with the values correlated or predicted using different theoretical models such as Maxwell [93], Hamilton-Crosser (H-C) [94], Nan et al. [95], Murshed et al. [96] and Xue [97]. As an example, in the case of s-MWCNT/PEG400 system, experimental and calculated data exhibited average absolute deviations of 5.5% (Murshed), 5.6% (H-C), and 2.6% (Xue).

The densities (ρ) of NePCM and base fluids were measured for fGnP/PEG400, synthetized MWCNT/PEG400 and PVP-Ag/PEG400. The density of NePCM increases (regarding base PEG400) with the addition of solid nanoparticles. Those increases in density were 0.33% for fGnP(0.5wt.%)/PEG400, 0.42% for s-MWCNT(1.0wt.%)/PEG400 and 2.2% for PVP-Ag(1.1wt.%)/PEG400. As expected, density reduced with rising temperature for base materials and NePCM. The temperature dependence of density was also investigated throughout the isobaric thermal expansivity (α_p). Maximum reductions in α_p (regarding the base fluid) of 2.6% and 1.8% were obtained for fGnP(0.5wt.%)/PEG400 and s-MWCNT(1.0wt.%)/PEG400 samples, respectively.

Dynamic viscosity (η) was studied for the five NePCM sets. Table 2 presents the experimental conditions at which those assays were conducted, as well as the maximum increases in dynamic viscosity due to the addition of the nanoadditives. fGnP/PEG400 viscosities were investigated in the temperature range 283-373 K with a SVM 3000 rotational Stabinger viscometer-densimeter (Anton Paar, Graz, Austria); rheological flow curves were determined for s-MWCNT/PEG400, c-MWCNT/PEG300 and c-MWCNT/PEG200 systems by means of a Physica MCR 101 rotational rheometer (Anton Paar, Austria), while PVP-Ag/PEG400 samples were investigated with an AR-G2 rotational magnetic bearing rheometer (TA Instruments, New Castle, DE, USA). As expected, dynamic viscosity increased with the addition of nanoadditives. Maximum rises in dynamic viscosity (in comparison with the corresponding base fluid) were 24% and 29.6% for the fGnP/PEG400 dispersion loaded with 0.5 wt.% and the s-MWCNT/PEG400 sample containing 1.0 wt.% of s-MWCNT, respectively. These results are much lower than the increases in dynamic viscosity (regarding the base fluid) of 102% and 71% obtained for 0.70 wt.% concentrations of commercial MWCNTs in PEG200 and PEG300, respectively. Finally, a rise of 5.4% was obtained for the for PVP-capped Ag(1.1% wt.) dispersion (in comparison with neat PEG400). The dispersion of commercial MWCNT to PEG200 and PEG300 also leaded to stronger non-Newtonian behaviours than the dispersion of synthesized MWCNTs in PEG400. Thus, while PEG400-based NePCMs showed a pseudoplastic non-Newtonian behaviour for concentrations of synthesized MWCNT higher than 0.05%, commercial MWCNT dispersion in

PEG200 and PEG300 exhibited shear thinning viscosity even at the lowest investigated nanoparticle concentration (0.025 wt.%). The temperature dependence of dynamic viscosity was described by means of the Vogel-Fulcher-Tammann equation, with maximum deviations (between experimental and correlated data) ranging from 1.2% to 3.8% for fGnP/PEG400 and c-MWCNT/PEG200, respectively. Relative dynamic viscosity (*i.e.* the ratio between NePCM viscosity to the viscosity of the corresponding base fluid) was also described as a function of nanoparticle volume fraction by means of Einstein [98], Batchelor [99], Brinkman [100], Krieger-Dougherty [101], Maron-Pierce [102] or Brenner-Condiff models [103]. Values provided by Maron-Pierce model were the most consistent with experimental results, with absolute average deviations lower than 5%. Finally, rheological oscillatory experiments were also conducted for c-MWCNT/PEG200 and c-MWCNT/PEG300 systems in order to identify the linear-viscoelastic region and provide an insight on the analysis of the viscoelastic behaviour of designed dispersions.

Table 2. Experimental conditions at which the viscosities, η, of the different NePCM sets were investigated and maximum increase in viscosity (regarding the corresponding base fluid).

Nanofluid sets	Nanoadditive Concentrations	Temperature range	Shear rate range	Max η increase
c-MWCNT/PEG200	0, 0.025, 0.050, 0.10, 0.20, 0.50 and 0.70 wt%	278–313 K	0.2-1000 s^{-1}	**102%**
c-MWCNT/PEG300	0, 0.025, 0.050, 0.10, 0.20, 0.50 and 0.70 wt%	278–313 K	0.2-1000 s^{-1}	**71%**
s-MWCNT/PEG400	0, 0.010, 0.050, 0.10, 0.30, 0.50 and 0.75 wt%	273–313 K	~1-1000 s^{-1}	**29.6%**
fGnP/PEG400	0, 0.10, 0.25 and 0.50 wt%	283-373 K	-	**24%**
PVP-Ag/PEG400	0, 0.10, 0.50 and 1.1 wt%	278-343 K	80-1600 s^{-1}	**5.4%**

Surface tension was determined for neat-PEG400 and PEG400-based nanofluids loaded with 0.10, 0.50 and 1.1 wt.% of silver nanoparticles by means of a DSA30 drop shape analyzer (Krüss GmBH, Hamburg, Germany) working with appropriate syringes of 15-gauge needle and 1.835 mm outside diameter. Tests were carried out in a TC40 environmental chamber (also from Krüss GmBH), in which the sample temperature was stabilized from 288.15 to 328.15 K. The surface tension of base fluid and NePCMs decreased with rising temperature by ~(0.21–0.22)% every 10 K. A reduction in surface tension was also observed for this NePCM system as the concentration in silver nanoparticles increased. These decreases, which reached 2.2% for the PVP-Ag(1.1wt.%)/PEG400 sample may be attributed to the presence of PVP surfactant.

3.1 Influence of molecular mass of PEG on rheological behaviour of MWCNT-based nanofluids for thermal energy storage†

†Marco A. Marcos, Luis Lugo, Sergei V. Ageev, Nikita E. Podolsky, David Cabaleiro, Viktor N. Postnov, Konstantin N. Semenov, Influence of molecular mass of PEG on rheological behaviour of MWCNT-based nanofluids for thermal energy storage, *Journal of Molecular Liquids,* 318 (2020) 113965.

†Marco A. Marcos, Luis Lugo, Sergei V. Ageev, Nikita E. Podolsky, David Cabaleiro, Viktor N. Postnov, Konstantin N. Semenov, Influence of molecular mass of PEG on rheological behaviour of MWCNT-based nanofluids for thermal energy storage, Journal of Molecular Liquids, 318 (2020) 113965. https://doi.org/10.1016/j.molliq.2020.113965

3.2 MWCNT in PEG-400 nanofluids for thermal applications: A chemical, physical and thermal approach†

†Marco A. Marcos, Nikita E. Podolsky, David Cabaleiro, Luis Lugo, Alexey O. Zakharov, Viktor N. Postnov, Nikolay A. Charykov, Sergei V. Ageev, Konstantin N. Semenov, MWCNT in PEG-400 nanofluids for thermal applications: A chemical, physical and thermal approach, *Journal of Molecular Liquids,* 294 (2019) 111616.

†Marco A. Marcos, Nikita E. Podolsky, David Cabaleiro, Luis Lugo, Alexey O. Zakharov, Viktor N. Postnov, Nikolay A. Charykov, Sergei V. Ageev, Konstantin N. Semenov, MWCNT in PEG-400 nanofluids for thermal applications: A chemical, physical and thermal approach, Journal of Molecular Liquids, 294 (2019) 111616. https://doi.org/10.1016/j.molliq.2019.111616

3.3 PEG 400-based phase change materials nano-enhanced with functionalized graphene nanoplatelets†

†Marco A Marcos, David Cabaleiro, María JG Guimarey, María JP Comuñas, Laura Fedele, Josefa Fernández, Luis Lugo, PEG 400-based phase change materials nano-enhanced with functionalized graphene nanoplatelets, *Nanomaterials,* 8 (2018) 16.

nanomaterials

MDPI

Article

PEG 400-Based Phase Change Materials Nano-Enhanced with Functionalized Graphene Nanoplatelets

Marco A. Marcos [1], David Cabaleiro [1,2,*], María J. G. Guimarey [3], María J. P. Comuñas [3], Laura Fedele [2], Josefa Fernández [3] and Luis Lugo [1]

1 Departamento de Física Aplicada, Universidade de Vigo, 36310 Vigo, Spain; mmarcosm@uvigo.es (M.A.M.); luis.lugo@uvigo.es (L.L.)
2 Institute of Construction Technologies, National Research Council, 35127 Padova, Italy; laura.fedele@itc.cnr.it
3 Laboratorio de Propiedades Termofísicas, Grupo NaFoMat, Departamento de Física Aplicada, Universidade de Santiago de Compostela, 15782 Santiago de Compostela, Spain; mariajesus.guimarey@usc.es (M.J.G.G.); mariajp.comunas@usc.es (M.J.P.C.); josefa.fernandez@usc.es (J.F.)
* Correspondence: dacabaleiro@uvigo.es; Tel.: +34-986-813-771

Received: 17 November 2017; Accepted: 25 December 2017; Published: 29 December 2017

Abstract: This study presents new Nano-enhanced Phase Change Materials, NePCMs, formulated as dispersions of functionalized graphene nanoplatelets in a poly(ethylene glycol) with a mass-average molecular mass of 400 g·mol^{-1} for possible use in Thermal Energy Storage. Morphology, functionalization, purity, molecular mass and thermal stability of the graphene nanomaterial and/or the poly(ethylene glycol) were characterized. Design parameters of NePCMs were defined on the basis of a temporal stability study of nanoplatelet dispersions using dynamic light scattering. Influence of graphene loading on solid-liquid phase change transition temperature, latent heat of fusion, isobaric heat capacity, thermal conductivity, density, isobaric thermal expansivity, thermal diffusivity and dynamic viscosity were also investigated for designed dispersions. Graphene nanoplatelet loading leads to thermal conductivity enhancements up to 23% while the crystallization temperature reduces up to in 4 K. Finally, the heat storage capacities of base fluid and new designed NePCMs were examined by means of the thermophysical properties through Stefan and Rayleigh numbers. Functionalized graphene nanoplatelets leads to a slight increase in the Stefan number.

Keywords: graphene nanoplatelets; poly(ethylene glycol); NePCM; solid-liquid phase change; thermal conductivity; dynamic viscosity; volumetric behaviour

1. Introduction

Thermal energy storage (TES) is considered one of the key technologies for the energy production of the future, especially in the case of renewable systems for which the intermittency and less predictable nature of energy sources are major issues [1,2]. Among different types of heat storage, it is worth mentioning the higher densities of energy storage and almost isothermal characteristics of those storage processes that take advantage of the energy involved in a phase change, in comparison to those methods which simply utilize the sensible heat due to a temperature difference [3,4]. Those materials that use latent heat to store and release energy, increasing thermal inertia of those systems in which are integrated, are also known as phase change materials, PCMs [4,5]. Over the last decades, many different groups of materials have been proposed as PCMs, like inorganic compounds (salt and salt hydrates), organic compounds (paraffins, alcohols, fatty acids and polymers), or eutectics [2,3]. In particular, polymeric materials such as poly(ethylene glycols), PEGs, have been extensively studied as potential solid-liquid PCMs due to their promising characteristics such as appropriate phase change temperature and

enthalpy, which can be tuned through the molecular mass, congruent melting behaviour, non-toxicity, low vapour pressure and competitive price, among others [2,5,6]. However, as many other organic phase change materials, PEGs exhibit low thermal conductivities which prolongs storing and releasing process and limits their usage in practice [5,7]. In order to overcome this limitation and to develop high-performance phase change materials, the dispersion of nano-sized materials with high thermal conductivity has gained increasing attention, given rise to what is known as Nano-enhanced Phase Change Materials, NePCMs, or nano-PCMs [8,9].

Owing to their properties, poly(ethylene glycols), which are a type of polyglycols or polyols, are among the most adaptable chemical ingredients and processing aids available to formulators and manufacturers of a wide range of products. In particular, special attention must also be paid to their potential use as hydraulic fluids and lubricants since poly(alkylene glycols) are considered to exhibit excellent lubricating ability for gears and compressors, for example [10,11]. Cooling and decreasing friction between moving parts, preventing corrosion and sealing and cleaning engines are among lubricant main functions. Thus, the development of new advanced lubricants that allow reducing friction between mechanical elements in motion is a key issue to improve machinery efficiency and component durability and, in turn minimize harmful gas emissions to the environment. In this sense, one of the used, current and promising strategies to improve performance of machinery lubrication and coolant applications is the use of nanoadditives [12,13].

Regarding colloidal dispersions using PEGs as carrier fluids, SiO_2 is the most studied additive in the development of new phase change materials with improved thermal properties [6,14–17]. Tang et al. [15] prepared form-stabilized SiO_2/PEG composites with latent heats over 100 $J \cdot g^{-1}$ using polymeric chains with mass-average molecular masses ranging from 1000 to 6000 $g \cdot mol^{-1}$ as base fluids. Min et al. [14], Quian et al. [6] and Wang et al. [17] also utilized SiO_2 to increase thermal conductivity and form-stabilized PEG 4000 in the two first studies and PEG 10000 in the latter. Wang et al. [18] formulated new composite PCMs from a SiO_2 gel and a PEG 1000 solution at 15/85 ratio doped with β-aluminium nitride at concentrations ranging from 5% to 30% and obtained remarkable enhancements in thermal conductivity, up to 157% higher than the pure poly(ethylene glycol), with suitable latent heats of fusion and slight modifications of melting and crystallization temperatures. Tang and co-workers studied SiO_2/PEG 6000 composite PCMs doped in situ with Cu [19], Al_2O_3 [7] and Ti_4O_7 [20] and reported thermal conductivity improvements compared to the SiO_2/PEG 6000 matrix of 14%, 11% and 73.1% with 2.1% mass concentration of copper, 3.3 wt % Al_2O_3 loading and 3 wt % Ti_4O_7 concentration, respectively. A reduction in subcooling of about 7 K was found for Cu-doped NePCMs compared to pure PEG 6000 [19]. Zafarani-Moattar et al. [21,22] analysed the thermophysical properties and rheological behaviour of ZnO dispersions in PEG 400, while Zendehasbagh et al. [22] prepared NiO nanofluids based on poly(ethylene glycols) mixtures of PEG 400 with PEG 2000 or PEG 6000.

In recent years carbon allotropes have risen great interest in the preparation of nanostructured materials due to their unique physical properties and its relative ease and cost of synthesis on a large scale [23–26]. Thus, certain carbon-based nanostructures exhibit thermal conductivities much higher than metallic or metal oxide nanoparticles [27]. Regarding PCMs, expanded carbon based microstructures or nanostructures have proven to be remarkably effective as thermal conductivity enhancers and shaper stabilizers of different phase change materials such as paraffins [28–31], fatty acids [32–35], or polymers [25,36–42], with acceptable reductions in latent storage heat. In the case of poly(ethylene glycols), Wang et al. [36] reported reductions in melting temperature of PEG 6000—based NePCMs with the addition of different surface-functionalized graphene oxides. Authors attributed these diminutions, especially noticeable with the presence of carboxylic groups, to the strong interactions created between nanomaterial surfaces and polymeric chains. Wang et al. [37] presented a novel solid-solid phase change material also formulated as functionalized graphene oxide (GO) dispersions in poly(ethylene glycol) 6000. Qi et al. [25] prepared a novel form-stable nanocomposite by simple blending and impregnation method with PEG 6000 as thermal storage material and graphene oxide as supporting substance. Authors reported melting temperatures quite

similar at different composite ratios, while crystallization temperatures did not show a clear loading of graphene oxide dependence. Otherwise, Wang et al. [40] used a dynamic impregnating absorption method to design a nanocomposite based on microporous carbon supporting matrix using PEG 4000. Their new proposal materials show noticeable thermal conductivity enhancements in relation to the pure PEG. Zhang et al. [39] prepared novel white carbon black/PEG 4000 form-stable composite PCMs by super ultrasound assisted. Thermal conductivity of these materials presented improvements up to 50% in relation to those of pure PEG.

Zhang et al. [38] analysed the thermal conductivity of poly(ethylene glycol) phase change materials nano-enhanced with carbon coated with Cu, Al and Fe nanoparticles and found 49%, 40% and 30% enhancements in thermal conductivity for 1.5 wt % nanoadditive loadings, respectively. Hybrid NePCMs were also designed by Liu et al. [41] and Tang et al. [42] consisting of SiO_2/PEG 6000 matrices doped with carbon fibres in the former case and with Multiwall Carbon Nanotubes, MWCNTs, in the later. Carbon nanostructures are also adequate solid nanoadditives to promote new nanostructured lubricants [13]. Thus, Gupta et al. [13] have recently studied the effect of the concentration of reduced graphene oxide in poly(ethylene glycol) PEG 200 on the decrease of wear and coefficient of friction on steel surfaces lubricated with this type of dispersions.

In this paper, new nano-enhanced phase change materials and nanolubricants designed as dispersions of functionalized graphene nanoplatelets (fGnP) in a poly(ethylene glycol) with a mass-average molecular mass of 400 g·mol^{-1}, PEG 400, were developed. Specifically, it was studied four different mass concentrations of (0.05, 0.10, 0.25 and 0.50) wt %, which correspond to (0.0003, 0.0005, 0.0013 and 0.0025) volume fractions, respectively, considering a density value of 2.25 g·cm^{-3} for the fGnP nanopowder [43]. In order to analyse thermal energy storage capabilities, the influences of nanoadditive loading on the thermophysical properties of density, dynamic viscosity, thermal conductivity and heat capacity were experimentally studied in a wide temperature range. In addition, temperatures and enthalpy changes associated with (solid-liquid) phase change transitions were also investigated for the designed dispersions.

2. Materials and Methods

2.1. Materials

Functionalized graphene nanoplatelets, fGnP, were provided by Iolitec with declared mass purity of 99.5% and average thickness of 11–15 nm. fGnP nanopowder was used as supplied, no further chemical treatment of nanoplatelet surface or surfactant addition was taken into consideration in this work. A pharmaceutical-grade poly(ethylene glycol) PEG 400 was purchased from Panreac AppliChem (Barcelona, Spain). A Mettler AE-200 analytical balance (Mettler Toledo, Greifensee, Switzerland) with an accuracy of 1×10^{-5} g was used to weigh reagents and samples.

2.2. Graphene and Poly(Ethylene Glycol) Characterization

Morphology and size of graphene nanostructure were observed under a scanning electron microscope (SEM) JEOL JSM-6700F (JEOL, Tokyo, Japan) operating at an accelerator voltage of 20 kV in backscattering electron image (YAG type detector). In order to prepare SEM samples, a drop of graphene in methanol was deposited on the top of a formvar-covered copper transmission electron microscopy grid and then the solvent was evaporated at atmospheric conditions. Typical SEM images of the graphene nanopowders are presented in Figure 1a.

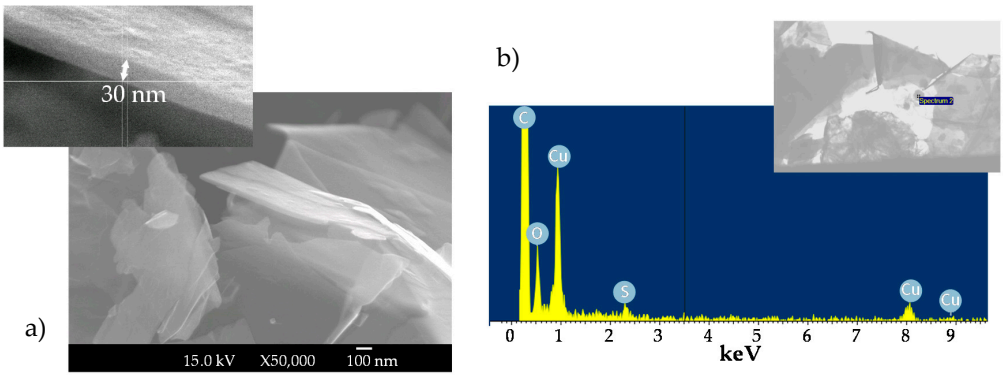

Figure 1. (**a**) SEM images at two magnifications: ×50,000 and ×300,000 (insertion) and (**b**) EDS microanalysis of fGnP powder.

In a first inspection, it is observed that in the commercial powder graphene is stacked forming domains of up to several micrometres. By studying the specimen in more detail, it is possible to differentiate several nanometre-thick laminar structures of rough surfaces, which correspond with the lamellar morphology previously reported for graphene platelets [44,45]. SEM technique was also combined with energy dispersive X-ray spectroscopy (EDS Oxford Inca Energy 300 SEM, Oxford Instruments, Abingdon, UK) in order to analyse the elemental composition of the dry graphene nanopowder. Figure 1b shows an example of EDS microanalysis and, as expected, results indicate the predominant presence of carbon and oxygen in the sample. Marginal contents of other elements such as sodium, calcium, or sulphur were also detected; their presence in the nanopowder can be due to the route used to synthesize the nanomaterial.

Thermal stabilities of as received nanopowder and base material were studied using a TGA/DSC1 thermogravimetric analyser (Mettler-Toledo GmbH, Greifensee, Switzerland). About 25 mg of sample was subject to temperature sweeps from ambient temperature to 1073 K at a heating rate of 10 K/min and under an inert nitrogen atmosphere. Figure 2 shows TGA profiles of graphene nanoplatelets and poly(ethylene glycol).

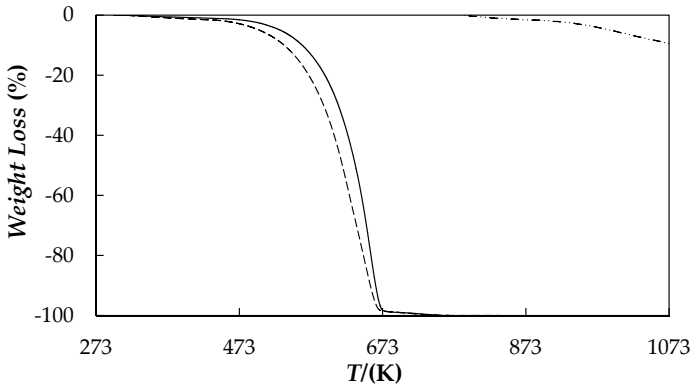

Figure 2. TGA curves of: PEG 400 (— —), fGnP nanopowder (– ·· –) and 0.5 wt % fGnP/PEG 400 NePCM (—) under nitrogen atmosphere.

A gradual weight loss was found for functionalized graphene nanoplatelets as temperature increases, with a total weight loss lower than 9.5% for the entire analysed temperature range. However, when air is introduced into the chamber at the highest temperature the nanopowder sample was almost completely calcined, with an additional weight loss of about 82%. For the PEG 400 used as base material, the weight loss step occurs mainly at temperatures between 460 K and 670 K, with a weight loss less than 5% for temperatures below 503 K and a T_{onset} degradation temperature of about

507 K. T_{onset} temperatures were obtained as the temperature of the crossing point between thermogram baseline and the tangent line to derivative weight loss curve at the inflection point.

Purity and molecular mass of the poly(ethylene glycol) were analysed by electrospray ionization mass spectrometry (ESI-MS) on an APEXQe FT-ICR MS mass spectrometer (Bruker Daltonics, Billerica, MA, USA) equipped with a 7 T actively shielded magnet. A Combi MALDI-electrospray ionization (ESI) source was used to produce ionization with a voltage of 4.5 kV applied to the needle and a counter voltage of 300 V applied to the capillary. A PEG sample was dissolved in a spray solution of CH_3OH/H_2O/formic acid (70:29.9:0.1 by volume). Data were acquired using the ApexControl software version 3.0.0 and the spectrum was processed using the DataAnalysis software version 4.0, both software from Bruker Daltonics. Figure 3 reports the ESI mass spectrum of the PEG 400 used as base material.

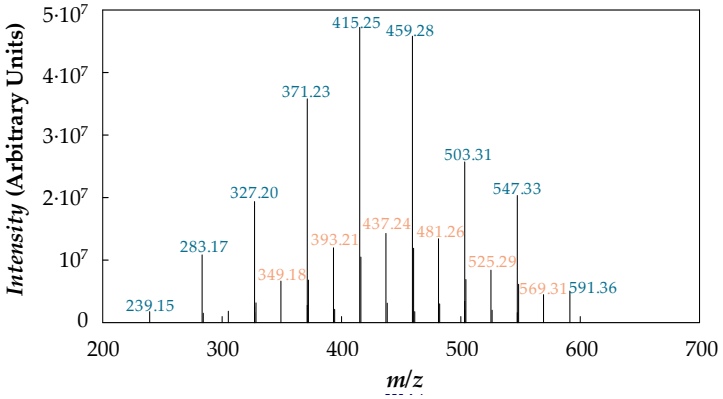

Figure 3. Electrospray mass spectrum of PEG 400.

Taking into account the molecular structure of the polymer, HO–[CH_2–CH_2–O]$_n$–H, all peaks present in the mass spectrum are attributable to PEG molecules cationized with H^+ (m/z = 19.02 + 44.03 n with n = 5–13) or Na^+ (m/z = 41 + 44.03 n with n = 7–12). Hence, the degree of impurities in the specimen can be considered negligible. The distribution of the molecular mass is uniform with a number average of M_n = 417.4 g·mol^{-1}, an average value $M_w = \sum N_i \cdot M_i^2 / \sum N_i \cdot Mi$ of 427.2 g·mol^{-1} where N_i is the number of moles of species i, and a polydispersity index, M_w/M_n = 1.023, which indicates that the polymer is quasi-monodisperse.

Water content in PEG 400, which was determined using a Metrohm 870 Karl Fischer KF Titrino (Metrohm, Herisau, Switzerland) with a Titran 2 (Merck, Darmstadt, Germany), is less than 300 ppm of water.

2.3. NePCM Preparation, Stability and Chemical Interactivity Analysis

NePCMs were prepared following a two-step method combining mechanical stirring with a vortex mixer and ultrasonication. Two different ultrasonic devices were considered: (i) an Ultrasounds (JP Selecta SA, Barcelona, Spain) 9 L ultrasonic bath at 20 kHz and power of 200 W and (ii) a Bandelin Sonopuls HD2200 (Bandelin, Berlin, Germany) ultrasonic disruptor, with a maximum power output of 200 W and a frequency of 20 kHz, working with a 3 mm diameter titanium microtip at a fixed 20% amplitude. In order to select the best conditions for the preparation of the graphene nanofluids based on PEG 400, a study of the sonication time influence on the apparent nanoparticle size distributions of dispersions prepared with these two sonication devices was carried out by using a Zetasizer Nano ZS (Malvern Instruments, Malvern, UK) based on Dynamic Light Scattering, DLS, technique. It must be mention that size distributions obtained from the random changes in the intensity of light scattered using DLS technique are based on the assumption that particles are spherical while studied nanoadditives are sheet-like shaped. Measurements were carried out at 298.15 K using a scattering angle of 173°. Figure 4 shows size distribution of 0.25 wt % fGnP/PEG 400 dispersions prepared

using both methods, as an example. These results are similar to those obtained for the rest of the concentrations. A reduction in average apparent size of nanoparticle aggregates was observed by increasing sonication time, minimum values being 881 nm and 700 nm for 240 min of ultrasonication bath and 45 min of disruptor, respectively. Thus, the last sonication device was considered more appropriated to PEG 400-based fluids. In addition, although no reduction in size measurements was observed between 45 min and 70 min of ultrasonication with the disruptor, 70 min sample exhibits slightly better temporal stability. Therefore, the ultrasonic probe and 70 min sonication time were selected to prepare all the studied fGnP/PEG NePCMs.

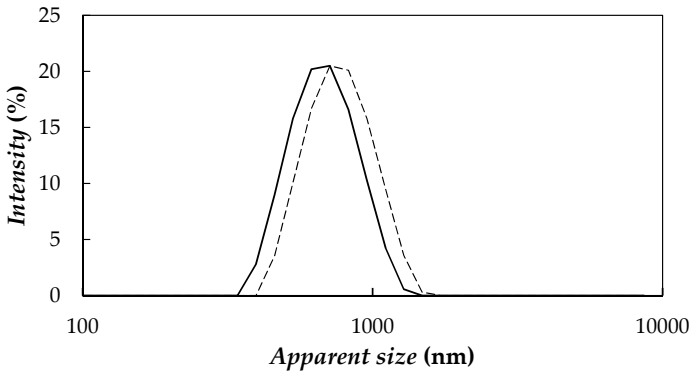

Figure 4. Apparent size distributions of 0.25 wt % fGnP/PEG 400 dispersions prepared by using ultrasonic bath for 240 min (—) and ultrasonic probe for 70 min (— —).

Thermal stability of 0.5 wt % fGnP/PEG 400 dispersion was also analysed in the same conditions as base materials by thermo-gravimetric analysis and results were incorporated in Figure 2. The weight loss profile of the NePCM is very similar to that of PEG 400, which indicates that the addition of the nanoadditive does not lead to any PEG transformation. However, a slight improvement in thermal stability, with a displacement in weight loss-temperature curve of 18 K to the right for the studied NePCM, is observed with the addition of the graphene. This result is attributed to the better thermal stability of nanopowder, higher than 1000 K, in comparison to the poly(ethylene glycol). Similar results were also reported in previous studies [46,47].

In order to analyse possible new chemical interactions between the base fluid and nanoadditives, Fourier Transform Infrared (FT-IR) spectra were recorded for the PEG 400 and 0.5 wt % NePCM in the wavenumber range from 400 to 4000 cm^{-1} by using FTIR spectroscopy (Varian 670-IR with PIKE GladiATR accessory, Agilent Technologies, Santa Clara, CA, USA). FT-IR spectra of the two samples are shown in Figure 5.

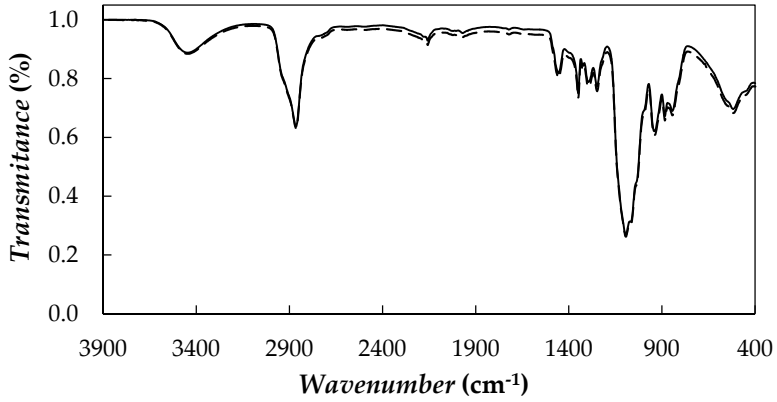

Figure 5. FT-IR spectrum of PEG 400 (— —) and 0.5 wt % fGnP/PEG 400 (—).

In the case of pure PEG 400, typical bands of these polymers [7,19,48] can be observed at wavenumbers of 3446 (O–H stretching), 2865 (–CH_3 stretching) and 1094 cm^{-1} (C–O–C symmetrical stretching). Tang et al. [7,19] observed the same bands when performing FT-IR measurements for a PEG with a molecular mass of 6000 $g{\cdot}mol^{-1}$. In that case, the bands were shown at 3440, 2917, 1106 cm^{-1} [7] or 3430, 2917 and 1106 cm^{-1} [19]. No new spectral peaks or shifts are found for the dispersions prepared at the highest nanoparticle loading, which would indicate that no chemical bonds between the poly(ethylene glycol) and graphene were formed in the NePCMs.

2.4. Thermophysical Characterization

(Solid-liquid) phase transitions of poly(ethylene glycol) and nano-enhanced phase change materials were experimentally obtained in the temperature range from 188 to 313 K using a differential scanning calorimeter, DSC, Q2000 (TA Instruments, New Castle, DE, USA). The instrument is equipped with a refrigerated cooling system RSC90 and nitrogen with mole fraction purity higher than 0.99999 was used as purge gas. General calibration of the device was carried out according to manufacturer procedure. Approximately 10 μg of sample was hermetically encapsulated in 20 μL Tzero aluminium pans able to withstand pressures up to 0.4 MPa. Pans were weighed before and after tests to verify that no loss of mass had taken place and therefore validate measurements. Before experiments, samples were heated up at a temperature of 313 K, at least 20 K above their melting point and held for 10 min to remove any prior thermal history of the materials. Data analysis was performed using Universal Analysis 2000 software V4.5A (TA Instruments, New Castle, DE, USA). Estimated uncertainties for transition temperatures and enthalpies are 0.3 K (with a repeatability of 0.1 K) and 1.2 $J{\cdot}g^{-1}$ (with a repeatability of 0.7 $J{\cdot}g^{-1}$), respectively [49].

Isobaric heat capacities, C_p, of PEG 400 and graphene nanoplatelet powder were measured between 233 and 373 K employing the differential scanning calorimeter DSC Q2000. Measurements were performed using a quasi-isothermal Temperature-Modulated Differential Scanning Calorimetry (TMDSC) method by which the sample temperature sinusoidally varies with amplitude of 0.5 K and oscillation period of 80 s for at least 40 min. Estimated experimental uncertainty for this property in the studied temperature range is 3% [50].

Thermal conductivities, k, were measured in liquid phase and at temperatures ranging from 283 to 333 K by means of a KD2 Pro Thermal Properties Analyser (Decagon Devices, Inc., Pullman, WA, USA). This device was used together with a KS-1 sensor made of stainless steel with a length of 60 mm and a diameter of 1.3 mm and which is appropriate for measuring thermal conductivities of liquids between 0.020 and 4 $W{\cdot}m^{-1}{\cdot}K^{-1}$. In order to remove thermal gradients and ensure a uniform initial temperature, samples were fully immersed in a Grant GP200 (Grant Instruments, Cambridge, UK) oil bath and a delay of at least 15 min was waited between consecutive measurements. The estimated expanded uncertainty of this instrument is lower than 10 $mW{\cdot}m^{-1}{\cdot}K^{-1}$ for thermal conductivities below 200 $mW{\cdot}m^{-1}{\cdot}K^{-1}$ [51].

Dynamic viscosity, η and density, ρ, were experimentally obtained at temperatures between 283 K and 373 K with a SVM 3000 rotational Stabinger viscometer-densimeter (Anton Paar, Graz, Austria). Density determinations are based on the well-known vibrating tube technique, whereas the cell for viscosity measurements is based on a modification of Couette principle. Schematic set up and basic operation principles are described in a European Patent, EP 0 926 481 A2. Viscosity values can be traced back to a single rotational speed, which is measured by an electronic system (Hall effect sensor) that counts the frequency of the rotating magnetic field. Kinematic viscosities fulfil repeatability, reproducibility and comparability requirements of ASTM D445. Expanded uncertainties of 0.02 K in temperature, 1% in viscosity and 0.05% in density were estimated [52].

3. Results

3.1. Phase Change Characterization

(Solid-liquid) transitions of the PEG 400 used as base material and three NePCMs (0.10, 0.25, 0.50) wt % were analysed by means of temperature sweeps with cooling rates ranging from 1 to 10 K·min^{-1} and heating rates of 1 and 2 K·min^{-1}. After the cycles necessary to analyse the samples at the different cooling/heating rates, an additional DSC scan was performed using the same conditions of the first DSC run in order to check that there was not any difference in the (solid-liquid) phase characteristics and therefore validate the results. In addition, it must be pointed out that no significant differences with cycling were observed, specially checked for unmodified PEG 400 and highest mass concentration after 50 melting-freezing processes at 10 K·min^{-1}. Figure 6a,b shows the thermograms obtained for PEG 400 and 0.5 wt % dispersion of nanoplatelets at different cooling rates, 2 K·min^{-1} being the heating rate.

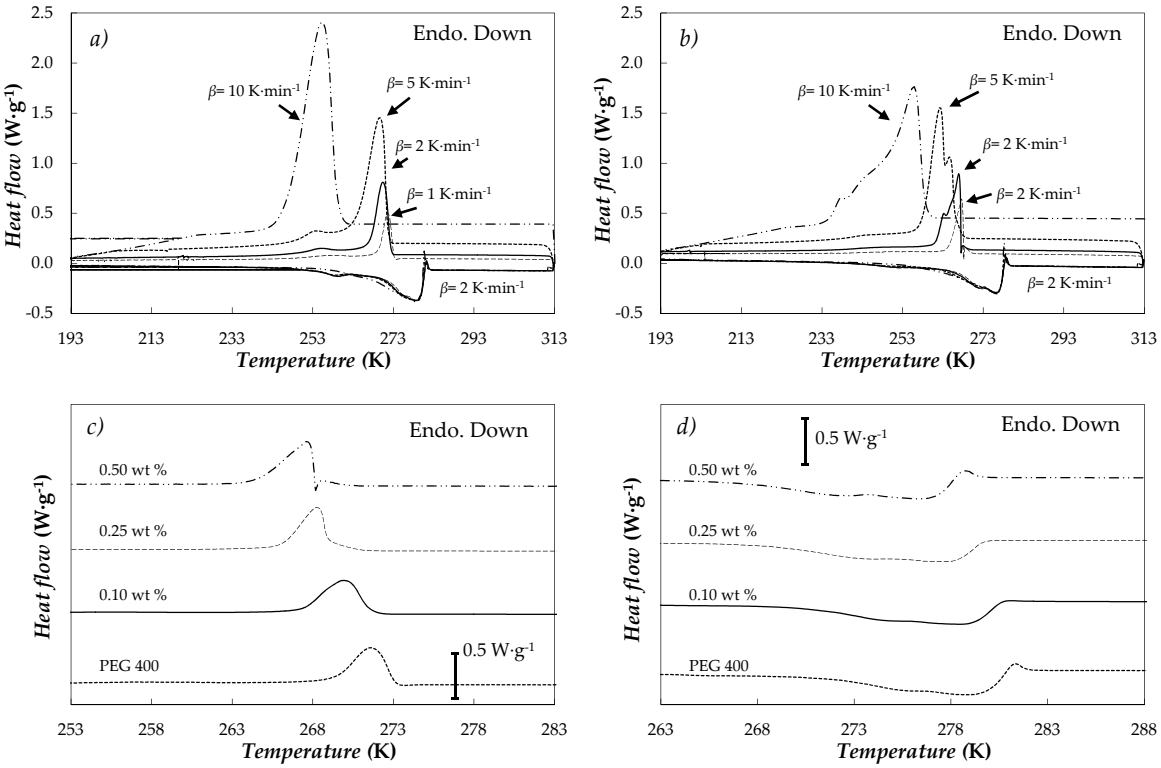

Figure 6. DSC thermograms of (**a**) PEG 400 and (**b**) 0.5 wt % fGnP/PEG 400 concentration at different cooling rates, β and a heating rate of β = 2 K·min^{-1}. (**c**) Cooling and (**d**) heating scans of the different NePCMs at β = 1 K·min^{-1} rates.

Recrystallization temperature of PEG 400 decreases with the increasing cooling rate. This same behaviour was also observed by Pielichowski et al. [53] for poly(ethylene glycols) consisting of longer polymeric chains with molecular masses between (1000 and 35,000) g·mol^{-1}. This phenomenon is attributed to the different thicknesses of the formed crystals during the solidification of this type of materials because of the multiple folds of the polymer chains [53,54]. The behaviour for 0.5% concentration is also exhibited by the other analysed NePCMs. Figure 6c,d present crystallization and melting curves of PEG 400 and studied NePCMs obtained at 1 K·min^{-1} rates. Crystallization and melting temperatures and melting heats obtained at those conditions are gathered in Table 1.

Table 1. Crystallization, T_{crys}, and melting temperatures, T_m, and latent heat of fusion, ΔH_m, of PEG 400 and NePCMs obtained with heating and cooling rates of 1 K·min^{-1}.

Nanoparticle Concentration, wt %	T_{crys} (K)	T_m (K)	ΔH_m (J·g^{-1})
PEG 400, base fluid 0%	271.6	278.8	105.3
fGnP/PEG400 NePCM, 0.10 wt %	269.9	278.5	104.4
fGnP/PEG400 NePCM, 0.25 wt %	268.3	277.7	100.7
fGnP/PEG400 NePCM, 0.50 wt %	267.6	276.3	97.2

Within the studied concentration range, graphene addition reduces crystallization temperature by up to 4 K. Similarly, the temperature range in which the melting transition takes place also decreases in 2.5 K with the loading of nanopowder. Wang et al. [36,47] found the same effects when they studied graphene oxide and reduced graphene oxides nanocomposites in poly(ethylene glycol) PEG 6000. These authors attributed this behaviour to a possible reduction in the movement of the poly(ethylene glycol) segments during melting and crystallization processes due to the presence of nanoadditives. Functionalized graphene nanoplatelets used as nanoadditive are not an active PCM in the studied temperature range. Therefore, a reduction in latent heat of fusion is expected as fGnP loading increases. However, the lower sample fraction which undergoes melting transition due to fGnP addition cannot by itself explain the observed diminutions in ΔH_m. This further reduction was attributed to a diminution in poly(ethylene glycol) crystallinity as a consequence of nanomaterial dispersion in the literature [36,47]. This effect can be characterized by using the degree of crystallinity, X_c:

$$X_c = \frac{\Delta H_m}{(1-\varphi)\cdot \Delta H_{m,pure}} \quad (1)$$

where ΔH_m and $\Delta H_{m,pure}$ are the melting heats of sample and pure PEG 400, respectively and φ is nanoplatelet mass fraction. In this case, a reduction in degree of crystallinity from 90% to 83% was observed with, considering $\Delta H_{m,pure}$ = 117.6 J·g^{-1} [2].

3.2. Isobaric Heat Capacity

Isobaric heat capacity was experimentally determined for the base fluid and nanopowder. Obtained values for PEG 400 show an average absolute deviation, AAD%, of 3% with respect to those data published by Francesconi et al. [55]. Nanopowder C_p values range from 0.44 to 1.14 J·K^{-1}·g^{-1} within the studied temperature range, which is in agreement with the values reported by Pop et al. [43]. For NePCMs, C_p values were obtained using the following equation [56,57].

$$C_{p,nf} = \varphi \cdot C_{p,np} + (1-\varphi)\cdot C_{p,bf} \quad (2)$$

where φ is the mass fraction of nanoplatelets and nf, np and bf subscripts correspond to nanofluid, nanopowder and base fluid, respectively. Figure 7 presents the temperature dependence of C_p values for base fluid and the highest studied concentrations together with modifications of NePCM isobaric heat capacities regarding the PEG 400 at different temperatures. The obtained C_p values decrease slightly with the concentration of functionalized graphene nanoplatelets up to 0.34% for the highest analysed concentration, the 0.5 wt % NePCM. These reductions are lower as temperature rises.

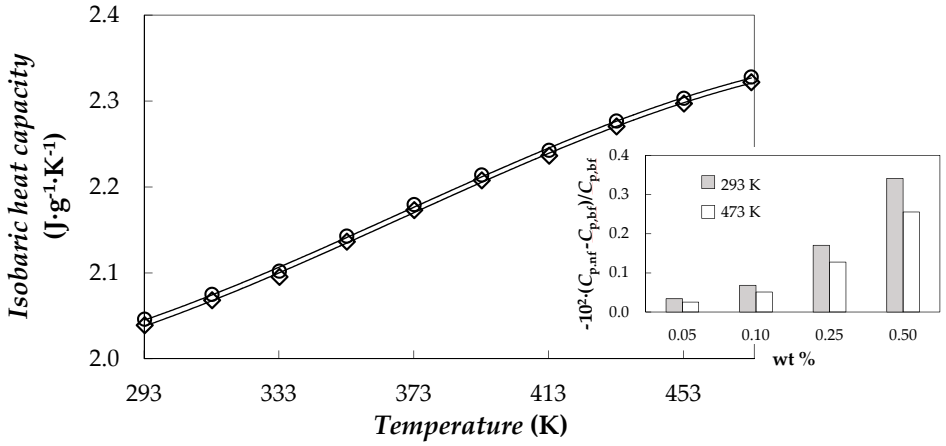

Figure 7. Temperature dependence of isobaric heat capacity, C_p, of PEG 400 and 0.5 wt % NePCM. Inset: isobaric heat capacity decreases, $-10^2 \cdot (C_{p,nf} - C_{p,bf})/C_{p,bf}$, vs. mass concentration, wt %, at different temperatures.

3.3. Thermal Conductivity

The influence of the fGnP loading on thermal conductivity was analysed for (0.05, 0.10, 0.25 and 0.50)% mass concentrations. Figure 8 shows thermal conductivity behaviour in relation to temperature for the base fluid and studied NePCMs.

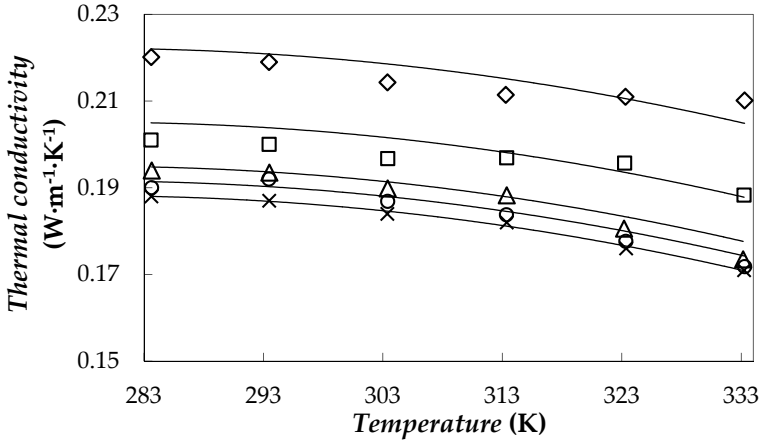

Figure 8. Thermal conductivity against temperature for PEG 400 (×) and for 0.05% (○), 0.10% (△), 0.25% (□) and 0.50% (◇) fGnP/PEG 400 nanofluids. Nan et al. equation [58] (—).

Experimental tests show that the thermal conductivity increases with the loading of fGnPs, with enhancements up to 23% for the highest concentration. In order to describe the effect of dispersed nanoparticles on thermal conductivity, Nan et al. model [58] was used:

$$k_{nf} = k_{bf} \cdot \frac{3 + \phi \cdot [2 \cdot \beta_{11} \cdot (1 - L_{11}) + \beta_{33} \cdot (1 - L_{33})]}{3 - \phi \cdot (2 \cdot \beta_{11} \cdot L_{11} + \cdot \beta_{33} \cdot L_{33})} \quad (3)$$

where L_{ii} are geometric parameters that take values of $L_{11} = 0$ and $L_{33} = 1$ in the case of graphene lamellar nanostructures such as that used in this work [59,60], ϕ is the volumetric fraction of nanoplatelets and β_{ii} is a coefficient defined as:

$$\beta_{ii} = \frac{k_{np} - k_{bf}}{k_{bf} + L_{ii} \cdot \left(k_{np} - k_{bf}\right)} \quad (4)$$

In this study, the Nan equation was used as a correlation with the in-plane thermal conductivity of the graphene, k_{np}, as fitting parameter. A description of the thermal conductivities of the whole system with an AAD% between experimental and correlated data of 1% was obtained with k_{np} = 20 W·m^{-1}·K^{-1}. This result of in-plane thermal conductivity is slightly higher than the values of 11 and 17 W·m^{-1}·K^{-1} obtained by Kole and Dey [59] or Cabaleiro et al. [60], respectively, when they studied graphene oxide dispersions in water-ethylene glycol mixtures.

3.4. Volumetric Behaviour

Density was experimentally obtained for PEG 400 and four fGnP/PEG 400 nanofluids. A comparison between our density values for the base fluid and those previously reported in the literature for poly(ethylene glycols) with molar masses ranging from 365 to 414 g·mol^{-1} [55,61–64], shows average deviations below 0.1%. Temperature behaviour of density is plotted for base fluid and 0.10 and 0.50 wt % NePCMs in Figure 9a.

NePCM density increases with the concentration of nanoadditives as usual in nanostructured thermal materials. The temperature does not practically influence these density increments for temperatures below 333.15 K. However, density improvements rise with temperature at values higher than 333.15 K, ranging from 0.25% to 0.33% for 0.5 wt % fGnP/PEG 400 nanofluid, as an example. The isobaric thermal expansivities, $\alpha_p = -(1/\rho)(\partial\rho/\partial T)_p$, were numerically calculated from the derivatives of the polynomial density adjustments. As can be seen in Figure 9b, α_p increases with temperature up to 9% in the studied range while this coefficient decreases with the concentration of nanoplatelets, up to 2.6% in the case of 0.5 wt % fGnP/PEG 400 nanofluid at 368 K.

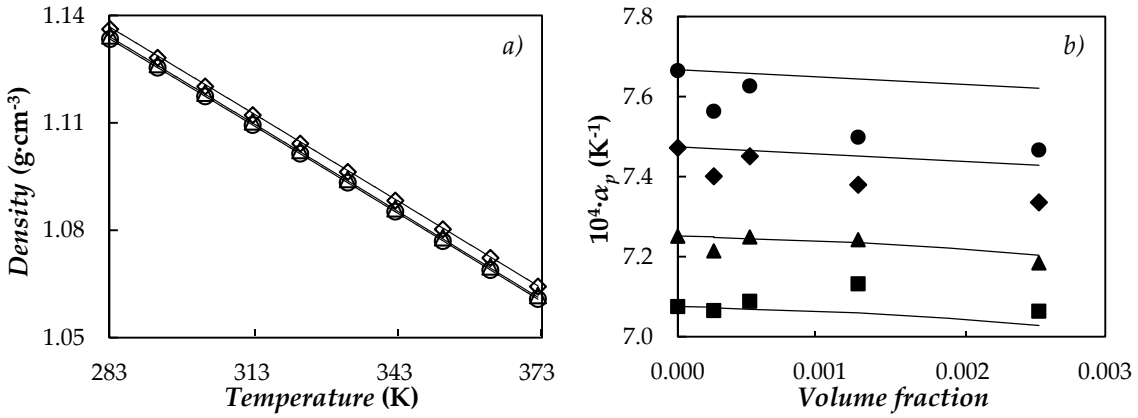

Figure 9. (**a**) Temperature dependence of density at different mass fractions: PEG 400 (○), 0.10% (△) and 0.5% (◇). (—) Equation (5). (**b**) Isobaric thermal expansivity, α_p, vs. volume fraction at different temperatures: 288.15 K (■), 313.15 K (▲), 343.15 K (◆) and 368.15 K (●). (—) Equation (6).

Densities and isobaric thermal expansivities here reported for NePCMs were also compared with values predicted by the following equations:

$$\rho_{nf} = \phi \cdot \rho_{np} + (1 - \phi) \cdot \rho_{bf} \quad (5)$$

$$\alpha_{p,nf} = \phi \cdot \alpha_{p,np} + (1 - \phi) \cdot \alpha_{p,fb} \quad (6)$$

where ϕ is the volume fraction of the nanoplatelets, while the values of ρ_{np} and $\alpha_{p,np}$ were obtained from literature [43,65]. The maximum deviations obtained between the experimental values and data from Equations (5) and (6) are less than 0.1% for density and 2.4% for isobaric thermal expansivity.

3.5. Thermal Diffusivity

In non-steady state or transient conditions, the ability of materials to transfer thermal energy is described by thermal diffusivity, α, which relates thermal conductivity and volumetric heat capacity:

$$\alpha = \frac{k}{\rho \cdot C_p} \tag{7}$$

Materials with high α exhibit fast responses to thermal changes in the environment and thus are preferred when it comes to transferring stored heat. In this work, thermal diffusivity was obtained for the PEG 400 and NePCMs from our experimental k, ρ and C_p data. In order to calculate thermal conductivities and isobaric heat capacities at the exact temperature values, the temperature dependence of these two properties was first described by using a linear correlation in the case of k and a second-order polynomial fitting for C_p. Obtained thermal diffusivities for PEG 400 and NePCMs are plotted in Figure 10.

Thermal diffusivity rises with nanoparticle loading and the decrease in temperature. The best results in terms of thermal diffusivity are obtained for 0.5 wt % NePCM, with a maximum enhancement compared to the base material of 21% at 333.15 K. Obtained maximum increases are lower than those reported by Babapoor et al. [66] for paraffin nanoparticle composite phase change materials. However, it should be taken into account that they used loadings of up to 8 wt % of metallic oxides as nanoadditives. Moreover, absolute thermal diffusivities of fGnPs/PEG400 are twice superior than those of those paraffin nanoparticle composites [66]. Lower absolute thermal diffusivities than these here reported were also reported for expanded graphite/stearic acid and carbon nanotubes/stearic acid NePCMs by Cheng et al. [67]. Finally, results in thermal diffusivity also show a potential use for the proposed NePCMs in distinctive thermal management applications.

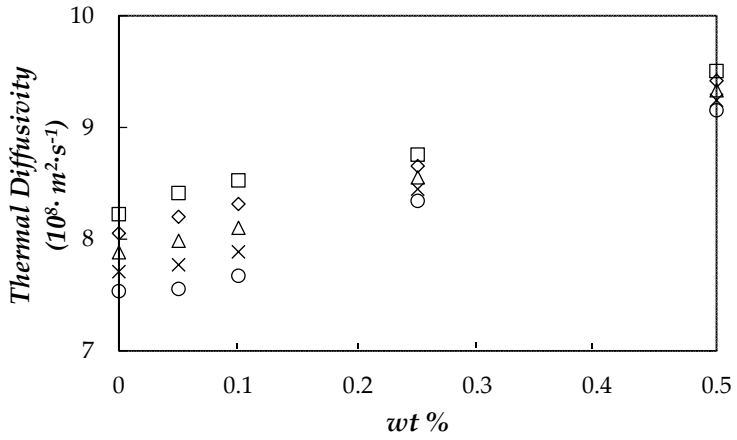

Figure 10. Mass fraction, wt %, dependence of thermal diffusivity at different temperatures: 293.15 K (□), 303.15 K (◇), 313.15 K (△), 323.15 K (×) and 333.15 K (○).

3.6. Viscosity

Values obtained for PEG 400 present a good agreement with viscosity data reported for poly(ethylene glycols) with mass-average molecular masses ranging from 365 to 400 g·mol^{-1} [55,62,63,68]. An average deviation of 1.9% is obtained. Figure 11 shows the temperature dependence of the dynamic viscosity for the base fluid and two NePCMs.

As expected, dynamic viscosity decreases considerably with temperature. This behaviour can be described using the Vogel-Fulcher-Tamman equation (VFT):

$$\ln\ \eta(T) = \ln\ \eta_0 + \frac{D \cdot T_0}{T - T_0} \tag{8}$$

where η_0, D and T_0 are the setting parameters. AADs% between experimental values and those from Equation (8) are equal to or less than 1.2%.

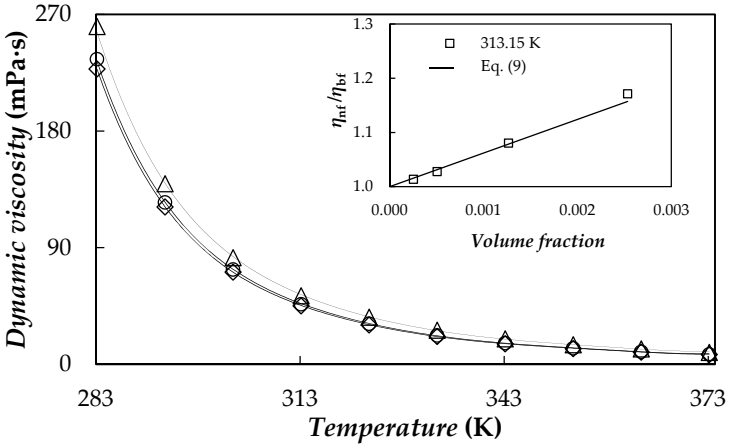

Figure 11. Temperature dependence of dynamic viscosity, η, for: PEG 400 (◇), 0.10% (○) and 0.50% (△) mass concentrations. VFT equation (—). Inset: viscosity ratios, η_{nf}/η_{bf}, vs. nanoadditive volume fraction, together with the values provided by using Equation (9) with ϕ_m = 0.032.

In order to show the effectiveness of the fit, the values obtained by using Equation (8) are also depicted in Figure 11 together with the experimental results. Viscosity ratios of the four studied nanofluids at 313.15 K are plotted in the insert of Figure 11. NePCM viscosities rise with the concentration of graphene platelets up to 24%. The influence of material dispersion with different aspect ratios such as fibres or flakes can be described using the Maron and Piece model [69]:

$$\frac{\eta_{nf}}{\eta_{bf}} = \left(1 - \frac{\phi_a}{\phi_m}\right)^{-2} \tag{9}$$

where ϕ_a is the effective volumetric fraction of aggregates, which reduces to the volume fraction of nanoplatelets in absence of aggregates and ϕ_m is the maximum packing volume fraction [70]. In this study, an AAD% of 1.4% was obtained using ϕ_m as adjustment parameter, obtaining an overall value of ϕ_m = 0.032 for the whole temperature range, which is about ten times larger than the highest volume fraction, for the whole temperature range. AAD% is reduced to 0.9% by considering temperature dependence of ϕ_m, which takes values ranging from 0.030 to 0.051. The goodness of this model can be observed in the inset of Figure 11.

3.7. Evaluation Based on the Studied Properties

With the aim of evaluating storage and heat transfer potentials for proposed NePCMs in relation to base material, PEG 400, the Figures of Merit (FOMs) known as Stefan and Rayleigh numbers were analysed. Stefan dimensionless number, *Ste*, represents the ratio between sensible heat, $C_p \cdot \Delta T$ and latent heat, L_f, in the storage medium:

$$Ste = \frac{C_p \cdot \Delta T}{L_f} \tag{10}$$

where $\Delta T = T - T_m$ is the difference between the temperature considered for the liquid phase, T and the melting temperature, T_m. Figure 12 presents the concentration dependence of Stefan number at different temperatures. As stated above, no significant modification in the isobaric heat capacities was observed in comparison with the PEG 400 used as base material. However, decreases in temperature and enthalpy of melting transition with the addition of graphene nanoplatelets lead to a slight increase

in Stefan number. This increasing trend with fGnP concentration is reduced when high liquid phase temperatures are considered.

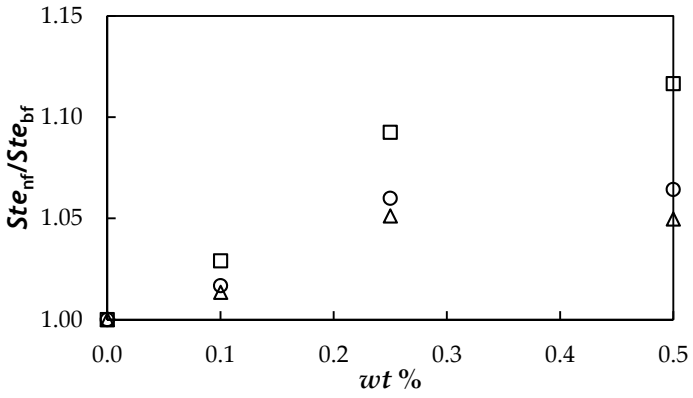

Figure 12. Concentration dependence of the ratio between Stefan numbers, Ste_{nf}/Ste_{bf}, at different temperatures: 293.15 K (□), 313.15 K (○) and 333.15 K (△).

Rayleigh number, Ra, represents the ratio between buoyancy force driving convection and viscous force resisting movement in the fluid and can be expressed in a dimensionless way, Ra_0, as follows:

$$Ra_0 = \frac{Ra}{\Delta T \cdot L^3} = \frac{g \cdot \rho^2 \cdot \alpha_p \cdot C_p}{\eta \cdot k} \tag{11}$$

where the temperature difference, ΔT and length, L, correspond to the geometric and operating conditions of the system and g is the acceleration of gravity. Figure 13 shows the fGnPs concentration dependence of the ratio between the Rayleigh numbers, Ra_0, obtained for each NePCM and base fluid.

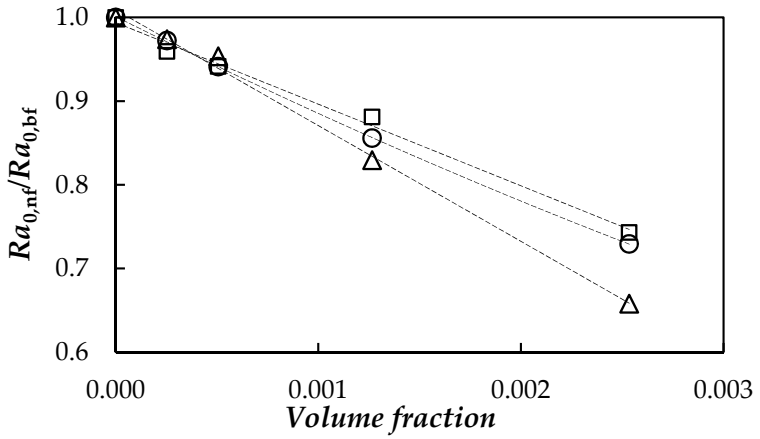

Figure 13. Rayleigh numbers ratio, $Ra_{0,nf}/Ra_{0,bf}$, vs. volume fraction at different temperatures: 293.15 K (□), 313.15 K (○) and 333.15 K (△).

As can be observed, Rayleigh number decreases with the dispersion of nanoplatelets due to the highest influence of the modifications in viscosity and thermal conductivity. A decrease in the Rayleigh number indicates a higher prevalence of the conduction processes in comparison to those of convection, which is more pronounced at higher temperatures.

4. Conclusions and Future Works

Four dispersions of functionalized graphene nanoplatelets up to 0.5 wt % in a poly(ethylene glycol), PEG 400, were designed and characterized for their possible use as NePCMs. Nanoplatelets present a rough laminar structure with thicknesses of several nanometres, while the poly(ethylene glycol) used as base PCM is a quasi monodisperse polymer with an mass-average molecular mass of 427.2 g·mol^{-1}. According to the study of temporal dispersion stability, the optimal preparation conditions consist of a sonication treatment with an ultrasonic homogenizer for 70 min combined with mechanical stirring. Crystallization temperature decreases with the cooling rate for both PEG 400 and NePCMs. Nanoplatelet dispersion reduces crystallization temperature and the interval in which melting occurs up to in 4 K and 2.5 K, respectively. Good agreement was found between thermophysical property results here presented for the base fluid and those previously reported in literature. Thermal conductivity enhancements reach 23% for 0.50% fGnP/PEG 400 nanofluid. In relation to nanoparticle concentration dependence of isobaric heat capacity, density, thermal diffusivity and viscosity of NePCMs, we have found the characteristic behaviour in nanostructured thermal materials. Maximum modifications with respect to base fluid in C_p, ρ, α and η are 0.34%, 0.33%, 21% and 23%, respectively. Lower melting temperatures of NePCMs in comparison to PEG 400 leads to a slight increase in Stefan number, while Rayleigh number decreases with the dispersion of nanoplatelets due to viscosity and thermal conductivity increases. Other nanoadditives (such as metallic nanoparticles, different carbon nanostructures or other functionalizations) and/or poly(ethylene glycols) with different mass-average molar masses should be considered in future works in order to analyse the influence of nanoadditive nature and polymer chain length on PEG-based NePCMs.

Acknowledgments: This work was supported by the "Ministerio de Economía y Competitividad" (Spain) and the FEDER program through the ENE2014-55489-C2-2-R and ENE2014-55489-C2-1-R Projects. Authors acknowledge the financial support by the Xunta de Galicia through GRC ED431C 2016-034, GRC ED431C 2016/001 and AGRUP2015/11 Programs. D.C. was recipient of a postdoctoral fellowship from Xunta de Galicia (Spain). Authors acknowledge CACTI (Univ. de Vigo) and CACTUS (Univ. Santiago Compostela) for technical assistance.

Author Contributions: M.A.M. and D.C. designed the NePCMs, measured thermal properties, analysed results and drafted the manuscript. M.J.G.G. and M.J.P.C. carried out density and dynamic viscosity experiments and contributed to the data interpretation of results concerning material characterization and thermophysical properties. L.F., J.F. and L.L. conceived the study, planned the experiments and took an active role in the preparation of the manuscript. All authors read and approved the final manuscript.

Conflicts of Interest: The authors declare no conflict of interest.

References

1. Karaman, S.; Karaipekli, A.; Sarı, A.; Biçer, A. Polyethylene glycol (PEG)/diatomite composite as a novel form-stable phase change material for thermal energy storage. *Sol. Energy Mater. Sol. Cells* **2011**, *95*, 1647–1653. [CrossRef]
2. Pielichowska, K.; Pielichowski, K. Phase change materials for thermal energy storage. *Prog. Mater. Sci.* **2014**, *65*, 67–123. [CrossRef]
3. Sharma, A.; Tyagi, V.V.; Chen, C.R.; Buddhi, D. Review on thermal energy storage with phase change materials and applications. *Renew. Sustain. Energy Rev.* **2009**, *13*, 318–345. [CrossRef]
4. Cabeza, L.F.; Martorell, I.; Miró, L.; Fernández, A.I.; Barreneche, C. *Introduction to Thermal Energy Storage (TES) Systems*; Woodhead Publishing: Cambridge, UK, 2015; pp. 1–28.
5. Sun, Q.; Yuan, Y.; Zhang, H.; Cao, X.; Sun, L. Thermal properties of polyethylene glycol/carbon microsphere composite as a novel phase change material. *J. Therm. Anal. Calorim.* **2017**, *130*, 1741–1749. [CrossRef]
6. Qian, T.; Li, J.; Ma, H.; Yang, J. The preparation of a green shape-stabilized composite phase change material of polyethylene glycol/SiO_2 with enhanced thermal performance based on oil shale ash via temperature-assisted sol–gel method. *Sol. Energy Mater. Sol. Cells* **2015**, *132*, 29–39. [CrossRef]
7. Tang, B.; Wu, C.; Qiu, M.; Zhang, X.; Zhang, S. PEG/SiO_2–Al_2O_3 hybrid form-stable phase change materials with enhanced thermal conductivity. *Mater. Chem. Phys.* **2014**, *144*, 162–167. [CrossRef]

8. Ma, Z.; Lin, W.; Sohel, M.I. Nano-enhanced phase change materials for improved building performance. *Renew. Sustain. Energy Rev.* **2016**, *58*, 1256–1268. [CrossRef]
9. Gerard, F.; Camila, B.; Aran, S.; José Enrique, J.; Luisa, F.C. Recent patents on nano-enhanced materials for use in thermal energy storage (TES). *Recent Pat. Nanotechnol.* **2017**, *11*, 101–108.
10. Fandiño, O.; Lugo, L.; Comuñas, M.J.P.; López, E.R.; Fernández, J. Temperature and pressure dependences of volumetric properties of two poly(propylene glycol) dimethyl ether lubricants. *J. Chem. Thermodyn.* **2010**, *42*, 84–89. [CrossRef]
11. Paredes, X.; Fandiño, O.; Pensado, A.S.; Comuñas, M.J.P.; Fernández, J. Pressure-viscosity coefficients for polyalkylene glycol oils and other ester or ionic lubricants. *Tribol. Lett.* **2012**, *45*, 89–100. [CrossRef]
12. Zin, V.; Barison, S.; Agresti, F.; Colla, L.; Pagura, C.; Fabrizio, M. Improved tribological and thermal properties of lubricants by graphene based nano-additives. *RSC Adv.* **2016**, *6*, 59477–59486. [CrossRef]
13. Gupta, B.; Kumar, N.; Panda, K.; Dash, S.; Tyagi, A.K. Energy efficient reduced graphene oxide additives: Mechanism of effective lubrication and antiwear properties. *Sci. Rep.* **2016**, *6*, 18372. [CrossRef] [PubMed]
14. Min, X.; Fang, M.; Huang, Z.; Liu, Y.; Huang, Y.; Wen, R.; Qian, T.; Wu, X. Enhanced thermal properties of novel shape-stabilized PEG composite phase change materials with radial mesoporous silica sphere for thermal energy storage. *Sci. Rep.* **2015**, *5*, 12964. [CrossRef] [PubMed]
15. Tang, B.; Cui, J.; Wang, Y.; Jia, C.; Zhang, S. Facile synthesis and performances of PEG/SiO_2 composite form-stable phase change materials. *Sol. Energy* **2013**, *97*, 484–492. [CrossRef]
16. Wang, P.; Li, N.; Zhao, C.; Wu, L.; Han, G. A phase change storage material that may be used in the fire resistance of building structure. *Procedia Eng.* **2014**, *71*, 261–264. [CrossRef]
17. Wang, W.; Yang, X.; Fang, Y.; Ding, J. Preparation and performance of form-stable polyethylene glycol/silicon dioxide composites as solid–liquid phase change materials. *Appl. Energy* **2009**, *86*, 170–174. [CrossRef]
18. Wang, W.; Yang, X.; Fang, Y.; Ding, J.; Yan, J. Enhanced thermal conductivity and thermal performance of form-stable composite phase change materials by using β-aluminium nitride. *Appl. Energy* **2009**, *86*, 1196–1200. [CrossRef]
19. Tang, B.; Qiu, M.; Zhang, S. Thermal conductivity enhancement of PEG/SiO_2 composite PCM by in situ Cu doping. *Sol. Energy Mater. Sol. Cells* **2012**, *105*, 242–248. [CrossRef]
20. Tang, B.; Wei, H.; Zhao, D.; Zhang, S. Light-heat conversion and thermal conductivity enhancement of PEG/SiO_2 composite PCM by in situ Ti_4O_7 doping. *Sol. Energy Mater. Sol. Cells* **2017**, *161*, 183–189. [CrossRef]
21. Zafarani-Moattar, M.T.; Majdan-Cegincara, R. Investigation on stability and rheological properties of nanofluid of ZnO nanoparticles dispersed in poly(ethylene glycol). *Fluid Phase Equilib.* **2013**, *354*, 102–108. [CrossRef]
22. Zendehasbagh, S.; Majdan-Cegincara, R. Magnetorheological and volumetric properties of starch and polyethylene glycol solutions in the presence of nio nanoparticles. *Phys. Chem. Res.* **2018**, *6*, 45–66.
23. Amiri, A.; Sadri, R.; Shanbedi, M.; Ahmadi, G.; Chew, B.T.; Kazi, S.N.; Dahari, M. Performance dependence of thermosyphon on the functionalization approaches: An experimental study on thermo-physical properties of graphene nanoplatelet-based water nanofluids. *Energy Convers. Manag.* **2015**, *92*, 322–330. [CrossRef]
24. Mehrali, M.; Sadeghinezhad, E.; Latibari, S.T.; Kazi, S.N.; Mehrali, M.; Zubir, M.N.B.M.; Metselaar, H.S.C. Investigation of thermal conductivity and rheological properties of nanofluids containing graphene nanoplatelets. *Nanoscale Res. Lett.* **2014**, *9*, 15. [CrossRef] [PubMed]
25. Qi, G.Q.; Liang, C.L.; Bao, R.Y.; Liu, Z.Y.; Yang, W.; Xie, B.H.; Yang, M.B. Polyethylene glycol based shape-stabilized phase change material for thermal energy storage with ultra-low content of graphene oxide. *Sol. Energy Mater. Sol. Cells* **2014**, *123*, 171–177. [CrossRef]
26. Żyła, G.; Fal, J.; Estellé, P. The influence of ash content on thermophysical properties of ethylene glycol based graphite/diamonds mixture nanofluids. *Diam. Relat. Mater.* **2017**, *74*, 81–89. [CrossRef]
27. Khodadadi, J.M.; Fan, L.; Babaei, H. Thermal conductivity enhancement of nanostructure-based colloidal suspensions utilized as phase change materials for thermal energy storage: A review. *Renew. Sustain. Energy Rev.* **2013**, *24*, 418–444. [CrossRef]
28. Zhang, Z.; Fang, X. Study on paraffin/expanded graphite composite phase change thermal energy storage material. *Energy Convers. Manag.* **2006**, *47*, 303–310. [CrossRef]
29. Sarı, A.; Karaipekli, A. Thermal conductivity and latent heat thermal energy storage characteristics of paraffin/expanded graphite composite as phase change material. *Appl. Therm. Eng.* **2007**, *27*, 1271–1277. [CrossRef]

30. Kim, S.D.L.T. High latent heat storage and high thermal conductive phase change materials using exfoliated graphite nanoplatelets. *Sol. Energy Mater. Sol. Cells* **2009**, *93*, 136–142. [CrossRef]
31. Bahiraei, F.; Fartaj, A.; Nazri, G.-A. Experimental and numerical investigation on the performance of carbon-based nanoenhanced phase change materials for thermal management applications. *Energy Convers. Manag.* **2017**, *153*, 115–128. [CrossRef]
32. Sari, A.; Karapekl, A.; Kaygusuz, K. Fatty acid/expanded graphite composites as phase change material for latent heat thermal energy storage. *Energy Sources Part A* **2008**, *30*, 464–474. [CrossRef]
33. Sarı, A.; Karaipekli, A. Preparation, thermal properties and thermal reliability of palmitic acid/expanded graphite composite as form-stable PCM for thermal energy storage. *Sol. Energy Mater. Sol. Cells* **2009**, *93*, 571–576. [CrossRef]
34. Karaipekli, A.; Sarı, A.; Kaygusuz, K. Thermal conductivity improvement of stearic acid using expanded graphite and carbon fiber for energy storage applications. *Renew. Energy* **2007**, *32*, 2201–2210. [CrossRef]
35. Li, C.; Xie, B.; Chen, J. Graphene-decorated silica stabilized stearic acid as a thermal energy storage material. *RSC Adv.* **2017**, *7*, 30142–30151. [CrossRef]
36. Wang, C.; Wang, W.; Xin, G.; Li, G.; Zheng, J.; Tian, W.; Li, X. Phase change behaviors of PEG on modified graphene oxide mediated by surface functional groups. *Eur. Polym. J.* **2016**, *74*, 43–50. [CrossRef]
37. Wang, F.; Zhang, P.; Mou, Y.; Kang, M.; Liu, M.; Song, L.; Lu, A.; Rong, J. Synthesis of the polyethylene glycol solid-solid phase change materials with a functionalized graphene oxide for thermal energy storage. *Polym. Test.* **2017**, *63*, 494–504. [CrossRef]
38. Zhang, H.; Wu, Q.; Lin, J.; Chen, J.; Xu, Z. Thermal conductivity of polyethylene glycol nanofluids containing carbon coated metal nanoparticles. *J. Appl. Phys.* **2010**, *108*, 124304. [CrossRef]
39. Zhang, X.; Huang, Z.; Ma, B.; Wen, R.; Min, X.; Huang, Y.; Yin, Z.; Liu, Y.; Fang, M.; Wu, X. Preparation and performance of novel form-stable composite phase change materials based on polyethylene glycol/white carbon black assisted by super-ultrasound-assisted. *Thermochim. Acta* **2016**, *638*, 35–43. [CrossRef]
40. Wang, Z.; Zhang, X.; Jia, S.; Zhu, Y.; Chen, L.; Fu, L. Influences of dynamic impregnating on morphologies and thermal properties of polyethylene glycol-based composite as shape-stabilized PCMs. *J. Therm. Anal. Calorim.* **2017**, *128*, 1039–1048. [CrossRef]
41. Liu, Z.; Wei, H.; Tang, B.; Xu, S.; Shufen, Z. Novel light–driven CF/PEG/SiO_2 composite phase change materials with high thermal conductivity. *Sol. Energy Mater. Sol. Cells* **2018**, *174*, 538–544. [CrossRef]
42. Tang, B.; Wang, Y.; Qiu, M.; Zhang, S. A full-band sunlight-driven carbon nanotube/PEG/SiO_2 composites for solar energy storage. *Sol. Energy Mater. Sol. Cells* **2014**, *123*, 7–12. [CrossRef]
43. Pop, E.; Varshney, V.; Roy, A.K. Thermal properties of graphene: Fundamentals and applications. *MRS Bull.* **2012**, *37*, 1273–1281. [CrossRef]
44. Mehrali, M.; Tahan Latibari, S.; Mahlia, T.M.I.; Metselaar, H.S.C.; Naghavi, M.S.; Sadeghinezhad, E.; Akhiani, A.R. Preparation and characterization of palmitic acid/graphene nanoplatelets composite with remarkable thermal conductivity as a novel shape-stabilized phase change material. *Appl. Therm. Eng.* **2013**, *61*, 633–640. [CrossRef]
45. Agromayor, R.; Cabaleiro, D.; Pardinas, A.A.; Vallejo, J.P.; Fernandez-Seara, J.; Lugo, L. Heat transfer performance of functionalized graphene nanoplatelet aqueous nanofluids. *Materials* **2016**, *9*, 455. [CrossRef] [PubMed]
46. Qian, T.; Li, J.; Feng, W.; Nian, H.E. Single-walled carbon nanotube for shape stabilization and enhanced phase change heat transfer of polyethylene glycol phase change material. *Energy Convers. Manag.* **2017**, *143*, 96–108. [CrossRef]
47. Wang, C.; Feng, L.; Yang, H.; Xin, G.; Li, W.; Zheng, J.; Tian, W.; Li, X. Graphene oxide stabilized polyethylene glycol for heat storage. *Phys. Chem. Chem. Phys.* **2012**, *14*, 13233–13238. [CrossRef] [PubMed]
48. Qian, T.; Li, J.; Ma, H.; Yang, J. Adjustable thermal property of polyethylene glycol/diatomite shape-stabilized composite phase change material. *Polym. Compos.* **2016**, *37*, 854–860. [CrossRef]
49. Cabaleiro, D.; Gracia-Fernández, C.; Lugo, L. (Solid + liquid) phase equilibria and heat capacity of (diphenyl ether + biphenyl) mixtures used as thermal energy storage materials. *J. Chem. Thermodyn.* **2014**, *74*, 43–50. [CrossRef]
50. Cabaleiro, D.; Colla, L.; Agresti, F.; Lugo, L.; Fedele, L. Transport properties and heat transfer coefficients of ZnO/(ethylene glycol + water) nanofluids. *Int. J. Heat Mass Transf.* **2015**, *89*, 433–443. [CrossRef]

51. Cabaleiro, D.; Nimo, J.; Pastoriza-Gallego, M.J.; Piñeiro, M.M.; Legido, J.L.; Lugo, L. Thermal conductivity of dry anatase and rutile nano-powders and ethylene and propylene glycol-based TiO_2 nanofluids. *J. Chem. Thermodyn.* **2015**, *83*, 67–76. [CrossRef]
52. Gaciño, F.M.; Regueira, T.; Lugo, L.; Comuñas, M.J.P.; Fernández, J. Influence of molecular structure on densities and viscosities of several ionic liquids. *J. Chem. Eng. Data* **2011**, *56*, 4984–4999. [CrossRef]
53. Pielichowski, K.; Flejtuch, K. Differential scanning calorimetry studies on poly(ethylene glycol) with different molecular weights for thermal energy storage materials. *Polym. Adv. Technol.* **2002**, *13*, 690–696. [CrossRef]
54. Wunderlich, B. *Macromolecular Physics: Crystal Nucleation, Growth, Annealing*; Academic Press: New York, NY, USA, 1976; pp. 11–12.
55. Francesconi, R.; Bigi, A.; Rubini, K.; Comelli, F. Molar heat capacities, densities, viscosities and refractive indices of poly(ethylene glycols) + 2-methyltetrahydrofuran at (293.15, 303.15 and 313.15) K. *J. Chem. Eng. Data* **2007**, *52*, 2020–2025. [CrossRef]
56. O'Hanley, H.; Buongiorno, J.; McKrell, T.; Hu, L.W. Measurement and model validation of nanofluid specific heat capacity with differential scanning calorimetry. *Adv. Mech. Eng.* **2015**, *4*, 181079. [CrossRef]
57. Zhou, S.Q.; Ni, R. Measurement of the specific heat capacity of water-based Al_2O_3 nanofluid. *Appl. Phys. Lett.* **2008**, *92*, 093123. [CrossRef]
58. Nan, C.W.; Birringer, R.; Clarke, D.R.; Gleiter, H. Effective thermal conductivity of particulate composites with interfacial thermal resistance. *J. Appl. Phys.* **1997**, *81*, 6692–6699. [CrossRef]
59. Kole, M.; Dey, T.K. Investigation of thermal conductivity, viscosity and electrical conductivity of graphene based nanofluids. *J. Appl. Phys.* **2013**, *113*, 084307. [CrossRef]
60. Cabaleiro, D.; Colla, L.; Barison, S.; Lugo, L.; Fedele, L.; Bobbo, S. Heat transfer capability of (ethylene glycol + water)-based nanofluids containing graphene nanoplatelets: Design and thermophysical profile. *Nanoscale Res. Lett.* **2017**, *12*, 53. [CrossRef] [PubMed]
61. Afzal, W.; Mohammadi, A.H.; Richon, D. Volumetric properties of mono-, di-, tri- and polyethylene glycol aqueous solutions from (273.15 to 363.15) K: Experimental measurements and correlations. *J. Chem. Eng. Data* **2009**, *54*, 1254–1261. [CrossRef]
62. Niu, Y.; Gao, F.; Zhu, R.; Sun, S.; Wei, X. Solubility of dilute SO_2 in mixtures of n,n-dimethylformamide + polyethylene glycol 400 and the density and viscosity of the mixtures. *J. Chem. Eng. Data* **2013**, *58*, 639–647. [CrossRef]
63. Živković, N.V.; Šerbanović, S.S.; Kijevčanin, M.L.; Živković, E.M. Volumetric and viscometric behavior of binary systems 2-butanol + PEG 200, + PEG 400, + tetraethylene glycol dimethyl ether and + n-methyl-2-pyrrolidone. *J. Chem. Eng. Data* **2013**, *58*, 3332–3341. [CrossRef]
64. Trivedi, S.; Pandey, S. Densities of 1-butyl-3-methylimidazolium hexafluorophosphate + poly(ethylene glycol) in the temperature range (283.15 to 363.15) K. *J. Chem. Eng. Data* **2011**, *56*, 2168–2174. [CrossRef]
65. Yoon, D.; Son, Y.-W.; Cheong, H. Negative thermal expansion coefficient of graphene measured by raman spectroscopy. *Nano Lett.* **2011**, *11*, 3227–3231. [CrossRef] [PubMed]
66. Babapoor, A.; Karimi, G. Thermal properties measurement and heat storage analysis of paraffinnanoparticles composites phase change material: Comparison and optimization. *Appl. Therm. Eng.* **2015**, *90*, 945–951. [CrossRef]
67. Cheng, X.; Li, G.; Yu, G.; Li, Y.; Han, J. Effect of expanded graphite and carbon nanotubes on the thermal performance of stearic acid phase change materials. *J. Mater. Sci.* **2017**, *52*, 12370–12379. [CrossRef]
68. Bajić, D.M.; Ivaniš, G.R.; Visak, Z.P.; Živković, E.M.; Šerbanović, S.P.; Kijevčanin, M.L. Densities, viscosities and refractive indices of the binary systems (PEG 200 + 1,2-propanediol, + 1,3-propanediol) and (PEG 400 + 1,2-propanediol, + 1,3-propanediol) at (288.15 to 333.15) K and atmospheric pressure: Measurements and modeling. *J. Chem. Thermodyn.* **2013**, *57*, 510–529. [CrossRef]
69. Maron, S.H.; Pierce, P.E. Application of ree-eyring generalized flow theory to suspensions of spherical particles. *J. Colloid Sci.* **1956**, *11*, 80–95. [CrossRef]
70. Halelfadl, S.; Estellé, P.; Aladag, B.; Doner, N.; Maré, T. Viscosity of carbon nanotubes water-based nanofluids: Influence of concentration and temperature. *Int. J. Therm. Sci.* **2013**, *71*, 111–117. [CrossRef]

3.4 NePCM based on silver dispersions in poly (ethylene glycol) as a stable solution for thermal storage†

†Marco A Marcos, David Cabaleiro, Samah Hamze, Laura Fedele, Sergio Bobbo, Patrice Estellé, Luis Lugo, NePCM based on silver dispersions in poly (ethylene glycol) as a stable solution for thermal storage, *Nanomaterials,* 10 (2020) 19.

nanomaterials

MDPI

Article

NePCM Based on Silver Dispersions in Poly(Ethylene Glycol) as a Stable Solution for Thermal Storage

Marco A. Marcos [1,2], David Cabaleiro [1,2,3,*], Samah Hamze [3], Laura Fedele [2], Sergio Bobbo [2], Patrice Estellé [3] and Luis Lugo [1]

1 Departamento de Física Aplicada, Universidade de Vigo, E–36310 Vigo, Spain; mmarcosm@uvigo.es (M.A.M.); luis.lugo@uvigo.es (L.L.)
2 Institute of Construction Technologies, National Research Council, I–35127 Padova, Italy; laura.fedele@itc.cnr.it (L.F.); bobbo@itc.cnr.it (S.B.)
3 Université Rennes 1, LGCGM, EA3913, F–35704 Rennes, France; samah.hamze@univ-rennes1.fr (S.H.); patrice.estelle@univ-rennes1.fr (P.E.)
* Correspondence: dacabaleiro@uvigo.es; Tel.: +34-986813771

Received: 18 November 2019; Accepted: 16 December 2019; Published: 19 December 2019

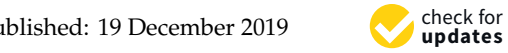

Abstract: The main objective of this study is to design and characterize silver suspensions based on poly(ethylene glycol) PEG400, Ag/PEG400, as energy storage media for low-temperature applications. A polyvinylpyrrolidone (PVP) treatment was applied to ~22 nm silver nanoparticles to ensure good stability in poly(ethylene glycol). An array of different experimental techniques was utilized to analyze the molecular mass and purity of base poly(ethylene glycol), morphology of dry PVP-capped Ag nanoparticles, hydrodynamic average size of dispersed Ag particles, as well as thermal stability of PEG400 and Ag/PEG400 dispersions. Samples exhibited good temporal stabilities with average hydrodynamic diameter around 50 nm according to dynamic light scattering analyses. Melting and solidification transitions were investigated in terms of temperature and enthalpy from differential scanning calorimeter (DSC) thermograms. The thermophysical characterization was completed with thermal conductivity (k), dynamic viscosity (η), isobaric heat capacity (C_p), density (ρ), and surface tension (σ) measurements of designed materials using a Hot Disk thermal conductivimeter, a rotational rheometer, a DSC calorimeter working with a quasi-isothermal modulated method, a U-tube densimeter and a drop shape analyzer, respectively. For a nanoparticle loading of only 1.1% in mass, sub-cooling reduced by 7.1% and thermal conductive improved by 3.9%, with almost no penalization in dynamic viscosity (less than 5.4% of increase). Maximum modifications in C_p, ρ, and σ were 0.9%, 2.2%, and 2.2%, respectively. Experimental results were compared with the values provided by using different theoretical or semi-empirical equations. In particular, good descriptions of dynamic viscosity as functions of temperature and nanoparticle volume concentration were obtained by using the Vogel–Fulcher–Tammann equation and a first-order polynomial $\eta(\phi_{v,np})$ correlation, with absolute average deviations of 2.2% and 0.55%, respectively.

Keywords: silver nanoparticles; PEG400; NePCM; heat storage; thermal conductivity; dynamic viscosity; surface tension

1. Introduction

Better integration of renewable energy in power systems and enhancement of energy efficiency in thermal facilities are essential pathways to improve energy-related environmental issues [1]. In this sense, thermal energy storage (TES) is a useful strategy to address the intermittency of renewable sources and assist an effective utilization of energy by relieving the mismatch between power supply and demand. TES methods are commonly categorized as latent heat using phase change materials

(PCMs), sensible heat, and thermochemical storage technologies [2]. PCMs or latent heat storage media are attracting particular attention due to the high energy storage density (5 to 14 times larger than with only sensible heat [3]) and fewer degradation/reversibility issues throughout a large number of cycles when compared to thermochemical approaches. In recent years numerous materials have been proposed as potential solid–liquid or solid–solid PCMs for applications such as smart housing [2], heat management of electronics [4], or energy generation [5], among others. Refrigeration, one of the major energy consuming processes, has not been an exception. Thus, the use of phase change materials for cold thermal energy storage is also raising increasing interest [6–9].

PCMs are categorized into different groups according to material nature [10]. Among non-paraffinic organic PCMs, poly(ethylene glycol), PEGs, are some of the most promising candidates with melting transitions that can be selected within a wide range of temperatures, from 277 to 343 K, by means of molecular mass [11–13]. In particular, the poly(ethylene glycol) with an average molecular mass of 400 $g{\cdot}mol^{-1}$, PEG400, used as based material in this work, has its melting transition at ~277 K, which is attractive for cold thermal energy storage [8,14]. PEGs exhibit good chemical stabilities, small volume variations, and high latent heats of fusion [15]. However, as with other organic PCMs, the main disadvantage of poly(ethylene glycol) is their low thermal conductivity, which can unacceptably slow the heat transfer rate of stored energy, precluding practical implementation [14].

Different techniques have been proposed to face the low thermal conductivity of PCMs, such as inclusion of high-conductive particles, encapsulation, shape stabilization, metal foams, or embedding in finned/porous structures, among others [16–18]. In recent years, the addition of nanostructures has been found particularly effective not only to increase thermal conductivity, but also to reduce the large sub-cooling characteristic of different PCMs [19]. Latent media obtained from the dispersion of nano-sized particles in phase change materials are known as nano-enhanced phase change materials (NePCMs) or nano-PCMs [4,20,21].

A proper evaluation of NePCMs or other nanotechnology-derived PCMs as both heat transfer and storage media relies on the characterization of melting and solidification transitions, but also on the study of other thermophysical properties such as thermal conductivity (k), viscosity (η), isobaric heat capacity (C_p), density (ρ), or surface tension (σ).

Thus, modifications in rheological behavior or dynamic viscosity can considerably affect pumping power and even flow nature of designed fluids [22–24] while mass flow rate depends on C_p and ρ [25,26]. Although less studied, surface tension also plays an important role in heat and mass transfer processes with low Bond dimensionless numbers, such as microfluidic or systems working under microgravity conditions, for instance [27,28]. A revision of previous studies on storage materials or nanofluids formulated using poly(ethylene glycol) and/or Ag nanoparticles is presented below.

Singh et al. [29] evaluated different techniques to enhance the heat transfer performance of PEG1000, including the addition of carbon powder or the inclusion of either aluminum or carbon fins to the PCM system. An improvement in thermal conductivity of ~31% was observed when 2.5 wt% of carbon powder was dispersed in PEG1000. This enhancement is marginal when compared with the rise in k of more than 40 and 30 times obtained with aluminum and carbon fins, respectively. However, aluminum fin stack occupies ~22.7% of storage system volume (which represents ~42.5% in mass), while carbon framework corresponds to ~24.7% of volume (~34% in mass). Thus, larger reductions in storage capacity are expected for the strategies aiming at enhancing the heat transfer rate by using fins (in comparison with approaches based on carbon powder loading). Marcos et al. [30] formulated dispersions of functionalized graphene nanoplatelets (GnPs) in PEG400 and experimentally investigated the influence that GnP loading has on solid–liquid phase change transition temperatures, latent heat of fusion, thermal conductivity, or thermal diffusivity. A maximum thermal conductivity enhancement of 23% and a reduction in crystallization temperature of 4 K was obtained for a graphene nanoplatelet concentration of 0.5 wt%. Yang et al. [31] prepared PEG1000-based PCMs for efficient light-to-heat conversion, collection, and storage using graphene nanoplatelets (GnPs) and boron nitride (BN). The PCM-composite formulated at a BN:PEG:GnP ratio of 30%:69%:1% showed enhancements in

thermal conductivity up to 336% and reductions in sub-cooling up to 2 K, in both cases in comparison to pure PEG1000. Multi-walled carbon nanotube/PEG400 dispersions were proposed by Marcos et al. [32] from a chemical, physical, and thermal approach. For the maximum nanoadditive content (1% in mass), thermal conductivity and diffusivity improved by 12.7% and 13.5%, while maximum modifications in density and isobaric heat capacity did not exceed 0.42% and 3%, respectively.

Conversely, authors observed that the incorporation of additives reduced latent heat capacity by ~30%. Babapoor, Karimi and Khorram [15] produced NePCM nanofibers using PEG1000, polyamid6 (PA6), and several nanoparticles (SiO_2, Al_2O_3, Fe_2O_3, and ZnO). The highest enhancement in thermal conductivity (above 40% when compared with the former PEG1000) was observed for the PEG:PA6 mixture at a 1:2 ratio and containing 4 wt% of Al_2O_3 nanoparticles. Anghel et al. [33] formulated spherical macrocapsules of PEG6000 in epoxy resin using an aluminum nanopowder as filler to reduce charging and discharging processes. Several sets of PEG/SiO_2 composite form stable phase change materials doped (or not) with other nanoadditives were designed by [34–36], Feng et al. [37], Yang et al. [38], or Li et al. [39], among others. PEG/SiO_2 composite materials containing multi-walled carbon nanotubes [40], active carbon [37], or carbon fibers [41] did not only prove excellent shape-stability and high thermal conductivity but also unique characteristics such as wider absorption range for sunlight, high light-to-heat conversion or energy storage efficiencies.

Despite some carbon nanostructures such as carbon nanotubes or graphene exhibiting thermal conductivities about one order of magnitude higher than those of copper, gold, or silver, large enhancements in the thermal conductivity of common heat transfer fluids were also obtained when dispersing small amounts of metallic nanoparticles [42–44]. Zeng et al. [45] investigated Ag dispersions in 1–Tetradecanol as organic phase change material. These authors indicated that thermal conductivity rises with increasing Ag loading but did not report any value of how much those enhancements were. Deng et al. [46] prepared advanced PCMs based on PEG4000 using expanded vermiculite (EVM) as a shape stabilizer and silver nanowires as a thermal conductivity nano-enhancer. Prepared composites exhibited reductions in super-cooling by 7 K (for the EVM:PEG:Ag composition of 28.2%:64.7%:7.1%) and a thermal conductivity 11.3 times higher than that of PEG4000 (in the case of the EVM:PEG:Ag composition of 1.9%:58.8%:19.3%). Qian et al. [47] modified PEG4000 using Ag nanoparticle-decorated diatomite. The presence of additives (either silver or diatomite) did not significantly reduce the sub-cooling (less than 4 K). However, thermal conductivity increased by 127% (in comparison to the mixture of PEG and diatomite used as based) when the shape-stabilized PCM was doped with a silver loading of 7.2 wt%. As a consequence, absorption and release of thermal energy during the phase change was considerably reduced.

The surface tension of silver dispersions in water was studied by Chen et al. [48] and Godson et al. [49]. Chen et al. [48] observed decreases in σ with either surfactant addition or Ag concentration (especially when nanoparticle loading overcame 0.2 wt%). Also a decreasing trend with silver content was detected by Godson et al. [49]. In this last study, maximum reductions in surface tension reached 10.3% at 323.15 K for the highest analyzed silver concentration (1.2 vol%). Silver-particle colloids have been considered as potential conductive inks for inkjet printing. Thus, Lee et al. [50] designed silver colloids based on a diethylene glycol–water mixture (50:50 in mass) and stabilized with a $40{\cdot}10^3$ molecular weight PVP (with an Ag:PVP ratio of 1:8), and the authors studied the effect of Ag concentration on the dynamic viscosity and surface tension of designed samples. Both properties were found to increase with nanoparticle loading, reaching enhancements of ~3% (σ) and ~400% (η) at the highest Ag concentration (35 wt%). Also important increases in dynamic viscosity were reported by Ankireddy et al. [51] when they studied dispersions (up to 66 wt%) of carboxylic-acid-encapsulated silver nanoparticles in toluene. However, the authors observed that surface tension decreased with the addition of nanoparticles, with maximum diminutions of ~29% for the highest Ag content. Reductions in this property were attributed to a lessening in the interactions between toluene molecules at the droplet surface.

There is still substantial need for further investigative techniques to improve the thermal conductivity of organic PCMs [29]. Thus, the present study aims to develop and characterize stable phase change materials based on poly(ethylene glycol) PEG400 and containing Ag silver nanoparticles as a new stable solution for thermal storage. The effectiveness of Ag loading reducing sub-cooling effect or improving the thermal conductivity and diffusivity is experimentally investigated. Moreover, the thermophysical characterization is completed with the analysis of the dynamic viscosity, isobaric heat capacity, density, and surface tension of presented phase change materials for a wide range of temperatures.

2. Materials and Methods

2.1. Materials

A NePCM based on poly(ethylene glycol) PEG400 and containing 1.1 wt% of silver nanoparticles was specifically prepared for this investigation by NANOGAP Sub-NM-Powder S.A. (A Coruña, Spain). PVP-capped Ag nanoparticles (DS0476, also commercialized by NANOGAP Sub-NM-Powder) were subjected to a surfactant treatment with polyvinylpyrrolidone, PVP, (at a fixed PVP:Ag ratio of 0.068) in order to ensure good temporal stability in poly(ethylene glycol). Merck PEG400 (Merck, Sigma–Aldrich Darmstadt, Germany) poly(ethylene glycol) for synthesis was used as based fluid. This same PEG400 was employed to prepare the other two studied nanofluid concentrations (0.10 wt% and 0.50 wt%) by dilution from 1.1 wt% dispersion. In order to ensure homogeneous composition of the samples, dilutions were sonicated for 2 min in a low power ultrasonic bath (Ultrasounds, JP Selecta S.A., Barcelona, Spain). Density values of 10.49 $g{\cdot}cm^{-3}$ corresponding to crystalline silver [52] and 1.20 $g{\cdot}cm^{-3}$ for PVP were considered in this investigation. In the case of base PEG400, density was experimentally measured in this work. Therefore, at room temperature studied 0.10%, 0.50%, and 1.1% mass fractions ($\phi_{m,np}$) of silver nanoparticles corresponded to volume fractions ($\phi_{v,np}$) of 0.011%, 0.057%, and 0.13%, respectively. A Mettler AE-200 analytical balance (Mettler Toledo, Greifensee, Switzerland) with an accuracy of $1{\cdot}10^{-5}$ g was utilized to weigh reagents and samples.

2.2. Nanoparticle and Base Fluid Characterization

UV–Vis spectroscopy is considered a reliable technique in the primary identification of synthesized nanoparticles [53]. In silver NPs, the proximity of conduction and valence bands allows free movement of electrons between both bands. This electron freedom gives rise to a surface plasmon resonance (SPR) absorption band, which confers unique optical properties at certain wavelengths of light [53]. The UV–Vis absorption spectrum of nanoparticles in wavelengths from 300 nm to 800 nm (Figure 1) was recorded on an HP 8452 UV–Vis diode array spectrophotometer (Hewlett Packard, Palo Alto, CA, USA). A highly diluted aliquot of initial Ag/PEG400 dispersion (containing 1.1 wt%) was studied in a standard 10 mm quartz cuvette.

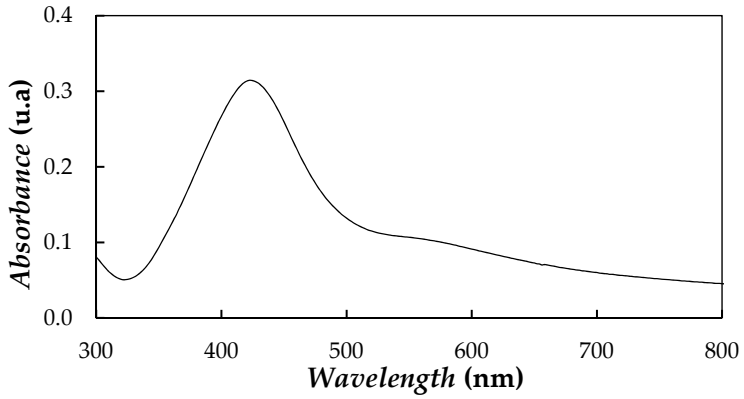

Figure 1. Absorption UV–Vis spectrum of diluted silver dispersion based on PEG400.

The UV–Vis spectrum of Ag nanoparticles exhibited an absorption peak at ~418–428 nm. The presence of a peak close to ~420 nm and ascribed to SPR was well documented in literature [54–57] for other silver nanoparticles of sizes ranging from 2 nm to 100 nm.

Morphology of silver nanoparticles was examined in a JEOL JEM-1011 (JEOL, Tokyo, Japan) scanning transmission electron microscope (S-TEM) working at an acceleration voltage of 100 kV. One drop of diluted NePCM was deposited on a Formvar-covered 400 mesh copper grid and allowed to evaporate at room temperature. Figure 2 shows a representative S-TEM image in which the quasi-spherical morphology of silver nanoparticles can be observed.

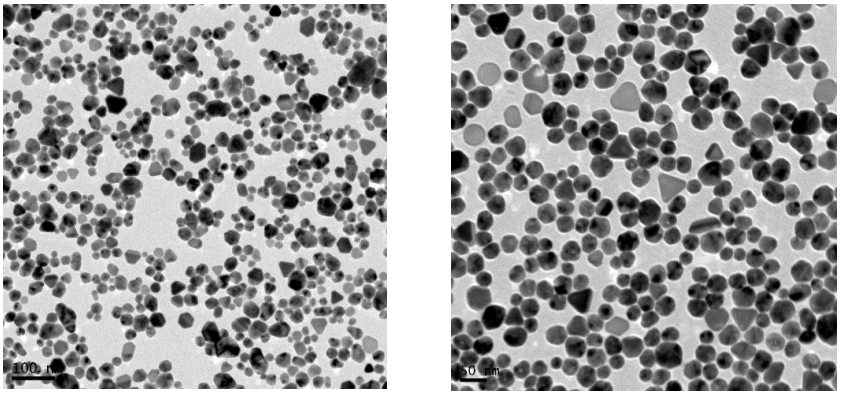

(**a**) (**b**)

Figure 2. Scanning transmission electron microscope images of DS0476 silver nanoparticles capped with polyvinylpyrrolidone at two different magnifications.

Particle size distribution was obtained by measuring the diameter of a representative number of nanoparticles using ImageJ software (http://rsb.info.nih.gov/ij/). Nanoparticle diameters were mainly in the range of 20 nm to 30 nm (with an average value of 22 ± 7 nm), which agreed with the size of 28 ± 8 nm reported by the supplier for other silver nanoparticles from the DS0476 product.

Molecular mass and purity of poly(ethylene glycol) PEG400 were determined by electrospray ionization mass spectrometry (ESI-MS). Experiments were conducted in a high-resolution APEX Qe FT–ICR mass spectrometer (Bruker Daltonics, Billerica, MA, USA). This device is equipped with a 7 Tesla magnet and configured for external ion accumulation in positive-ion mode. Identification was performed applying a voltage of 300 V to the capillary output. Figure 3 presents the ESI-MS spectrum obtained within the scanning range from 300 to 800 *m*/*z*. Poly(ethylene glycol) is a complex mixture of oligomers, with molecular structure: $HO–[CH_2–CH_2–O]_n–H$.

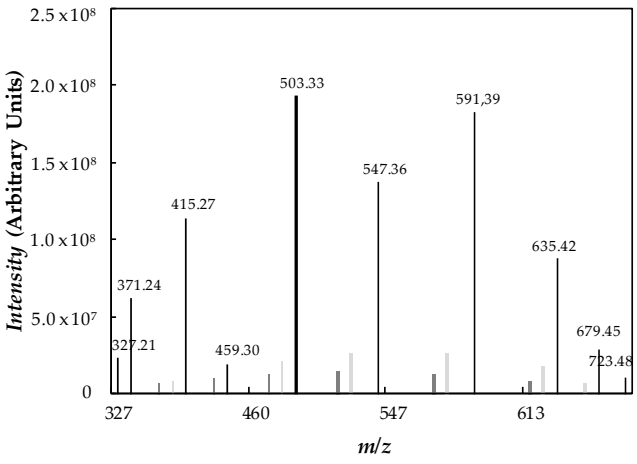

Figure 3. Positive-ion mode electrospray ionization (ESI) spectrum of PEG400.

All peaks present in the mass spectra correspond to molecules cationized with H^+ (m/z = 19.02 + 44.03·n, where n = 7–16), Na^+ (m/z = 41 + 44.03·n, where n = 8–13), or K^+ (m/z = 57.11 + 44.03 n, where n = 8–14). Therefore, average number molar mass is equal to M_n = 520.50 g·mol^{-1}, average mass molar mass being M_w = 532.94 g·mol^{-1} and polydispersity index M_w/M_n = 1.02 (quasi-monodisperse polymer). Molecular mass values obtained by ESI-MS were larger than expected for a poly(ethylene glycol) commercialized as PEG400 [30,32,58,59].

2.3. Thermal and Temporal Stability

Thermal stabilities of neat/base PEG400 and the three Ag/PEG400 dispersions of nanoparticles were investigated by thermogravimetric analysis (TGA) using a Setaram Setsys 1750 TG-DTA (Setaram Instrumentation, Caluire, France). Sample size determinations with this device had a precision of 0.04 µg, while temperature was measured with accuracy better than 2 K. About 30 mg to 35 mg of sample was tarred into ceramic crucibles. Experiments were performed in two steps. Temperature was first raised from 298 to 1023 K with a scanning rate of 1 K·min^{-1} under inert N_2 atmosphere (flow rate of 30 mL·min^{-1}). Then, air atmosphere was introduced in the chamber while temperature was further increased up to 1123 K. Figure 4 shows weight loss and differential weight loss curves obtained for neat PEG400 and the dispersion loaded with 1.1 wt% of silver nanoparticles.

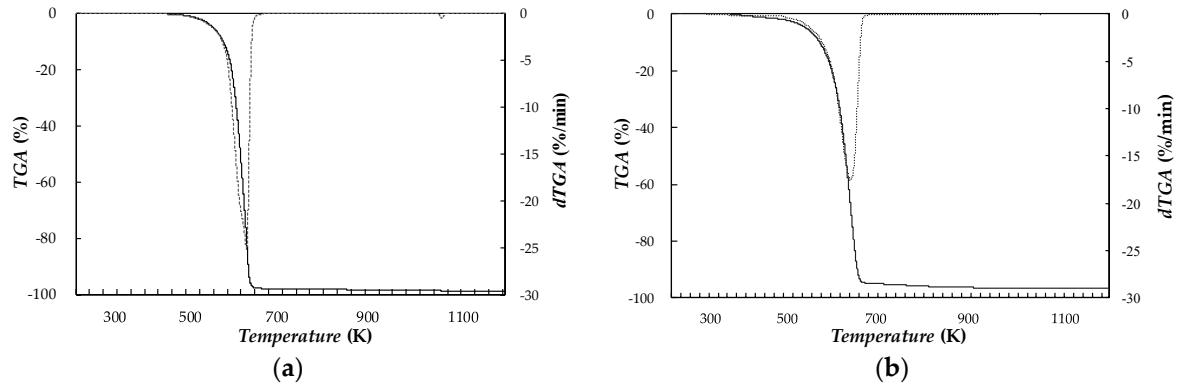

Figure 4. (—) weight loss, TGA, and (- - -) differential weight loss, dTGA, thermograms of (**a**) base fluid PEG400 and (**b**) 1.1 wt% Ag/PEG400 nano-enhanced phase change materials.

In the TGA thermogram of PEG400, a major weight loss step occurs in the temperature range between 510 and 690 K, while weight loss is lower than 5% for temperatures below 579 K, and T_{onset} degradation temperature is 609 K. A comparison between PEG400 and Ag(1.1 wt%)/PEG400 curves shows that the addition of Ag nanoparticles only leads to a slight shift (less than 10 K) to the left in the TGA curve.

The average hydrodynamic size of dispersed Ag nanoparticles in PEG400 was analyzed by means of a Zetasizer Nano ZS (Malvern Instruments, UK) based on dynamic light scattering (DLS). The experimental uncertainty in size measuring suspended particles was estimated to be 2%, further details can be found in Fedele et al. [60] and Colla et al. [61]. In order to ensure appropriate operation conditions, a diluted concentration was selected to carry out DLS investigations. Thus, in this work analyses were performed for an Ag/PEG400 dispersion containing 0.01 wt% of nanoparticles at 298 K and with a scattering angle of 173°. As previously reported for other nanostructured materials [61], hydrodynamic nanoparticle sizes of Ag/PEG400 samples at higher concentrations were expected to be similar to the diameters here obtained for 0.01 wt% loading. Figure 5a shows the nanoparticle size distribution of Ag(0.01 wt%)/PEG400 NePCM. For this last dispersion, the average hydrodynamic diameter is ~50 ± 1 nm. DLS value is almost twice the diameter observed by using transmission electron microscopy. The reason is that DLS size is not based on direct measurements of dry nanoparticles (as in the case of TEM investigations), but on an estimation of hydrodynamic size obtained from an analysis

of nanoparticle diffusion behavior. Differences between DLS and TEM size determinations were also reported in the literature for other silver nanofluids by different authors [54,55]. With the objective of evaluating Ag/PEG400 temporal stability, the evolution of average nanoparticle size was monitored in the timeframe of four weeks. Following a procedure similar to the one proposed by Fedele et al. [62], two DLS cuvettes were filled with ~1 mL of Ag(0.01 wt%)/PEG400 dispersion. The first cuvette was kept in static conditions, while the other was hand shaken for some seconds just before performing the measurements. Figure 5a shows the nanoparticle size distributions obtained at three different days after preparation for the static sample, while the temporal evolution of size determinations under static and shaken conditions is plotted in Figure 5b.

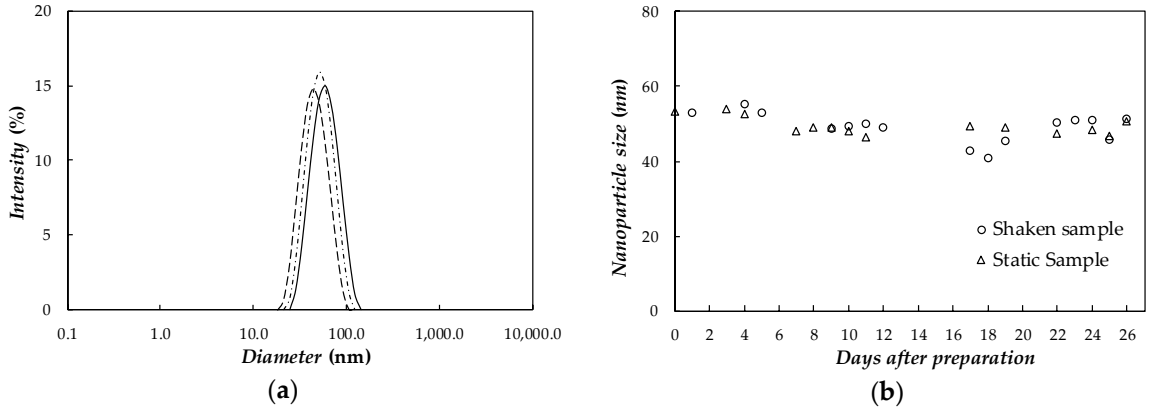

Figure 5. (**a**) Nanoparticle size distribution of static sample based on dynamic light scattering measurements: zero day (—), 7th day (- - -), and 26th day (- · - ·). (**b**) Temporal evolution of average nanoparticle size in Ag(0.01 wt%)/PEG400 dispersion under shaken and static conditions.

As it can be observed in Figure 5, in both samples (under static and shaken conditions) average nanoparticle size remains centered at ~50 nm for the whole analyzed period. This allows us to rule out the presence of any nanoparticle agglomeration or aggregation phenomena and confirm the good stability of designed NePCMs.

2.4. Thermophysical Characterization

Solid–liquid phase change characteristics were determined for PEG400 and the three NePCMs by means of a heat-flux differential scanning calorimeter (DSC) Q2000 (TA Instruments, New Castle, DE, USA) equipped with a refrigerated cooling system RSC90. Analyses were conducted at cooling and heating rates ranging from β = 1 to 10 K·min^{-1} in a nitrogen atmosphere (mole fraction purity better than 0.99999) flowing at 50 mL·min^{-1}. Each measurement condition was repeated at least three times for three different aliquots. Uncertainties in the characterization of thermal events are 0.3 K (temperature) and 1.2 J·g^{-1} (enthalpy). A further description of this instrument and experimental method can be found in Cabaleiro et al. [63].

Thermal conductivity, k, was obtained at temperatures ranging from 283.15 to 333.15 K for PEG400 and Ag/PEG400 suspensions using a Hot Disk Thermal Constants Analyzer (Hot Disk AB, Göteborg, Sweden). This device works with the transient plane source (TPS) technique [64]. In this case, a Hot Disk probe consisting of a double spiral made of nickel (2 mm in diameter) and appropriate to measure the thermal conductivity of liquids was selected. Experiments were performed using a low thermal power, 20 to 25 mW, and a short power input time, 4 s. At least four different tests were performed for each sample. The instrument accuracy declared by the supplier was 5%, however, previous tests with deionized water [60] showed deviations with literature [65] better than 2%. More details can be found in Fedele et al. [60].

Shear rate dependence of dynamic viscosity, η, was studied for base PEG400 and NePCMs at shear rates between 80 and 1600 s^{-1} and temperatures from 278.15 to 343.15 K. Flow curve rheological tests

were developed on an AR-G2 rotational magnetic bearing rheometer (TA Instruments, New Castle, DE, USA). This device is based on a combined motor and transducer instrument and utilizes an induction motor to minimize the friction. Tests were conducted in a cone–plate geometry with a diameter of 40 mm, a 1° steel cone and a truncation gap of 35 μm. Dynamic viscosity results reached repeatability, reproducibility, and comparability requirements of the ASTM D445 standard. An intermediate instrument calibration was performed every three measures to confirm results reliability. After each calibration and series of assays, a check was carried out with distilled water to verify that the rheometer was working in optimal conditions. Water measurements using this experimental device [66] showed accuracy better than 2% with Refprop 9.0 [65].

Isobaric heat capacity, C_p, was analyzed for base PEG400 and silver nanoparticles in the temperature range between 283 and 333 K. Measurements were performed using the DSC Q2000 calorimeter above described, working with a quasi-isothermal temperature-modulated differential scanning calorimetry (TMDSC) method. In this investigation, TMDSC analyses were carried out sinusoidally modulating sample temperature with amplitude of 0.5 K and a period of 80 s for at least 40 min. In the studied temperature range, an uncertainty of 3% was experimentally estimated for C_p [26].

Density, ρ, was measured within the temperature range from 288.15 to 313.15 K by means of an oscillating U-tube densimeter DMA 500 (Anton Paar, Graz, Austria). Water and toluene were selected as reference materials to perform device calibration. Relative uncertainty of density measurements with this device was established to be lower than 0.1% [67].

Surface tension, σ, at the air–sample surface was studied by means of a DSA30 drop shape analyzer (Krüss GmBH, Hamburg, Germany). Tests were performed in a TC40 environmental chamber (also from Krüss GmBH), in which the sample temperature was stabilized from 288.15 to 328.15 K each 10 K. σ was obtained from the shape analysis of sample drops suspended at the apex of a vertical syringe (15-gauge needle with an outer diameter of 1.835 mm) based on the Young–Laplace equation. Reported results were calculated from the study of at least three different drops (with a minimum of 10 recordings each). Necessary density values were experimentally obtained in this work at 288.15, 298.15, and 308.15 K while predicted values, at 318.15 and 328.15 K, were obtained by a second-order polynomial fitting based on the temperature dependence of PEG400 densities measured in Marcos et al. [30] and the influence of adding PVP-capped Ag nanoparticles on this physical property determined in the present study, following a procedure similar to that used by Berrada et al. [68]. Experimental uncertainty of surface tension measurements was previously estimated to be better than 1% [24]. A more detailed description of the experimental device and followed procedure can be found in Gómez-Villarejo et al. [69].

3. Results and Discussion

3.1. Phase Change Characterization

The solid–liquid phase transitions were studied by temperature scans at cooling/heating rates of 1, 2, 5, and 10 K·min^{-1} for PEG400 as base material, and three Ag/PEG400 mass concentrations (0.10%, 0.50%, 1.1%). After completing the necessary runs to study the samples at the predefined cooling/heating rates, some representative DSC scans were repeated to verify that no significant change occurred between the original test and replicate, and thus validate the characterization of phase change transitions. In addition, in order to analyze the reliability of designed materials, base PEG400 and NePCM loaded with 1.1% of silver nanoparticles were subjected to 100 heating–cooling cycles and no reduction in latent heat or shift in melting or solidification transitions was observed. As an example, Figure 6 shows the thermograms obtained at cooling and heating rates of 2 K·min^{-1}.

As it can be observed, the addition of nanoparticles did not significantly modify the onset temperature of the freezing process. Thus, while recrystallization started at around ~259.3 K for pure PEG400, this transition occurred at ~259.8 K in the case of the NePCM loaded with the highest nanoparticle concentration. However, with increasing silver loading, a slight shift towards lower

temperatures was found in the melting transition. These lower melting temperatures (due to the dispersion of nanoparticles), led to a reduction in sub-cooling of up to 7.1% in the case of the Ag(1.1 wt%)/PEG400 sample (in comparison with neat PEG400).

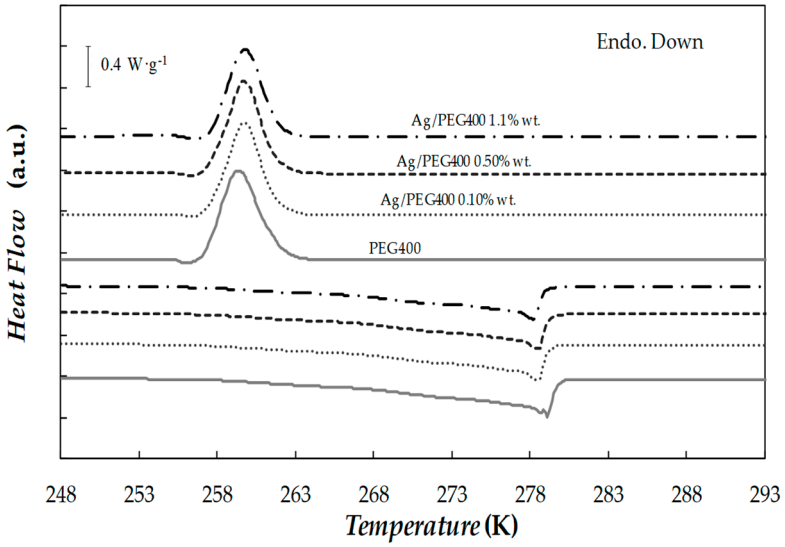

Figure 6. DSC cooling and heating thermograms obtained for base fluid and different Ag/PEG400 NePCMs at scanning rates of 2 K·min^{-1}.

3.2. Isobaric Heat Capacity

Experimental isobaric heat capacities, C_p, for PEG400, the dry powder of Ag nanoparticle, and the Ag(0.5 wt%)/PEG400 nanofluid in the temperature range from 283.15 to 333.15 K are shown in Figure 7.

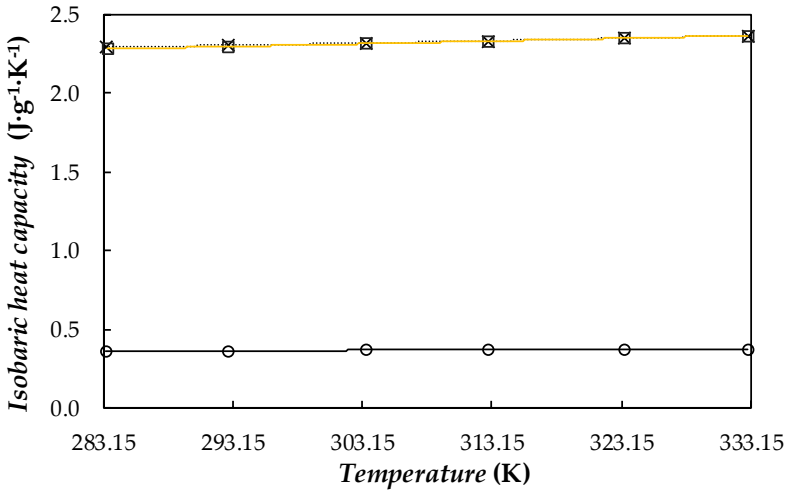

Figure 7. Temperature dependence of isobaric heat capacity of (×) PEG400, (○) dry Ag nanoparticles, and (□) Ag(0.50 wt%)/PEG400 nanofluid. (·····) Second-order polynomial fitting and (—) values provided for Ag(0.50 wt%)/PEG400 by using Equation (1).

Obtained values for base fluid exhibit a good agreement with data reported by Francesconi et al. [70] and Marcos et al. [30,32] for other poly(ethylene glycol) with similar average molecular weights, around 400 g·mol^{-1}. Results measured for dry silver nanoparticles were also compared with the values

recommended by Touloukian and Buyco [71] for bulk silver. In the case of the nanofluids, C_p values were determined by using the following weighted-average equation [72,73]:

$$c_{p,\mathrm{nf}} = \phi_{m,np} \cdot c_{p,\mathrm{np}} + \left(1 - \phi_{m,np}\right) \cdot c_{p,\mathrm{bf}} \quad (1)$$

where $\phi_{m,np}$ is the mass fraction of nanoparticles, while np, bf, and nf subscripts stand for nanoparticles, base fluid, and nanofluid, respectively. For comparison, the values estimated for the sample prepared with the silver loading 0.5 wt% are also plotted in Figure 7. In the studied temperature range, the specific heat capacities experimentally measured for the silver nanopowder are ~84% lower than the values obtained for base PEG400 at the corresponding temperature. C_p property slightly decreases with increasing mass concentration of silver nanoparticles, with reductions lower than 0.9% within studied concentration range of silver nanoparticles. This trend is in agreement with that predicted from C_p data measured in our laboratory for the base fluid and dry PVP-capped Ag nanoparticles by using Equation (1). Other studies on nanofluids using PEG400 as base fluid found diminutions of 3% for the concentration of 1wt% of multiwalled carbon nanotubes (MWCNT) [32], or 0.34% for a dispersion of 0.5 wt% using functionalized graphene nanoplatelets [30]. Hence, it can be concluded that the addition of the PVP-capped Ag nanoparticles does not lead to a significant reduction in the sensible heat capacity of the phase change material.

3.3. Thermal Conductivity

Experimental thermal conductivities obtained for the base fluid and the three Ag/PEG400 dispersions are shown in Figure 8. As it can be observed, the addition of nanoparticles slightly improved the thermal conductivity of the base phase change material. Those enhancements rose with increasing nanoparticle loading, a maximum improvement of 3.9% being reached in the case of the 1.1 wt% concentration. Other studies conducted with PEG400 as base fluid reported higher increases in thermal conductivity, 12.7% for 1 wt% MWCNT/PEG400 nanofluid [32] and 23% for a PEG400 dispersion containing 0.5 wt% of functionalized graphene nanoplatelets (fGnP) [30]. The PVP-capped procedure carried out with silver nanoparticles to favor the stability of the conceived dispersions entailed a penalty in the expected improvement of the intrinsic heat transfer of the sample. According to the results shown in the Figure 8, a slight improvement in thermal conductivity was observed. Modifications in this property were within the experimental uncertainty of this device. In any case, an upward trend with increasing mass fraction was obtained.

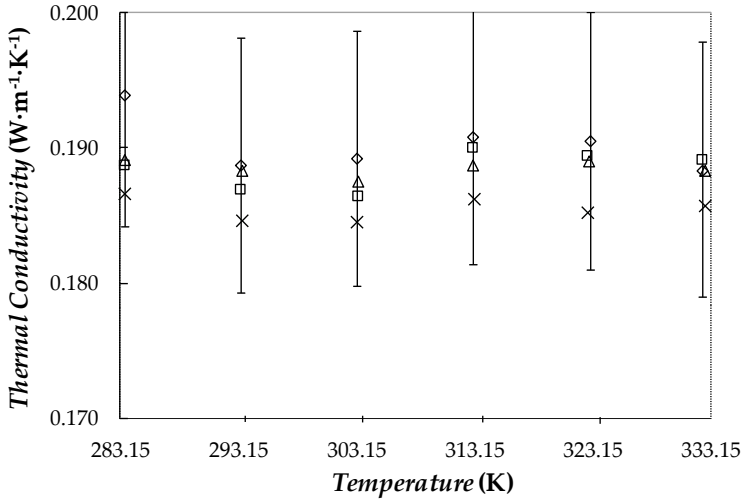

Figure 8. Temperature dependence of thermal conductivity for pure PEG400 (×) and the Ag/PEG400 nanofluids: (△) 0.10 wt%, (□) 0.50 wt% and (◇) 1.1 wt%. Error bars indicate 5% uncertainty regarding experimental data.

Over the last century, huge research efforts have been directed towards understanding and theoretically describing the thermal conductivity of solid–liquid colloidal systems.

In this work, results experimentally measured for Ag/PEG400 NePCMs were compared with the values provided by using some representative theoretical or semi-empirical equations. Maxwell [74] proposed the first equation to estimate the thermal conductivity of solid–liquid suspensions (in our case nanofluids, k_{nf}) from the volume concentration of particles, ($\phi_{v,np}$), and the thermal conductivities of base fluid, k_{bf}, and particles, k_{np}:

$$k_{nf} = \frac{k_{np}+2k_{bf} + 2(k_{np} - k_{bf})\phi_{v,np}}{k_{np}+2k_{bf} - (k_{np} - k_{bf})\phi_{v,np}} k_{bf} \quad (2)$$

However, the Maxwell model does not take into account several parameters such as particle size, agglomeration, or temperature, while those parameters have been found to strongly influence the thermal conductivity of several nanofluid systems [75–77]. Different studies have been developed [75–79] in order to identify the main mechanisms governing thermal conductivity in the solid–liquid interface.

Murshed et al. [80] proposed a model that considers the size of dispersed particles but also suggests the existence of an interfacial layer in which thermal conductivity takes an intermediate value between those of the base fluid and nanoparticles. According to the fundamental theory behind interfacial thermal resistance, heat exchange through the solid–liquid interfacial layer is an important function of the affinity between the two phases [81]. The Murshed et al. [80] equation can be expressed for spherical nanoparticles as follows:

$$k_{nf} = \frac{(k_{np} - k_{lr})\phi_{v,np}k_{lr}(2\gamma_1^3 - \gamma^3+1) + (k_{np}+2k_{lr})\gamma_1^3((\phi_{v,np}\gamma^3(k_{lr} - k_{bf})+k_{bf}))}{\gamma_1^3(k_{np}+2k_{lr}) - (k_{np} - k_{lr})\phi_{v,np}(\gamma_1^3+\gamma^3 - 1)} \quad (3)$$

where $\phi_{v,np}$ is the volume fraction of the nanoparticles in suspension, $\gamma_1 = 1 + h/r$ and $\gamma = 1 + h/2{\cdot}r$ relationships depend on the thickness of interfacial layer (h) and radius (r); while k_{lr}, k_{np}, and k_{bf} are the thermal conductivities of the interfacial layer, nanoparticles, and base fluid, respectively. In our analysis, a value of h = 12.5 nm was assumed for that interfacial layer considering that nanoparticles are spherical and the STEM and DLS average sizes are ~22 nm and ~53 nm (measurement of day 0), respectively.

A comparison between the experimental relative thermal conductivities and the values predicted by using the Maxwell and Murshed equations is graphically presented in Figure 9.

A thermal conductivity of k_{np} = 429 $W{\cdot}m^{-1}{\cdot}K^{-1}$ was considered in this work for the silver nanoparticles [71]. As it can be observed, experimental thermal conductivities for the nanofluids are larger than the values predicted by the Maxwell and Murshed models. For the highest nanoparticle loading, 1.1 wt% of silver, absolute average differences, *AAD%*, between experimental and theoretical data sets reach 2.1% (Maxwell) and 0.5% (Murshed). Other studies conducted with PEG400 as base fluid reported that Hamilton–Crosser, Murshed, Xue, or Nan models also underestimated thermal conductivity results. So, differences of 5.6% (H–C), 5.5% (Murshed) and 2.6% (Xue), were obtained when dispersed MWCNT [32] while the Nan correlation allowed obtaining 1% for GnP suspensions [30]. The cause of those larger experimental enhancements in thermal conductivity may be due to the size dependence of thermal conductivity. The smaller the particle size, the larger is the surface–volume ratio and, consequently, the heat transfer capacity of the nanoparticles also increases [82,83]. However, in the case of metallic nanoparticles, this is not always true. As an example, reductions in the thermal conductivity of copper or silver nanoparticles with decreasing particle size were previously published in the literature by Warrier and Teja [84] or Nath and Chopra [85].

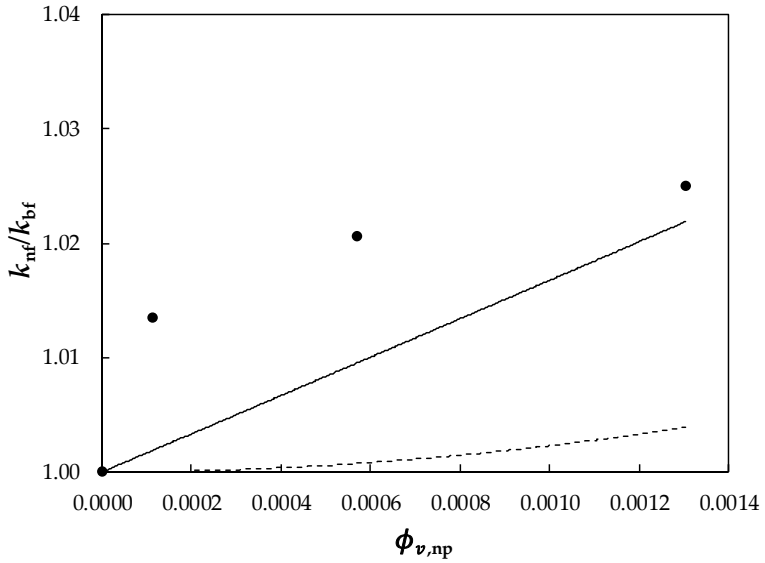

Figure 9. Relative thermal conductivity, k_{nf}/k_{bf}, as a function of volume fraction, $\phi_{v,np}$, for Ag/PEG400 nanofluids at 313.15 K. (●) Experimental results obtained in this work and predicted values by (- - -) Maxwell [74] and (—) Murshed et al. [80] models.

3.4. Density

Densities of base fluid and NePCMs at silver concentrations of 0.10, 0.50, and 1.1 wt% were measured at atmospheric pressure in the temperature range from 288.15 to 313.15 K. Experimental results are displayed for the four samples in Figure 10. According to the normal PEG density dependence on polymer molar mass [86], results obtained in this work for base PEG400 agree well with the ρ values reported in the literature for other poly(ethylene glycol) with similar molecular mass [58,86–88]. With the objective of evidencing this good agreement, some of those literature results are also plotted in Figure 10. As an example, ρ value determined in this study for PEG400 ($M_n \approx 520$ g·mol^{-1}) at 298.15 K is 0.07% higher than the result reported for PEG400 ($M_n = 415$ g·mol^{-1}) by [88] and 0.06% lower than the data provided for PEG600 by Trivedi, Bhanot and Pandey [86] at 293.15 K.

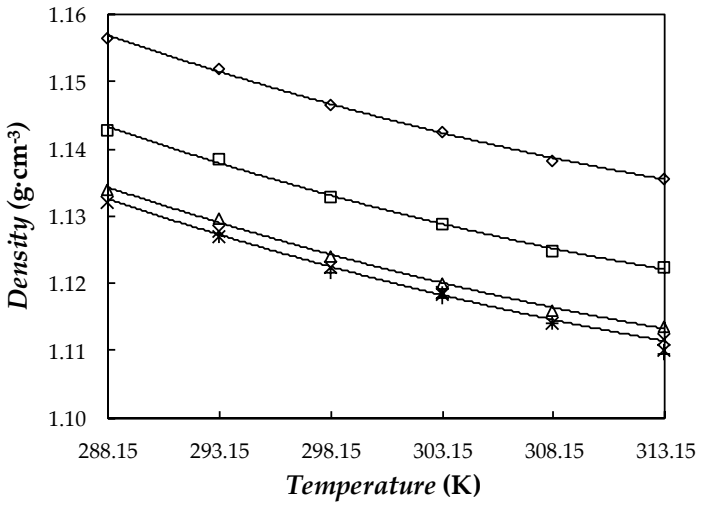

Figure 10. Temperature dependence of density (ρ) for: (×) base PEG400, (△) 0.10 wt%, (□) 0.50 wt%, and (◇) 1.1 wt% NePCMs. (—) Second-order polynomial fittings. Values reported for (+) PEG400 by Han et al. [88] and for (*) PEG600 by Trivedi, Bhanot and Pandey [86].

Density rises with the addition of nanoparticles and these enhancements do not depend on temperature. Average ρ rises (regarding base PEG400) for 0.10, 0.50, and 1.1 wt% PVP-capped Ag loadings are 0.16%, 0.94%, and 2.2%, respectively. Other studies in which PEG400 was used as base fluid observed a maximum increase of 0.42% for 1 wt% MWCNT/PEG400 nanofluid [32] or 0.33% for 0.5 wt% GnP/PEG400 one [30]. Our density modifications (2.2%) for the NePCM containing 0.10 wt% of PVP-capped silver nanoparticles are slightly larger than 0.03% reported by Nakhjavani et al. [89] for a 0.1 wt% Ag/water nanofluid or 0.09% to 0.11% reported by Bahiraei and Heshmatian [90] and Yarmand et al. [91] for aqueous hybrid nanofluids containing 0.1 wt% of graphene-decorated silver nanoadditives. Experimental results here obtained for Ag/PEG400 dispersions were also compared with the values provided by using the following weight-average equation:

$$\frac{1}{\rho_{n_f}} = \frac{\phi_{m,\,np}}{\rho_{np}} + \frac{\phi_{m,\,sf}}{\rho_{sf}} + \frac{1-\phi_{m,\,np}-\phi_{m,\,sf}}{\rho_{bf}} \tag{4}$$

where $\phi_{m,np}$ and $\phi_{m,sf}$ are the nanoparticle and surfactant volume fractions, while nf, np, sf, and bf subscripts stand for nanofluid, nanoparticle, surfactant, and base fluid, respectively. Maximum deviations between experimental results and values provided by Equation (5) are 1.1%.

As expected, density decreases with increasing temperature. This temperature dependence can be fitted with *AADs*% of 0.02% using second-order polynomial fittings. In the studied range, average density modifications each 5 K are 0.38% for base PEG400 and 1.1 wt% Ag/PEG400 considering a value of ρ_{np} = 10.49 g·cm^{-3} corresponding to crystalline silver [52].

3.5. Thermal Diffusivity

The higher the thermal diffusivity, α, of a material is, the faster the thermal energy is propagated. For that reason, thermal diffusivity becomes even more important than thermal conductivity when selecting NePCMs for energy storage. α is related to thermal conductivity, k, and heat capacity per unit of volume, $\rho{\cdot}C_p$, throughout the following expression:

$$\alpha = \frac{k}{\rho{\cdot}c_p} \tag{5}$$

Thermal diffusivities were calculated for base PEG400 and designed NePCMs from k, ρ, and C_p data above presented for these materials. In the studied temperature range, neat PEG400 exhibits α values from 7.13·10^{-8} to 7.15·10^{-8} m^2/s. These results are similar to the data reported in literature for other poly(ethylene glycol) with similar molecular mass [30]. Maximum improvements in thermal diffusivity were obtained for the highest concentration (1.1 wt%) nanoparticle loading, for which increases lower than 2% were obtained.

3.6. Viscosity

Shear viscosity was studied for base PEG400 and the three formulated NePCMs in the temperature range between 278.15 and 343.15 K. Taking into account that the dynamic viscosity of poly(ethylene glycol) is expected to increase with polymeric molecular mass [92], a good agreement is observed when comparing η values here obtained for base PEG400 (M_n = 520 g·mol^{-1}) and results previously reported for other PEGs [30,32,58,88]. As an example, Figure 11a,b shows shear rate–shear stress flow curves obtained for the four samples at 278.15 and 343.15 K.

A linear rise in shear stress with increasing shear rate was observed for all studied samples. This linear relationship, which is temperature independent, confirmed that like base fluid, designed dispersions are Newtonian. As pointed out by [93], this fact can be interpreted as an indication of the quality of dispersions and lack of agglomerates or aggregates in proposed NePCMs. This result agrees with the Newtonian behavior in the shear rate region of 1–200 s^{-1} observed by Tamjid and Guenther [94] when investigating di(ethylene glycol)-based nanofluids containing 0.11% and 0.22%

volume concentrations of silver nanoparticles. However, as reported in that study, larger amounts of nanoparticles led to a non-Newtonian or pseudoplastic behavior.

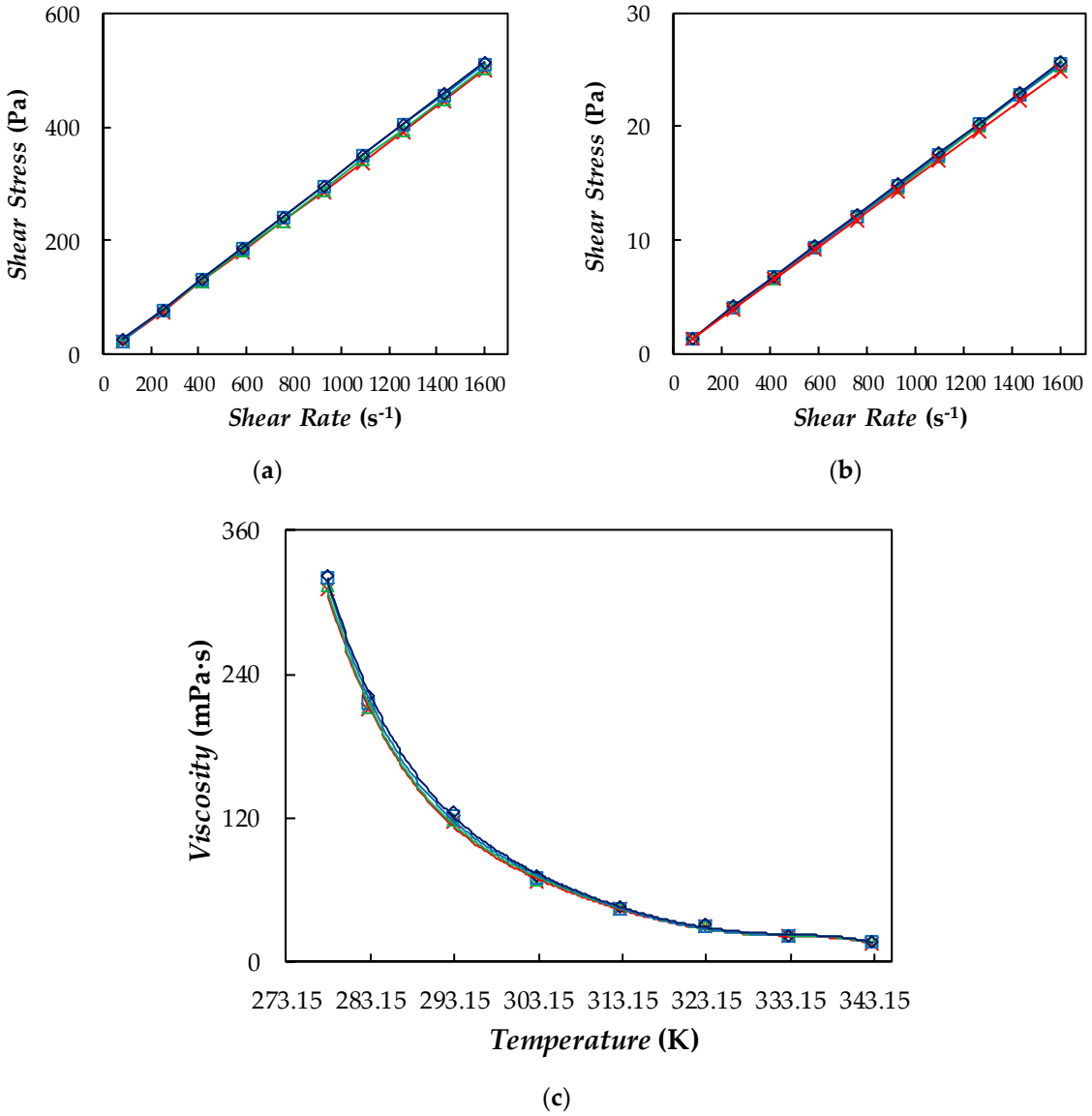

Figure 11. (**a**,**b**) Relationship between shear stress and shear rate at (**a**) 278 K and (**b**) 343 K. (**c**) Temperature dependence of dynamic viscosity. (×) base PEG400, 0 wt%; (△) 0.1 wt%; (□) 0.5 wt%; and (◇) 1.1 wt% Ag/PEG400 NePCMs. (—) Linear fittings, in (**a**,**b**); or VTF equation, Equation (6), in (**c**).

The evolution of dynamic viscosity with temperature is depicted in Figure 11c. As expected, this property exponentially decreased with increasing temperature. This behavior can be described by using the well-known Vogel–Fulcher–Tammann (VFT) equation:

$$\ln \eta = \ln \eta_0 + \frac{D \cdot T_0}{T - T_0} \tag{6}$$

where η_0, D, and T_0 are the fitting parameters. Table 1 reports the values of those three adjustable coefficients as well as *AADs*% between our experimental results and those values fitted by the VFT model.

Table 1. η_0, D, and T_0 fitting parameters, standard deviations, s, and $AADs\%$. from the VFT equation, Equation (6), at different mass fractions.

	Base Fluid (0 wt%)	0.10 wt%	0.50 wt%	1.1 wt%
η_0/mPa·s	0.0659	0.0672	0.0239	0.0246
D	6.37	6.37	9.93	9.92
T_0/K	158.19	158.08	135.41	135.57
s/mPa·s	1.4	1.3	2.4	2.1
$AAD\%$	1.2%	1.1%	2.2%	2.0%

The good description (with $AADs\%$ better than 2.2%) of the Vogel–Fulcher–Tammann equation is shown in Figure 11c. D coefficient is also known as the Angell strength parameter, while its inverse, $F = 1/D$, was defined as fragility by Angell et al. [95]. Studied NePCMs exhibited Angell strength coefficients similar to those of poly(propylene glycol) dimethyl ether [96] or ethylene glycol [97]. Reduced values of the D parameter were an indication of fluid fragility and that liquid configurational structure rapidly breaks down with rising temperature [98].

On the other hand, dynamic viscosity increased with nanoparticle loading. In Figure 12, the dynamic viscosity dependence with volume fraction is represented. In this case, average viscosity rises were 1.4%, 2.8%, and 5.4% for Ag/PEG400 dispersions containing 0.011%, 0.057%, and 0.13% in volume fraction of PVP-capped silver nanoparticles, respectively. These modifications were significantly lower than those reported by Zadeh and Toghraie [99] in their study on Ag–EG nanofluids, in which nanofluid apparent dynamic viscosity at 318 K rose by more than 90% as volume fraction increased from 0.25% to 2%.

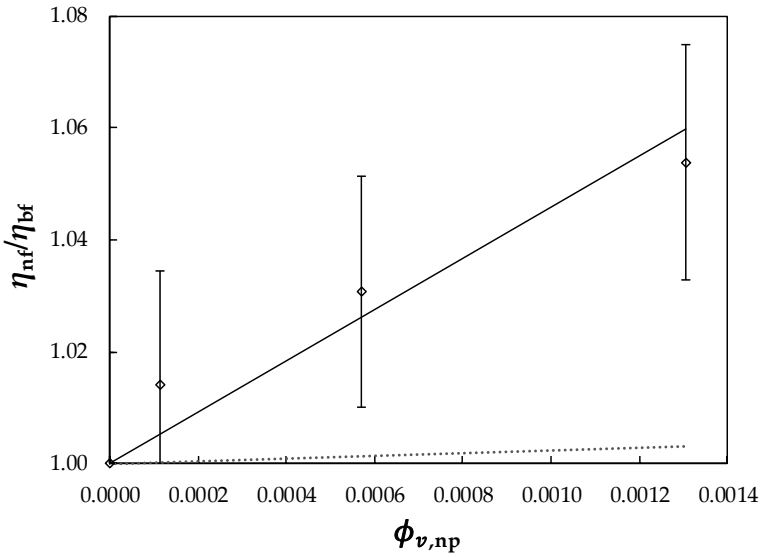

Figure 12. Viscosity ratios η_{nf}/η_{bf} vs. silver nanoparticles volume fraction, ($\phi_{v,\ np}$) at 313.15 K. (◇), experimental values; (·····) Einstein; (—) Equations (7) and (8). Error bars indicate 2% uncertainty.

Different equations have been proposed in the literature to describe $\eta(\phi_v)$ dependence of solid–liquid suspensions [22]. For dilute non-interacting suspensions of spherical-shaped particles, the well-known Einstein [100] predicted that viscosity linearly increases as a function of volume concentration:

$$\eta_r = 1 + 2.5\,\phi_{v,np} \tag{7}$$

where $\eta_r = \eta/\eta_0$ is the so-called reduced viscosity and $\phi_{v,np}$ is the nanoparticle volume concentration. With rising nanoparticle concentration, nanofluid viscosity usually increases in a non-linear manner and, consequently, the Einstein relationship may greatly underpredict η data.

According to Chow [101], the $\eta(\phi_{v,np})$ relationship of Newtonian colloids can be formally written as a virial of series:

$$\eta_r = \frac{\eta}{\eta_0} = 1 + \sum_{i=1}^{N} c_i \cdot \phi_{v,np}^{i} \quad (8)$$

where N is the degree of expansion and c_i are the fitting parameters which may vary from one sample to another [102].

Figure 12 shows a graphical comparison between experimental relative viscosities and the values provided by the predictive Einstein (1906) equation or a linear (N = 1) correlation based on Equation (8). In this case, values predicted using Einstein (1906) show *AADs*% with experimental data of 3%. A better description with an *AAD*% of 0.22%, was obtained utilizing a linear fitting based on Equation (8) with c_1 = 43.

3.7. Surface Tension

Surface tension at the air–sample surface was determined for base PEG400 and Ag/PEG400 suspensions. Obtained results for the four samples are depicted in Figure 13.

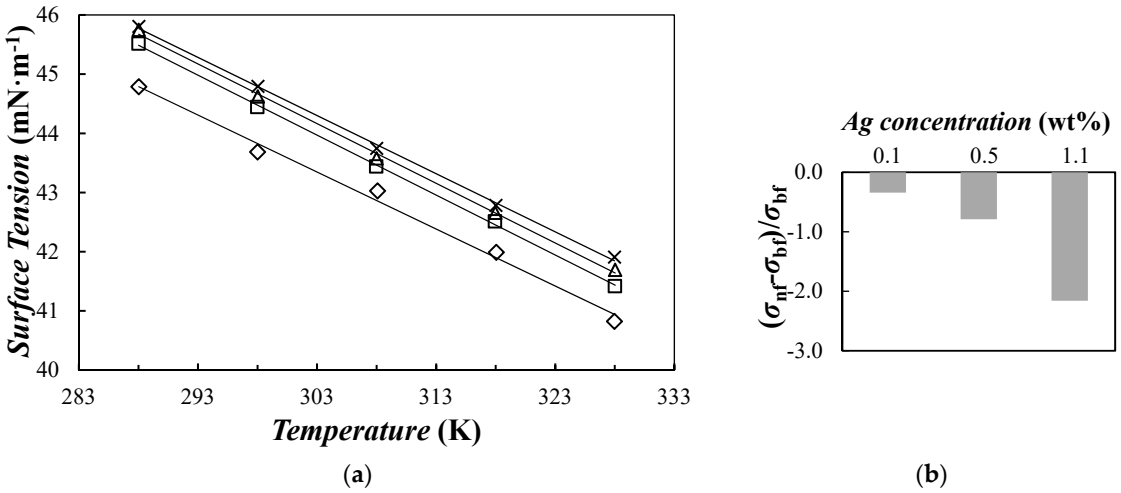

Figure 13. (**a**) Temperature dependence of surface tension: (×) base fluid, (△) 0.10 wt%, (□) 0.50 wt%, and (◇) 1.1 wt% nanoparticle concentrations of Ag/PEG400 nanofluids. (—) First–order polynomial fittings. (**b**) Average modifications in surface tension regarding base fluid, i.e., $(\sigma_{nf}-\sigma_{bf})/\sigma_{bf}$.

Our experimental values for base fluid showed maximum deviations lower than 0.9% with previous results reported in the range from 298 to 318 K for a similar PEG by Fu et al. [103]. Surface tension decreased with increasing temperature. In the studied temperature range, reductions of ~0.21–0.22% each 10 K were observed for base fluid and formulated NePCMs. This downward trend with increasing temperature can be described by using a first-order polynomial fitting with *ADDs*% lower than 0.25%. Lower surface tensions were also measured for formulated NePCMs when compared with neat PEG400 (see Figure 13b). These diminutions, that reach 2.2% for the Ag(1.1 wt%)/PEG400 sample, can be attributed to the presence of PVP surfactant used to stabilize silver nanoparticles (PVP:Ag ratio of 0.068) or other reagents remaining in the parent NePCM from the formulation process. Surfactants are surface active molecules that improve suspension stability by recovering nanoparticles and modifying particle–surface interaction forces. Surfactant molecules also place at the air–sample surface, which in turn, reduces nanofluid surface tension.

4. Conclusions

Three dispersions of PVP-capped silver nanoparticles in a poly(ethylene glycol) PEG400 at nanoparticle mass concentrations from 0.10% to 1.1% were specifically synthesized for this study. Such nanofluids were characterized for the purpose of being used as potential nano-enhanced phase change materials. The poly(ethylene glycol) utilized as base fluid was an almost monodisperse polymer with an average mass molar mass of 533 g·mol^{-1}. Dry silver nanoparticles exhibited a quasi-spherical morphology with an average diameter of ~22 nm. Once suspended in PEG400, nanoparticles showed DLS hydrodynamic diameters of ~50 nm, a value that remained constant over time indicating that no significant sedimentation or agglomeration occurred in the dispersion. The dispersion of PVP-capped silver nanoparticles improved the thermal conductivity of nanofluids, maximum enhancements reaching 3.9% for the Ag(1.1 wt%)/PEG400 sample. Calorimetry analyses showed that the addition of silver nanoparticles slightly reduced undesirable sub-cooling phenomena, in which a maximum improvement of 7.1% was found for the highest nanoparticle loading. Also at 1.1 wt% silver content, modifications in isobaric heat capacity, density, and surface tension were 0.9%, 2.2% and 2.2%, respectively. Studied NePCMs showed a Newtonian behavior with average increases ranging from 1.4% to 5.4%, in comparison to neat poly(ethylene glycol). Obtained improvements in the sub-cooling phenomenon and thermal conductivity evidence the potential that nanoparticle addition has in the development of phase change materials with enhanced thermal properties. However, more research in the selection of nanoadditives and the design of NePCMs is still necessary so that those materials achieve a competitive edge over conventional thermal storage materials.

Author Contributions: M.A.M., D.C., and S.H. performed experimental measurements and first drafted the manuscript. S.B. and P.E. took an active role in the interpretation of the results. L.F. and L.L. conceived the study, planned the experiments and revised the manuscript. All authors have read and agreed to the published version of the manuscript.

Funding: This work was supported by the Ministerio de Economía y Competitividad (Spain) and FEDER program through ENE2014–55489–C2–2–R and ENE2017–86425–C2–1–R projects. Authors also acknowledge the financial support by Xunta de Galicia, GRC ED431C 2016–034. This work was partially supported by EU COST Action CA15119: Overcoming Barriers to Nanofluids Market Uptake (NANOUPTAKE) in the framework of the Short Term Scientific Mission program COST-STSM-CA15119–41564 and COST-STSM-CA15119–42472. P.E. acknowledges the European Union through the European Regional Development Fund (ERDF), the Ministry of Higher Education and Research, the French region of Brittany and Rennes Métropole for the financial support of surface tension experimental device. D.C. thanks Xunta de Galicia for a postdoctoral fellowship.

Acknowledgments: Authors acknowledge Ana Cabrerizo and CACTI (Univ. de Vigo) for technical assistance.

Conflicts of Interest: The authors declare no conflict of interest.

References

1. Xu, Y.; Ren, Q.; Zheng, Z.-J.; He, Y.-L. Evaluation and optimization of melting performance for a latent heat thermal energy storage unit partially filled with porous media. *Appl. Energy* **2017**, *193*, 84–95. [CrossRef]
2. de Gracia, A.; Cabeza, L.F. Phase change materials and thermal energy storage for buildings. *Energy Build.* **2015**, *103*, 414–419. [CrossRef]
3. Sharma, A.; Tyagi, V.V.; Chen, C.; Buddhi, D. Review on thermal energy storage with phase change materials and applications. *Renew. Sust. Energy Rev.* **2009**, *13*, 318–345. [CrossRef]
4. Colla, L.; Ercole, D.; Fedele, L.; Mancin, S.; Manca, O.; Bobbo, S. Nano-phase change materials for electronics cooling applications. *J. Heat Transf.* **2017**, *139*, 052406. [CrossRef]
5. Pandey, A.K.; Hossain, M.S.; Tyagi, V.V.; Abd Rahim, N.; Selvaraj, J.A.L.; Sari, A. Novel approaches and recent developments on potential applications of phase change materials in solar energy. *Renew. Sustain. Energy Rev.* **2018**, *82*, 281–323. [CrossRef]
6. Oró, E.; Miró, L.; Farid, M.M.; Cabeza, L.F. Thermal analysis of a low temperature storage unit using phase change materials without refrigeration system. *Int. J. Refrig.* **2012**, *35*, 1709–1714. [CrossRef]
7. Oró, E.; Miró, L.; Farid, M.M.; Cabeza, L.F. Improving thermal performance of freezers using phase change materials. *Int. J. Refrig.* **2012**, *35*, 984–991. [CrossRef]

8. Veerakumar, C.; Sreekumar, A. Phase change material based cold thermal energy storage: Materials, techniques and applications–a review. *Int. J. Refrig.* **2016**, *67*, 271–289. [CrossRef]
9. Yusufoglu, Y.; Apaydin, T.; Yilmaz, S.; Paksoy, H.O. Improving performance of household refrigerators by incorporating phase change materials. *Int. J. Refrig.* **2015**, *57*, 173–185. [CrossRef]
10. Sarbu, I.; Sebarchievici, C. *Solar Heating and Cooling Systems: Fundamentals, Experiments and Applications*; Academic Press.: London, UK, 2016.
11. Qian, T.; Li, J.; Ma, H.; Yang, J. Adjustable thermal property of polyethylene glycol/diatomite shape-stabilized composite phase change material. *Polym. Compos.* **2016**, *37*, 854–860. [CrossRef]
12. Pielichowska, K.; Pielichowski, K. Phase change materials for thermal energy storage. *Prog. Mater. Sci.* **2014**, *65*, 67–123. [CrossRef]
13. Pielichowski, K.; Flejtuch, K. Differential scanning calorimetry studies on poly (ethylene glycol) with different molecular weights for thermal energy storage materials. *Polym. Advan. Technol.* **2002**, *13*, 690–696. [CrossRef]
14. Cabeza, L.F.; Castell, A.; Barreneche, C.; de Gracia, A.; Fernández, A.I. Materials used as PCM in thermal energy storage in buildings: A review. *Renew. Sustain. Energy Rev.* **2011**, *15*, 1675–1695. [CrossRef]
15. Babapoor, A.; Karimi, G.; Khorram, M. Fabrication and characterization of nanofiber-nanoparticle-composites with phase change materials by electrospinning. *Appl. Therm. Eng.* **2016**, *99*, 1225–1235. [CrossRef]
16. Khodadadi, J.; Hosseinizadeh, S. Nanoparticle-enhanced phase change materials (NePCM) with great potential for improved thermal energy storage. *Int. Commun. Heat Mass* **2007**, *34*, 534–543. [CrossRef]
17. Nazir, H.; Batool, M.; Bolivar Osorio, F.J.; Isaza-Ruiz, M.; Xu, X.; Vignarooban, K.; Phelan, P.; Inamuddin; Kannan, A.M. Recent developments in phase change materials for energy storage applications: A review. *Int. J. Heat Mass Tran.* **2019**, *129*, 491–523. [CrossRef]
18. Zhao, C.Y.; Lu, W.; Tian, Y. Heat transfer enhancement for thermal energy storage using metal foams embedded within phase change materials (PCMs). *Sol. Energy* **2010**, *84*, 1402–1412. [CrossRef]
19. Liu, Y.; Li, X.; Hu, P.; Hu, G. Study on the supercooling degree and nucleation behavior of water-based graphene oxide nanofluids pcm. *Int. J. Refrig.* **2015**, *50*, 80–86. [CrossRef]
20. Pisello, A.L.; Paolini, R.; Diamanti, M.V.; Fortunati, E.; Castaldo, V.L.; Torre, L. Nanotech-based cool materials for building energy efficiency. In *Nano and Biotech Based Materials for Energy Building Efficiency*; Springer: Berlin/Heidelberg, Germany, 2016; pp. 245–278.
21. Shamshirgaran, S.R.; Khalaji, A.M.; Viswanatha, S.K. Application of nanomaterials in solar thermal energy storage. *Heat Mass Transf.* **2018**, *54*, 1555–1577. [CrossRef]
22. Murshed, S.S.; Estellé, P. A state of the art review on viscosity of nanofluids. *Renew. Sust. Energy Rev.* **2017**, *76*, 1134–1152. [CrossRef]
23. Vallejo, J.P.; Żyła, G.; Fernández-Seara, J.; Lugo, L. Rheological behaviour of functionalized graphene nanoplatelet nanofluids based on water and propylene glycol:water mixtures. *Int. Commun. Heat Mass* **2018**, *99*, 43–53. [CrossRef]
24. Żyła, G.; Fal, J.; Estellé, P. Thermophysical and dielectric profiles of ethylene glycol based titanium nitride (TiN–EG) nanofluids with various size of particles. *Int. J. Heat Mass Tran.* **2017**, *113*, 1189–1199. [CrossRef]
25. Żyła, G.; Vallejo, J.P.; Lugo, L. Isobaric heat capacity and density of ethylene glycol based nanofluids containing various nitride nanoparticle types: An experimental study. *J. Mol. Liq.* **2018**, *261*, 530–539. [CrossRef]
26. Cabaleiro, D.; Gracia-Fernández, C.; Legido, J.; Lugo, L. Specific heat of metal oxide nanofluids at high concentrations for heat transfer. *Int. J. Heat Mass Tran.* **2015**, *88*, 872–879. [CrossRef]
27. Estellé, P.; Cabaleiro, D.; Żyła, G.; Lugo, L.; Murshed, S.S. Current trends in surface tension and wetting behavior of nanofluids. *Renew. Sustain. Energy Rev.* **2018**, *94*, 931–944. [CrossRef]
28. Savino, R.; Di Paola, R.; Cecere, A.; Fortezza, R. Self-rewetting heat transfer fluids and nanobrines for space heat pipes. *Acta Astronaut.* **2010**, *67*, 1030–1037. [CrossRef]
29. Singh, R.; Sadeghi, S.; Shabani, B. Thermal conductivity enhancement of phase change materials for low-temperature thermal energy storage applications. *Energies* **2019**, *12*, 75. [CrossRef]
30. Marcos, M.; Cabaleiro, D.; Guimarey, M.; Comuñas, M.; Fedele, L.; Fernández, J.; Lugo, L. PEG400-based phase change materials nano-enhanced with functionalized graphene nanoplatelets. *Nanomaterials* **2017**, *8*, 16. [CrossRef]

31. Yang, J.; Tang, L.-S.; Bao, R.-Y.; Bai, L.; Liu, Z.-Y.; Yang, W.; Xie, B.-H.; Yang, M.-B. Largely enhanced thermal conductivity of poly (ethylene glycol)/boron nitride composite phase change materials for solar-thermal-electric energy conversion and storage with very low content of graphene nanoplatelets. *Chem. Eng. J.* **2017**, *315*, 481–490. [CrossRef]
32. Marcos, M.A.; Podolsky, N.E.; Cabaleiro, D.; Lugo, L.; Zakharov, A.O.; Postnov, V.N.; Charykov, N.A.; Ageev, S.V.; Semenov, K.N. MWCNT in PEG-400 nanofluids for thermal applications: A chemical, physical and thermal approach. *J. Mol. Liq.* **2019**, *294*, 111616. [CrossRef]
33. Anghel, E.M.; Pavel, P.M.; Constantinescu, M.; Petrescu, S.; Atkinson, I.; Buixaderas, E. Thermal transfer performance of a spherical encapsulated PEG6000-based composite for thermal energy storage. *Appl. Energy* **2017**, *208*, 1222–1231. [CrossRef]
34. Tang, B.; Cui, J.; Wang, Y.; Jia, C.; Zhang, S. Facile synthesis and performances of PEG/SiO_2 composite form-stable phase change materials. *Sol. Energy* **2013**, *97*, 484–492. [CrossRef]
35. Tang, B.; Qiu, M.; Zhang, S. Thermal conductivity enhancement of PEG/SiO_2 composite PCM by in situ Cu doping. *Sol. Energy Mat. Sol. Cells* **2012**, *105*, 242–248. [CrossRef]
36. Tang, B.; Wu, C.; Qiu, M.; Zhang, X.; Zhang, S. PEG/SiO_2–Al_2O_3 hybrid form-stable phase change materials with enhanced thermal conductivity. *Mater. Chem. Phys.* **2014**, *144*, 162–167. [CrossRef]
37. Feng, L.; Zheng, J.; Yang, H.; Guo, Y.; Li, W.; Li, X. Preparation and characterization of polyethylene glycol/active carbon composites as shape-stabilized phase change materials. *Sol. Energy Mat. Sol. Cells* **2011**, *95*, 644–650. [CrossRef]
38. Yang, H.; Feng, L.; Wang, C.; Zhao, W.; Li, X. Confinement effect of SiO_2 framework on phase change of peg in shape-stabilized PEG/SiO_2 composites. *Eur. Polym. J.* **2012**, *48*, 803–810. [CrossRef]
39. Li, J.; He, L.; Liu, T.; Cao, X.; Zhu, H. Preparation and characterization of PEG/SiO_2 composites as shape-stabilized phase change materials for thermal energy storage. *Sol. Energy Mat. Sol. Cells* **2013**, *118*, 48–53. [CrossRef]
40. Tang, B.; Wang, Y.; Qiu, M.; Zhang, S. A full-band sunlight-driven carbon nanotube/PEG/SiO_2 composites for solar energy storage. *Sol. Energy Mat. Sol. Cells* **2014**, *123*, 7–12. [CrossRef]
41. Liu, Z.; Wei, H.; Tang, B.; Xu, S.; Shufen, Z. Novel light–driven CF/PEG/SiO_2 composite phase change materials with high thermal conductivity. *Sol. Energy Mat. Sol. Cells* **2018**, *174*, 538–544. [CrossRef]
42. Li, X.F.; Zhu, D.S.; Wang, X.J.; Wang, N.; Gao, J.W.; Li, H. Thermal conductivity enhancement dependent ph and chemical surfactant for Cu-H_2O nanofluids. *Thermochim. Acta* **2008**, *469*, 98–103. [CrossRef]
43. Patel, H.E.; Das, S.K.; Sundararajan, T.; Sreekumaran, N.A.; George, B.; Pradeep, T. Thermal conductivities of naked and monolayer protected metal nanoparticle based nanofluids: Manifestation of anomalous enhancement and chemical effects. *Appl. Phys. Lett.* **2003**, *83*, 2931–2933. [CrossRef]
44. Yu, W.; Xie, H.; Chen, L.; Li, Y. Investigation on the thermal transport properties of ethylene glycol-based nanofluids containing copper nanoparticles. *Powder Technol.* **2010**, *197*, 218–221. [CrossRef]
45. Zeng, J.L.; Sun, L.X.; Xu, F.; Tan, Z.C.; Zhang, Z.H.; Zhang, J.; Zhang, T. Study of a PCM based energy storage system containing Ag nanoparticles. *J. Therm. Anal. Calorim.* **2007**, *87*, 371–375. [CrossRef]
46. Deng, Y.; Li, J.; Qian, T.; Guan, W.; Li, Y.; Yin, X. Thermal conductivity enhancement of polyethylene glycol/expanded vermiculite shape-stabilized composite phase change materials with silver nanowire for thermal energy storage. *Chem. Eng. J.* **2016**, *295*, 427–435. [CrossRef]
47. Qian, T.; Li, J.; Min, X.; Guan, W.; Deng, Y.; Ning, L. Enhanced thermal conductivity of PEG/diatomite shape-stabilized phase change materials with Ag nanoparticles for thermal energy storage. *J. Mater. Chem. A* **2015**, *3*, 8526–8536. [CrossRef]
48. Chen, R.-H.; Phuoc, T.X.; Martello, D. Surface tension of evaporating nanofluid droplets. *Int. J. Heat Mass Tran.* **2011**, *54*, 2459–2466. [CrossRef]
49. Godson, L.; Raja, B.; Lal, D.M.; Wongwises, S. Experimental investigation on the thermal conductivity and viscosity of silver-deionized water nanofluid. *Exp. Heat Transf* **2010**, *23*, 317–332. [CrossRef]
50. Lee, H.-H.; Chou, K.-S.; Huang, K.-C. Inkjet printing of nanosized silver colloids. *Nanotechnology* **2005**, *16*, 2436. [CrossRef]
51. Ankireddy, K.; Vunnam, S.; Kellar, J.; Cross, W. Highly conductive short chain carboxylic acid encapsulated silver nanoparticle based inks for direct write technology applications. *J. Mater. Chem. C* **2013**, *1*, 572–579. [CrossRef]

52. Parker, W.; Jenkins, R.; Butler, C.; Abbott, G. Flash method of determining thermal diffusivity, heat capacity, and thermal conductivity. *J. Appl. Phys.* **1961**, *32*, 1679–1684. [CrossRef]
53. Mourdikoudis, S.; Pallares, R.M.; Thanh, N.T.K. Characterization techniques for nanoparticles: Comparison and complementarity upon studying nanoparticle properties. *Nanoscale* **2018**, *10*, 12871–12934. [CrossRef] [PubMed]
54. Ghaseminezhad, S.M.; Hamedi, S.; Shojaosadati, S.A. Green synthesis of silver nanoparticles by a novel method: Comparative study of their properties. *Carbohydr. Polym.* **2012**, *89*, 467–472. [CrossRef] [PubMed]
55. Huang, N.; Lim, H.; Radiman, S.; Khiew, P.; Chiu, W.; Hashim, R.; Chia, C.H. Sucrose ester micellar-mediated synthesis of Ag nanoparticles and the antibacterial properties. *Colloids Surf. A Physicochem. Eng. Asp.* **2010**, *353*, 69–76. [CrossRef]
56. Tomaszewska, E.; Soliwoda, K.; Kadziola, K.; Tkacz-Szczesna, B.; Celichowski, G.; Cichomski, M.; Szmaja, W.; Grobelny, J. Detection limits of dls and UV-Vis spectroscopy in characterization of polydisperse nanoparticles colloids. *J. Nanomater.* **2013**, *2013*, 10. [CrossRef]
57. Vigneshwaran, N.; Nachane, R.P.; Balasubramanya, R.H.; Varadarajan, P.V. A novel one-pot 'green' synthesis of stable silver nanoparticles using soluble starch. *Carbohyd. Res.* **2006**, *341*, 2012–2018. [CrossRef]
58. Ottani, S.; Vitalini, D.; Comelli, F.; Castellari, C. Densities, viscosities, and refractive indices of poly(ethylene glycol) 200 and 400 + cyclic ethers at 303.15 k. *J. Chem. Eng. Data* **2002**, *47*, 1197–1204. [CrossRef]
59. Ottani, S.; Vitalini, D.; Comelli, F.; Castellari, C. Densities, viscosities, and refractive indices of new mixtures of poly(ethylene glycols) + dialkyl carbonates at 313.15 k. *J. Chem. Eng. Data* **2004**, *49*, 148–154. [CrossRef]
60. Fedele, L.; Colla, L.; Bobbo, S. Viscosity and thermal conductivity measurements of water-based nanofluids containing titanium oxide nanoparticles. *Int. J. Refrig.* **2012**, *35*, 1359–1366. [CrossRef]
61. Colla, L.; Fedele, L.; Buschmann, M.H. Laminar mixed convection of TiO_2–water nanofluid in horizontal uniformly heated pipe flow. *Int. J. Therm. Sci.* **2015**, *97*, 26–40. [CrossRef]
62. Fedele, L.; Colla, L.; Bobbo, S.; Barison, S.; Agresti, F. Experimental stability analysis of different water-based nanofluids. *Nanoscale Res. Lett.* **2011**, *6*, 300. [CrossRef]
63. Cabaleiro, D.; Gracia-Fernández, C.; Lugo, L. (solid+liquid) phase equilibria and heat capacity of (diphenyl ether+biphenyl) mixtures used as thermal energy storage materials. *J. Chem. Thermodyn.* **2014**, *74*, 43–50. [CrossRef]
64. Rodríguez-Pérez, M.; Reglero, J.; Lehmhus, D.; Wichmann, M.; De Saja, J.; Fernández, A. The Transient Plane Source Technique (TPS) to Measure Thermal Conductivity and its Potential as A Tool to Detect In-Homogeneities in Metal Foams. In Proceedings of the International Conference "Advanced Metallic Materials", Smolenice, Slovakia, 5–7 November 2003; pp. 253–257.
65. Lemmon, E.; Huber, M.; McLinden, M. *NIST Standard Reference Database 23, Reference Fluid Thermodynamic and Transport Properties (Refprop)*, version 9.0; National Institute of Standards and Technology: Gaithersburg, MD, USA, 2010.
66. Bobbo, S.; Fedele, L.; Benetti, A.; Colla, L.; Fabrizio, M.; Pagura, C.; Barison, S. Viscosity of water based SWCNH and TiO_2 nanofluids. *Exp. Therm. Fluid Sci.* **2012**, *36*, 65–71. [CrossRef]
67. Żyła, G.; Vallejo, J.P.; Fal, J.; Lugo, L. Nanodiamonds—Ethylene glycol nanofluids: Experimental investigation of fundamental physical properties. *Int. J. Heat Mass Tran.* **2018**, *121*, 1201–1213. [CrossRef]
68. Berrada, N.; Hamze, S.; Desforges, A.; Ghanbaja, J.; Gleize, J.; Mare, T.; Vigolo, B.; Estellé, P. Surface tension of functionalized mwcnt-based nanofluids in water and commercial propylene-glycol mixture. *J. Mol. Liq.* **2019**, *293*, 111473. [CrossRef]
69. Gómez-Villarejo, R.; Aguilar, T.; Hamze, S.; Estellé, P.; Navas, J. Experimental analysis of water-based nanofluids using boron nitride nanotubes with improved thermal properties. *J. Mol. Liq.* **2019**, *277*, 93–103. [CrossRef]
70. Francesconi, R.; Bigi, A.; Rubini, K.; Comelli, F. Molar heat capacities, densities, viscosities, and refractive indices of poly (ethylene glycols)+ 2-methyltetrahydrofuran at (293.15, 303.15, and 313.15) K. *J. Chem. Eng. Data* **2007**, *52*, 2020–2025. [CrossRef]
71. Touloukian, Y.; Buyco, E. Specific heat-metallic elements and alloys. In *Thermophysical Properties of Matter*; The TPRC Data Series: West Lafayette, IN, USA, 1971; Volume 4.
72. Zhou, S.-Q.; Ni, R. Measurement of the specific heat capacity of water-based Al_2O_3 nanofluid. *Appl. Phys. Lett.* **2008**, *92*, 093123. [CrossRef]

73. O'Hanley, H.; Buongiorno, J.; McKrell, T.; Hu, L.-W. Measurement and model validation of nanofluid specific heat capacity with differential scanning calorimetry. *Adv. Mech. Eng.* **2012**, *4*, 181079. [CrossRef]
74. Maxwell, J.C. *A Treatise on Electricity and Magnetism*; Clarendon Press: Oxford, UK, 1873; Volume 1.
75. Azmi, W.H.; Sharma, K.V.; Mamat, R.; Najafi, G.; Mohamad, M.S. The enhancement of effective thermal conductivity and effective dynamic viscosity of nanofluids—A review. *Renew. Sust. Energy Rev.* **2016**, *53*, 1046–1058. [CrossRef]
76. Beck, M.P.; Yuan, Y.; Warrier, P.; Teja, A.S. The effect of particle size on the thermal conductivity of alumina nanofluids. *J. Nanopart. Res.* **2009**, *11*, 1129–1136. [CrossRef]
77. Timofeeva, E.V.; Gavrilov, A.N.; McCloskey, J.M.; Tolmachev, Y.V.; Sprunt, S.; Lopatina, L.M.; Selinger, J.V. Thermal conductivity and particle agglomeration in alumina nanofluids: Experiment and theory. *Phys. Rev. E* **2007**, *76*, 061203. [CrossRef]
78. Frank, M.; Drikakis, D. Solid-like heat transfer in confined liquids. *Microfluid Nanofluidics* **2017**, *21*, 148. [CrossRef] [PubMed]
79. Frank, M.; Drikakis, D.; Asproulis, N. Thermal conductivity of nanofluid in nanochannels. *Microfluid. Nanofluidics* **2015**, *19*, 1011–1017. [CrossRef]
80. Murshed, S.; Leong, K.; Yang, C. Investigations of thermal conductivity and viscosity of nanofluids. *Int. J. Therm. Sci.* **2008**, *47*, 560–568. [CrossRef]
81. Frank, M.; Drikakis, D. Thermodynamics at solid–liquid interfaces. *Entropy* **2018**, *20*, 362. [CrossRef]
82. Halté, V.; Bigot, J.-Y.; Palpant, B.; Broyer, M.; Prével, B.; Pérez, A. Size dependence of the energy relaxation in silver nanoparticles embedded in dielectric matrices. *Appl. Phys. Lett.* **1999**, *75*, 3799–3801. [CrossRef]
83. Özerinç, S.; Kakaç, S.; Yazıcıoğlu, A.G. Enhanced thermal conductivity of nanofluids: A state-of-the-art review. *Microfluid. Nanofluid.* **2010**, *8*, 145–170. [CrossRef]
84. Warrier, P.; Teja, A. Effect of particle size on the thermal conductivity of nanofluids containing metallic nanoparticles. *Nanoscale Res. Lett.* **2011**, *6*, 247. [CrossRef]
85. Nath, P.; Chopra, K.L. Thermal conductivity of copper films. *Thin Solid Film.* **1974**, *20*, 53–62. [CrossRef]
86. Trivedi, S.; Bhanot, C.; Pandey, S. Densities of {poly(ethylene glycol)+water} over the temperature range (283.15 to 363.15) K. *J. Chem. Thermodyn.* **2010**, *42*, 1367–1371. [CrossRef]
87. Afzal, W.; Mohammadi, A.H.; Richon, D. Volumetric properties of mono-, di-, tri-, and polyethylene glycol aqueous solutions from (273.15 to 363.15) K: Experimental measurements and correlations. *J. Chem. Eng. Data* **2009**, *54*, 1254–1261. [CrossRef]
88. Han, F.; Zhang, J.; Chen, G.; Wei, X. Density, viscosity, and excess properties for aqueous poly(ethylene glycol) solutions from (298.15 to 323.15) k. *J. Chem. Eng. Data* **2008**, *53*, 2598–2601. [CrossRef]
89. Nakhjavani, M.; Nikkhah, V.; Sarafraz, M.M.; Shoja, S.; Sarafraz, M. Green synthesis of silver nanoparticles using green tea leaves: Experimental study on the morphological, rheological and antibacterial behaviour. *Heat Mass Transf.* **2017**, *53*, 3201–3209. [CrossRef]
90. Bahiraei, M.; Heshmatian, S. Efficacy of a novel liquid block working with a nanofluid containing graphene nanoplatelets decorated with silver nanoparticles compared with conventional CPU coolers. *Appl. Therm. Eng.* **2017**, *127*, 1233–1245. [CrossRef]
91. Yarmand, H.; Gharehkhani, S.; Ahmadi, G.; Shirazi, S.F.S.; Baradaran, S.; Montazer, E.; Zubir, M.N.M.; Alehashem, M.S.; Kazi, S.; Dahari, M. Graphene nanoplatelets–silver hybrid nanofluids for enhanced heat transfer. *Energy Convers. Manag.* **2015**, *100*, 419–428. [CrossRef]
92. Nguyen, T.T.T.; Park, J.S. Fabrication of electrospun nonwoven mats of polyvinylidene fluoride/polyethylene glycol/fumed silica for use as energy storage materials. *J. Appl. Polym. Sci.* **2011**, *121*, 3596–3603. [CrossRef]
93. Chen, H.; Ding, Y.; Tan, C. Rheological behaviour of nanofluids. *New J. Phys.* **2007**, *9*, 367. [CrossRef]
94. Tamjid, E.; Guenther, B.H. Rheology and colloidal structure of silver nanoparticles dispersed in diethylene glycol. *Powder Technol.* **2010**, *197*, 49–53. [CrossRef]
95. Angell, C.; MacFarlane, D.; Oguni, M. The kauzmann paradox, metastable liquids, and ideal glasses. *Ann. N. Y. Acad. Sci* **1986**, *484*, 241–247. [CrossRef]
96. Paredes, X.; Pensado, A.S.; Comuñas, M.a.J.; Fernández, J. How pressure affects the dynamic viscosities of two poly (propylene glycol) dimethyl ether lubricants. *J. Chem. Eng. Data* **2010**, *55*, 4088–4094. [CrossRef]
97. Siongco, K.R.; Leron, R.B.; Li, M.-H. Densities, refractive indices, and viscosities of n,n-diethylethanol ammonium chloride–glycerol or –ethylene glycol deep eutectic solvents and their aqueous solutions. *J. Chem. Thermodyn.* **2013**, *65*, 65–72. [CrossRef]

98. Hodge, I.M. Strong and fragile liquids—A brief critique. *J. Non-Cryst. Solids* **1996**, *202*, 164–172. [CrossRef]
99. Zadeh, A.D.; Toghraie, D. Experimental investigation for developing a new model for the dynamic viscosity of silver/ethylene glycol nanofluid at different temperatures and solid volume fractions. *J. Therm. Anal. Calorim.* **2018**, *131*, 1449–1461. [CrossRef]
100. Einstein, A. Eine neue bestimmung der moleküldimensionen. *Ann. Phys.* **1906**, *324*, 289–306. [CrossRef]
101. Chow, T. Viscosities of concentrated dispersions. *Phys. Rev. E* **1993**, *48*, 1977. [CrossRef]
102. Pal, R.; Rhodes, E. Viscosity/concentration relationships for emulsions. *J. Rheol.* **1989**, *33*, 1021–1045. [CrossRef]
103. Fu, D.; Du, L.; Wang, H. Experiment and model for the surface tension of MEA-PEG400 and DEA-PEG400 aqueous solutions. *J. Chem. Thermodyn.* **2014**, *69*, 132–136. [CrossRef]

Chapter 4

Conclusions

4 Conclusions

This PhD Thesis has been done within the framework of two national research projects (ENE2014-55489-C2-1/2-R and ENE2017-86425-C2-1/2-R). Moreover, different training activities and scientific stays in other European research centres were carried out within the European COST Action Nanouptake – Overcoming Barriers to Nanofluids Market Uptake (COST Action CA15119). This PhD Thesis has been focused on the design and characterization of advanced phase change materials based on poly(ethylene glycol)s with molecular masses between 200 and 400 $g \cdot mol^{-1}$, to be proposed as potential cold storage media in renewable energy applications. The main conclusions are summarized as follows:

- Design of new stable NePCM by dispersing high thermal conductivity nanoparticles in poly(ethylene glycol)s of different molecular masses.

Four nanoadditives (*viz.* two different multi-walled carbon nanotubes, c-MWCNT and s-MWCNT, one commercial and the other synthesized in the framework of this Thesis, functionalized graphene nanoplatelets, fGnP, and polyvinylpyrrolidone-capped silver nanoparticles, PVP-Ag), and several poly(ethylene glycol)s of different molecular masses (200, 300 and 400 $g \cdot mol^{-1}$) were selected to design five different sets of nano-enhanced phase change materials (NePCMs).

Poly(ethylene glycol)s were characterized by electrospray ionization mass spectrometry (ESI-MS) to obtain the molecular mass and purity of base fluid. ESI-MS results proved the high purity of the polymers and showed polydispersity indexes close to 1. The morphology and the size of the different nanoadditives were investigated by using Transmission Electron Microscopy (TEM) and/or Scanning Electron Microscopy (SEM). Microscopy analyses revealed that MWCNTs showed a filament-like morphology with mean diameters of 7 ±3 nm and between 20-50 nm for the synthetized and commercial nanotubes, respectively. Graphene nanoplatelets presented a laminar morphology with thickness of around 30 nm. PVP-silver nanoparticles exhibited a quasi-spherical morphology with diameters in the range of 20-30 nm. The characterization of the nanoparticles was completed with Energy-Dispersive X-Ray Spectroscopy (EDS) and Raman studies.

The temporal stability of designed NePCMs was assessed from the evolution with time of hydrodynamic nanoparticle-sizes measured by dynamic light scattering (DLS). These determinations were periodically repeated along some weeks for samples under both shaken and static conditions in order to investigate sample stability in flow and storage

conditions. Finally, the thermal stabilities of neat poly(ethylene glycol)s and designed dispersions were also analysed by Thermogravimetric Analysis (TGA).

- Determination of solid-liquid phase change characteristics of the new designed NePCMs, investigating the effect of nanoparticle dispersion on latent heat and sub-cooling phenomenon.

Phase change transitions were investigated at different cooling and heating rates by means of differential scanning calorimetry (DSC) analyses. Melting and solidifying points were determined for the base fluids and NePCMs prepared at several nanoparticle mass concentrations. The dispersion of the nanoparticles slightly modified the fusion and crystallization temperatures of the poly(ethylene glycol)s used as based materials. Thus, shifts in melting transition towards lower temperatures of up to 2.5 K were observed in the case of fGnP(0.5 wt.%)/PEG400. In addition, a reduction in the undesirable sub-cooling effect of up to 7.1% was also achieved for the PEG400-based sample loaded with a PVP-Ag loading of 1.1 wt.%. Slight modifications in latent heat capacity were also observed for the different dispersions, with reductions lower than 3% for all analysed samples. The good accuracy of reported results was ensured by the repetition of DSC analyses. Some representative samples were also subject to cycling tests (50-100 heat-cooling processes) to confirm that no significant reduction in latent heat capacity or important modification in melting/crystallization temperatures occur and, therefore, validate the thermal reliability of the samples.

- The differences in thermal conductivity between new NePCMs and fluids were experimentally studied.

The behaviour of thermal conductivity (k) was experimentally investigated in a wide range of temperatures and at different nanoparticle concentrations. Experimental results showed that this property increased with rising nanoparticle concentration. The best thermal conductivity enhancements were obtained in the case carbon-based NePCMs. Special mention requires the 0.50% fGnP/PEG 400 sample with a thermal conductivity increase of 23% when compared with base fluid at the same conditions. These results are considerably higher than the increases of 12.7% and 3.1% obtained for s-MWCNT(1.0 wt.%)/PEG400 and PVP-Ag(1.1 wt%)/PEG400 samples, respectively.

- The rheological behaviour and dynamic viscosity of base fluid and new designed nanofluids were measured.

Dynamic viscosity studies as a function of temperature and/or shear rate were performed for base fluids and different designed nanofluids, namely 0.05-0.50 wt.% dispersions of fGnP/PEG400, 0.1-1.1wt.% contents of PVP-Ag/PEG400, 0.01-1.0 wt.% concentrations of s-MWCNT/PEG400 and 0.025-0.70 wt.% loadings of both c-MWCNT/PEG200 and c-MWCNT/PEG300 nanofluids. As expected, in all systems dynamic viscosity decreased with rising temperature and increased with rising nanoparticle loading. Maximum modifications (with respect to base fluid) in this property were 23%, 5.4% and 29.6% for dispersions of fGnP (0.5 wt.%), PVP-Ag (1.1 wt.%) and s-MWCNT (1.0 wt.%) in PEG400, respectively. The dispersion of commercial MWCNT in PEG200 and PEG300 leaded to increases in dynamic viscosity of 102% and 71%, respectively. Flow curves obtained for PVP-Ag/PEG400 nanofluids in the temperature range from 278 to 343 K showed a linear relationship between shear stress and shear rate, proving the Newtonian behaviour of those nano-enhanced phase change materials. In the case of s-MWCNT/PEG400, a shear-thinning behaviour (more pronounced with rising nanoparticle loading) was detected for dispersions prepared with concentration higher than 0.01 wt.%. In contrast, all investigated c-MWCNT/PEG200 and c-MWCNT/PEG300 nanofluids showed a non-Newtonian pseudoplastic behavior in the low shear rate region, that was even detected for those dispersions with the lowest concentrations of nanoparticles (0.025 wt.% of c-MWCNTs).

- The isobaric heat capacities and densities of base fluid and proposed nanofluids were analyzed.

The influence of temperature and nanoparticle concentration on the isobaric heat capacities (C_p) and densities (ρ) were carried out by means of a differential scanning calorimeter working with the quasi-isothermal temperature-modulated differential scanning calorimetry method and an oscillating U-tube densimeter, respectively. Results showed a slight reduction in the isobaric heat capacity with the increasing nanoparticle content in the dispersion. The minimum decrease was detected for the PVP-Ag(1.1% wt.)/PEG400 dispersion, for which C_p values were ~0.9% lower than those values for the base fluid. Instead, a maximum decrease of 3% (regarding the base fluid) was obtained for PEG400-based nanofluid prepared at a s-MWCNT concentration of 1 wt%. As expected, density decreased with rising temperature, and increased with the concentration of dispersed nanoparticles. The highest enhancements in this property were measured for the PVP-Ag/PEG400 dispersions, for which a maximum enhancement in density of 2.2% was obtained at the silver content of 1.1 wt%.

- Some theoretical or semi-empirical approaches were employed in order to compare/validate the experimental results for the new designed nanofluids regarding the different thermophysical properties.

Viscosity and thermal conductivity results experimentally obtained for base fluids and NePCMs were compared with some predictive models or described by fitting equations. Nan equation was used to correlate experimental thermal conductivities of fGnP/PEG set. A good agreement (with an *AAD%* of 1%) was obtained between experimental and fitted data when using a value of k_{np} = 20 $W \cdot m^{-1} \cdot K^{-1}$ as in-plane thermal conductivity of the graphene. Regarding s-MWCNT/PEG400 system, three different *k* models were considered and the average absolute deviations between experimental and predicted results were 2.6% (Xue), 5.5% (Murshed) and 5.6% (Hamilton-Crosser). The evolution of dynamic viscosity with temperature was described by using the Vogel-Fulcher-Tammann equation, with maximum deviations (between experimental and correlated data) ranging from 1.2% to 3.8% for fGnP/PEG400 and c-MWCNT/PEG200, respectively. Relative dynamic viscosity was also described as a function of nanoparticle volume fraction by means of Einstein, Batchelor, Brinkman, Krieger-Dougherty, Maron-Pierce or Brenner-Condiff models. Values provided by Maron-Pierce model were the most consistent with experimental results, with absolute average deviations lower than 5%.

- The thermophysical properties of the new nanofluids were compared with base fluids and other PCMs in the literature.

The results obtained for designed NePCMs were compared with others materials in the literature and with the neat poly(ethylene glycol) based material. In general, important increases in properties such as thermal conductivity have been achieved without too much penalizing other properties such as viscosity. Therefore, the nanofluids studied can be potentially useful as heat transfer materials or storage media for application in domestic or commercial refrigeration systems, for example.

References

References

1. Global energy & CO_2 status report. *IEA (International Energy Agency): Paris, France* **2019**.
2. Frigione, M.; Lettieri, M.; Sarcinella, A. Phase change materials for energy efficiency in buildings and their use in mortars. *Materials* **2019**, *12*, 1260.
3. Randolph, J.; Masters, G.M. Energy sources and sustainability. In *Energy for sustainability. Technology, Planning, Policy*, Springer: Island Press, Washington, DC, **2018**; pp 25-57.
4. Cabeza, L.F. *Advances in thermal energy storage systems: Methods and applications*. Woodhead publishing series in Energy, Elsevier: Cambridge, UK, **2015**.
5. Zhang, X.-P.; Cheng, X.-M. Energy consumption, carbon emissions, and economic growth in china. *Ecological Economics* **2009**, *68*, 2706-2712.
6. Grossman, G.M.; Krueger, A.B. *Environmental impacts of a North American Free Trade Agreement*; 3914; National Bureau of Economic Research: **1991**, 3914.
7. Luzzati, T.; Orsini, M. Investigating the energy-environmental kuznets curve. *Energy* **2009**, *34*, 291-300.
8. Chaudhry, S.M.; Ahmed, R.; Shafiullah, M.; Huynh, T.L.D. The impact of carbon emissions on country risk: Evidence from the G7 economies. *Journal of Environmental Management* **2020**, *265*, 110533.
9. Ozcan, B.; Tzeremes, P.G.; Tzeremes, N.G. Energy consumption, economic growth and environmental degradation in OECD countries. *Economic Modelling* **2020**, *84*, 203-213.
10. Yamamoto, J.; Graham, P. Buildings and climate change, united nations environment programme, sustainable buildings & climate initiative (UNEP, SBCY), Paris, France. **2009**.
11. World energy statistics and balances. *IEA (International Energy Agency): Paris, France* **2019**.
12. Bisegna, F.; Cirrincione, L.; Casto, B.M.L.; Peri, G.; Rizzo, G.; Scaccianoce, G.; Sorrentino, G. In *Fostering the energy efficiency through the energy savings: The case of the university of palermo*, **2019** IEEE International Conference on Environment and Electrical Engineering and 2019 IEEE Industrial and Commercial Power Systems Europe (EEEIC/I&CPS Europe), **2019**; IEEE: pp 1-6.
13. Heun, M.K.; Brockway, P.E. Meeting 2030 primary energy and economic growth goals: Mission impossible? *Applied Energy* **2019**, *251*, 112697.
14. IRENA. Global energy transformation: A roadmap to 2050. IEA (International Renewable Energy Agency), Abu Dhabi: **2018**.
15. Nations, U. Transforming our World: The 2030 agenda for sustainable development. *New York, USA: United Nations, Department of Economic and Social Affairs* **2015**.
16. Masson-Delmotte, V.; Zhai, P.; Pörtner, H.-O.; Roberts, D.; Skea, J.; Shukla, P.R.; Pirani, A.; Moufouma-Okia, W.; Péan, C.; Pidcock, R. Global warming of 1.5 C. *An IPCC Special Report on the impacts of global warming of* **2018**, *1*.
17. Tagliapietra, S.; Zachmann, G.; Edenhofer, O.; Glachant, J.-M.; Linares, P.; Loeschel, A. The european union energy transition: Key priorities for the next five years. *Energy Policy* **2019**, *132*, 950-954.
18. Long-term low greenhouse gas emission development strategy of the eu and its member states. https://ec.europa.eu/clima/policies/strategies/2050_en
19. Proposal for a regulation of the european parliament and of the council establishing the framework for achieving climate neutrality and amending regulation (EU) 2018/1999 (european climate law). https://eur-lex.europa.eu/legal-content/EN/TXT/?qid=1588581905912&uri=CELEX:52020PC0080
20. Pérez-Lombard, L.; Ortiz, J.; Pout, C. A review on buildings energy consumption information. *Energy and buildings* **2008**, *40*, 394-398.
21. Dusonchet, L.; Favuzza, S.; Massaro, F.; Telaretti, E.; Zizzo, G. Technological and legislative status point of stationary energy storages in the EU. *Renewable and Sustainable Energy Reviews* **2019**, *101*, 158-167.

22. Child, M.; Kemfert, C.; Bogdanov, D.; Breyer, C. Flexible electricity generation, grid exchange and storage for the transition to a 100% renewable energy system in Europe. *Renewable Energy* **2019**, *139*, 80-101.
23. Calderón, A.; Barreneche, C.; Hernández-Valle, K.; Galindo, E.; Segarra, M.; Fernández, A.I. Where is thermal energy storage (TES) research going? A bibliometric analysis. *Solar energy* **2020**, *200*, 37-50.
24. Ziskind, G. 12 - Modelling of heat transfer in phase change materials (PCMs) for thermal energy storage systems. In *Advances in thermal energy storage systems*, Cabeza, L.F., Ed. Woodhead Publishing: **2015**; pp 307-324.
25. Pukšec, T.; Markovska, N.; Foley, A.; Duić, N. Addressing the transition to sustainable energy systems: Special issue dedicated to the 2018 conferences on sustainable development of energy, water and environment systems (SDEWES). *Renewable and Sustainable Energy Reviews* **2020**, *119*, 109520.
26. Kim, K.-B.; Choi, K.-W.; Kim, Y.-J.; Lee, K.-H.; Lee, K.-S. Feasibility study on a novel cooling technique using a phase change material in an automotive engine. *Energy* **2010**, *35*, 478-484.
27. Jamekhorshid, A.; Sadrameli, S. Application of phase change materials (PCMs) in maintaining comfort temperature inside an automobile. *World Academy of Science, Engineering and Technology, International Journal of Chemical, Molecular, Nuclear, Materials and Metallurgical Engineering* **2012**, *6*, 33-35.
28. Hussain, A.; Tso, C.Y.; Chao, C.Y.H. Experimental investigation of a passive thermal management system for high-powered lithium ion batteries using nickel foam-paraffin composite. *Energy* **2016**, *115*, 209-218.
29. Moraga, N.O.; Xamán, J.P.; Araya, R.H. Cooling li-ion batteries of racing solar car by using multiple phase change materials. *Applied Thermal Engineering* **2016**, *108*, 1041-1054.
30. Javani, N.; Dincer, I.; Naterer, G.; Rohrauer, G. Modeling of passive thermal management for electric vehicle battery packs with pcm between cells. *Applied Thermal Engineering* **2014**, *73*, 307-316.
31. Javani, N.; Dincer, I.; Naterer, G.; Yilbas, B. Exergy analysis and optimization of a thermal management system with phase change material for hybrid electric vehicles. *Applied Thermal Engineering* **2014**, *64*, 471-482.
32. Rao, Z.; Wang, S.; Zhang, Y. Thermal management with phase change material for a power battery under cold temperatures. *Energy Sources, Part A: Recovery, Utilization, and Environmental Effects* **2014**, *36*, 2287-2295.
33. Cabeza, L.F. Thermal energy storage. *Comprehensive renewable energy* **2012**, *3*, 211-253.
34. Du, K.; Calautit, J.; Wang, Z.; Wu, Y.; Liu, H. A review of the applications of phase change materials in cooling, heating and power generation in different temperature ranges. *Applied Energy* **2018**, *220*, 242-273.
35. Mofijur, M.; Mahlia, T.M.I.; Silitonga, A.S.; Ong, H.C.; Silakhori, M.; Hasan, M.H.; Putra, N.; Rahman, S. Phase change materials (PCM) for solar energy usages and storage: An overview. *Energies* **2019**, *12*, 3167.
36. Pardiñas, Á.Á.; Alonso, M.J.; Diz, R.; Kvalsvik, K.H.; Fernández-Seara, J. State-of-the-art for the use of phase-change materials in tanks coupled with heat pumps. *Energy and buildings* **2017**, *140*, 28-41.
37. Sarbu, I.; Sebarchievici, C. *Solar heating and cooling systems: Fundamentals, experiments and applications*. Academic Press: **2016**.
38. Stark, J.; Swinerd, G. Spacecraft systems engineering. **2011**.
39. Wu, W.-f.; Liu, N.; Cheng, W.-l.; Liu, Y. Study on the effect of shape-stabilized phase change materials on spacecraft thermal control in extreme thermal environment. *Energy Conversion and Management* **2013**, *69*, 174-180.
40. Izenson, M.; Knaus, D.; Cox, J.; Sanders, J. In *Lightweight, durable pcm heat exchanger for spacecraft thermal control*, **2017**; 47th International Conference on Environmental Systems.
41. Kim, T.Y.; Hyun, B.-S.; Lee, J.-J.; Rhee, J. Numerical study of the spacecraft thermal control hardware combining solid–liquid phase change material and a heat pipe. *Aerospace Science and Technology* **2013**, *27*, 10-16.

42. Gilpin, M.R. Chapter 12 - ultra-high temperature space power applications. In *Ultra-high temperature thermal energy storage, transfer and conversion*, Datas, A., Ed. Woodhead Publishing: **2021**; pp 309-330.
43. Soibam, J. Numerical investigation of a phase change materials (PCM) heat exchanger-for small scale combustion appliances. NTNU, **2017**.
44. Rashidi, S.; Shamsabadi, H.; Esfahani, J.; Harmand, S. A review on potentials of coupling pcm storage modules to heat pipes and heat pumps. *Journal of Thermal Analysis and Calorimetry* **2019**, 1-59.
45. Abokersh, M.H.; Osman, M.; El-Baz, O.; El-Morsi, M.; Sharaf, O. Review of the phase change material (PCM) usage for solar domestic water heating systems (SDWHS). *International journal of energy research* **2018**, *42*, 329-357.
46. Arunkumar, N.; Kumar, P.V.; Karthikeyan, R. In *Experimental analysis of thermal energy storage system using $MgSO_4.7H_2O$ PCM for HAVC applications*, **2016**.
47. Navarro, L.; De Gracia, A.; Colclough, S.; Browne, M.; McCormack, S.J.; Griffiths, P.; Cabeza, L.F. Thermal energy storage in building integrated thermal systems: A review. Part 1. Active storage systems. *Renewable Energy* **2016**, *88*, 526-547.
48. Lin, W.; Ma, Z.; McDowell, C.; Baghi, Y.; Banfield, B. Optimal design of a thermal energy storage system using phase change materials for a net-zero energy solar decathlon house. *Energy and buildings* **2020**, *208*, 109626.
49. Souayfane, F.; Fardoun, F.; Biwole, P.-H. Phase change materials (PCM) for cooling applications in buildings: A review. *Energy and buildings* **2016**, *129*, 396-431.
50. Sharma, A.; Tyagi, V.V.; Chen, C.R.; Buddhi, D. Review on thermal energy storage with phase change materials and applications. *Renewable and Sustainable Energy Reviews* **2009**, *13*, 318-345.
51. Sharma, R.K.; Ganesan, P.; Tyagi, V.V.; Metselaar, H.S.C.; Sandaran, S.C. Developments in organic solid–liquid phase change materials and their applications in thermal energy storage. *Energy Conversion and Management* **2015**, *95*, 193-228.
52. Ibrahim, N.I.; Al-Sulaiman, F.A.; Rahman, S.; Yilbas, B.S.; Sahin, A.Z. Heat transfer enhancement of phase change materials for thermal energy storage applications: A critical review. *Renewable and Sustainable Energy Reviews* **2017**, *74*, 26-50.
53. Abhat, A. Low temperature latent heat thermal energy storage: Heat storage materials. *Solar energy* **1983**, *30*, 313-332.
54. Ma, T.; Li, Z.; Zhao, J. Photovoltaic panel integrated with phase change materials (PV-PCM): Technology overview and materials selection. *Renewable and Sustainable Energy Reviews* **2019**, *116*, 109406.
55. Pielichowska, K.; Pielichowski, K. Phase change materials for thermal energy storage. *Progress in materials science* **2014**, *65*, 67-123.
56. Humphries, W.R.; Griggs, E.I. *A design handbook for phase change thermal control and energy storage devices*. NASA Huntsville, AL, USA 1977.
57. Sivasamy, P.; Devaraju, A.; Harikrishnan, S. Review on heat transfer enhancement of phase change materials (PCMs). *Materials Today: Proceedings* **2018**, *5*, 14423-14431.
58. Mehling, H.; Cabeza, L.F. Phase change materials and their basic properties. In *Thermal energy storage for sustainable energy consumption*, Springer: **2007**; pp 257-277.
59. Safari, A.; Saidur, R.; Sulaiman, F.; Xu, Y.; Dong, J. A review on supercooling of phase change materials in thermal energy storage systems. *Renewable and Sustainable Energy Reviews* **2017**, *70*, 905-919.
60. Kumar Gupta, N.; Mishra, S.; Kumar Tiwari, A.; Kumar Ghosh, S. A review of thermo physical properties of nanofluids. *Materials Today: Proceedings* **2019**, *18*, 968-978.
61. Ma, Z.; Lin, W.; Sohel, M.I. Nano-enhanced phase change materials for improved building performance. *Renewable and Sustainable Energy Reviews* **2016**, *58*, 1256-1268.
62. Ferrer, G.; Barreneche, C.; Solé, A.; Enrique Julia, J.; F Cabeza, L. Recent patents on nano-enhanced materials for use in thermal energy storage (TES). *Recent patents on nanotechnology* **2017**, *11*, 101-108.

63. Halté, V.; Bigot, J.-Y.; Palpant, B.; Broyer, M.; Prével, B.; Pérez, A. Size dependence of the energy relaxation in silver nanoparticles embedded in dielectric matrices. *Applied Physics Letters* **1999**, *75*, 3799-3801.
64. Deng, Y.; Li, J.; Qian, T.; Guan, W.; Li, Y.; Yin, X. Thermal conductivity enhancement of polyethylene glycol/expanded vermiculite shape-stabilized composite phase change materials with silver nanowire for thermal energy storage. *Chemical Engineering Journal* **2016**, *295*, 427-435.
65. Popa, M.; Pradell, T.; Crespo, D.; Calderón-Moreno, J.M. Stable silver colloidal dispersions using short chain polyethylene glycol. *Colloids and Surfaces A: Physicochemical and Engineering Aspects* **2007**, *303*, 184-190.
66. Liang, W.; Wang, L.; Zhu, Z.; Qian, C.; Sun, H.; Yang, B.; Li, A. In situ preparation of polyethylene glycol/silver nanoparticles composite phase change materials with enhanced thermal conductivity. *ChemistrySelect* **2017**, *2*, 3428-3436.
67. Alawi, O.A.; Mallah, A.; Kazi, S.; Sidik, N.A.C.; Najafi, G. Thermophysical properties and stability of carbon nanostructures and metallic oxides nanofluids. *Journal of Thermal Analysis and Calorimetry* **2019**, *135*, 1545-1562.
68. Yapici, K.; Cakmak, N.K.; Ilhan, N.; Uludag, Y. Rheological characterization of polyethylene glycol based TiO_2 nanofluids. *Korea-Australia Rheology Journal* **2014**, *26*, 355-363.
69. Zafarani-Moattar, M.T.; Majdan-Cegincara, R. Stability, rheological, magnetorheological and volumetric characterizations of polymer based magnetic nanofluids. *Colloid and Polymer Science* **2013**, *291*, 1977-1987.
70. Zhang, H.; Yuan, Y.; Sun, Q.; Cao, X. Enhanced thermal energy storage performance of polyethylene glycol by using interfacial interaction of copper-based metal oxide. *Advanced Engineering Materials* **2017**, *19*, 1600601.
71. Poliks, B.; Sammakia, B. In *Molecular dynamics study of the influence of aggregation and percolation in Al_2O_3/polyethylene oxide nanofluids on the effective thermal conductivity*, 2020 IEEE 70th Electronic Components and Technology Conference (ECTC), **2020**; IEEE: pp 2033-2039.
72. Hou, J.; Wang, Y.; Liu, J.; Zhao, J.; Long, S.; Hao, J. Enhanced thermal conductivity of copper-doped polyethylene glycol/urchin-like porous titanium dioxide phase change materials for thermal energy storage. *International Journal of Energy Research* **2020**, *44*, 1909-1919.
73. Ansu, A.K.; Sharma, R.; Hagos, F.; Tripathi, D.; Tyagi, V. Improved thermal energy storage behavior of polyethylene glycol-based NEOPCM containing aluminum oxide nanoparticles for solar thermal applications. *Journal of Thermal Analysis and Calorimetry* **2020**, 1-12.
74. Liu, S.; Yan, Z.; Fu, L.; Yang, H. Hierarchical nano-activated silica nanosheets for thermal energy storage. *Solar Energy Materials and Solar Cells* **2017**, *167*, 140-149.
75. Tang, B.; Qiu, M.; Zhang, S. Thermal conductivity enhancement of PEG/SiO_2 composite PCM by in situ cu doping. *Solar Energy Materials and Solar Cells* **2012**, *105*, 242-248.
76. Zhang, Y.; Wang, J.; Qiu, J.; Jin, X.; Umair, M.M.; Lu, R.; Zhang, S.; Tang, B. Ag-graphene/PEG composite phase change materials for enhancing solar-thermal energy conversion and storage capacity. *Applied Energy* **2019**, *237*, 83-90.
77. Wang, C.; Chen, K.; Huang, J.; Cai, Z.; Hu, Z.; Wang, T. Thermal behavior of polyethylene glycol based phase change materials for thermal energy storage with multiwall carbon nanotubes additives. *Energy* **2019**, *180*, 873-880.
78. Qi, G.-Q.; Liang, C.-L.; Bao, R.-Y.; Liu, Z.-Y.; Yang, W.; Xie, B.-H.; Yang, M.-B. Polyethylene glycol based shape-stabilized phase change material for thermal energy storage with ultra-low content of graphene oxide. *Solar Energy Materials and Solar Cells* **2014**, *123*, 171-177.
79. Qian, T.; Zhu, S.; Wang, H.; Fan, B. Comparative study of carbon nanoparticles and single-walled carbon nanotube for light-heat conversion and thermal conductivity enhancement of the multifunctional peg/diatomite composite phase change material. *ACS Applied Materials & Interfaces* **2019**, *11*, 29698-29707.

80. Sun, Q.; Yuan, Y.; Zhang, H.; Cao, X.; Sun, L. Thermal properties of polyethylene glycol/carbon microsphere composite as a novel phase change material. *Journal of Thermal Analysis and Calorimetry* **2017**, *130*, 1741-1749.
81. Deng, Y.; He, M.; Li, J.; Yang, Z. Polyethylene glycol-carbon nanotubes/expanded vermiculite form-stable composite phase change materials: Simultaneously enhanced latent heat and heat transfer. *Polymers* **2018**, *10*, 889.
82. Cabaleiro, D.; Hamze, S.; Fal, J.; Marcos, M.A.; Estellé, P.; Żyła, G. Thermal and physical characterization of PEG phase change materials enhanced by carbon-based nanoparticles. *Nanomaterials* **2020**, *10*, 1168.
83. Song, S.; Qiu, F.; Zhu, W.; Guo, Y.; Zhang, Y.; Ju, Y.; Feng, R.; Liu, Y.; Chen, Z.; Zhou, J. Polyethylene glycol/halloysite@Ag nanocomposite PCM for thermal energy storage: Simultaneously high latent heat and enhanced thermal conductivity. *Solar Energy Materials and Solar Cells* **2019**, *193*, 237-245.
84. Qian, T.; Li, J.; Min, X.; Guan, W.; Deng, Y.; Ning, L. Enhanced thermal conductivity of PEG/diatomite shape-stabilized phase change materials with Ag nanoparticles for thermal energy storage. *Journal of Materials Chemistry A* **2015**, *3*, 8526-8536.
85. Xu, S.; Zhang, X.; Huang, Z.; Liu, Y.; Fang, M.; Wu, X.; Min, X. Thermal conductivity enhanced polyethylene glycol/expanded perlite shape-stabilized composite phase change materials with Cu powder for thermal energy storage. *Materials Research Express* **2018**, *5*, 095503.
86. Zhai, W.; Srikanth, N.; Kong, L.B.; Zhou, K. Carbon nanomaterials in tribology. *Carbon* **2017**, *119*, 150-171.
87. Haddad, Z.; Abid, C.; Oztop, H.F.; Mataoui, A. A review on how the researchers prepare their nanofluids. *International Journal of Thermal Sciences* **2014**, *76*, 168-189.
88. Fan, L.; Khodadadi, J.M. Thermal conductivity enhancement of phase change materials for thermal energy storage: A review. *Renewable and Sustainable Energy Reviews* **2011**, *15*, 24-46.
89. Krasser, E.; Senn, H. In *Simultaneous measurements at U-tube density sensors in fundamental and harmonic oscillation*, EUROCON 2007-The International Conference on "Computer as a Tool", 2007; IEEE: pp 551-555.
90. Hemmat Esfe, M.; Abbasian Arani, A.A.; Rezaie, M.; Yan, W.-M.; Karimipour, A. Experimental determination of thermal conductivity and dynamic viscosity of Ag–MgO/water hybrid nanofluid. *International Communications in Heat and Mass Transfer* **2015**, *66*, 189-195.
91. Saeedi, A.H.; Akbari, M.; Toghraie, D. An experimental study on rheological behavior of a nanofluid containing oxide nanoparticle and proposing a new correlation. *Physica E: Low-dimensional Systems and Nanostructures* **2018**, *99*, 285-293.
92. Estellé, P.; Cabaleiro, D.; Żyła, G.; Lugo, L.; Murshed, S.M.S. Current trends in surface tension and wetting behavior of nanofluids. *Renewable and Sustainable Energy Reviews* **2018**, *94*, 931-944.
93. Maxwell, J.C. *A treatise on electricity and magnetism*. Clarendon Press, Oxford, UK: **1873**; Vol. 1.
94. Hamilton, R.L.; Crosser, O. Thermal conductivity of heterogeneous two-component systems. *Industrial & Engineering chemistry fundamentals* **1962**, *1*, 187-191.
95. Nan, C.-W.; Birringer, R.; Clarke, D.R.; Gleiter, H. Effective thermal conductivity of particulate composites with interfacial thermal resistance. *Journal of Applied Physics* **1997**, *81*, 6692-6699.
96. Murshed, S.; Leong, K.; Yang, C. Investigations of thermal conductivity and viscosity of nanofluids. *International Journal of Thermal Sciences* **2008**, *47*, 560-568.
97. Xue, Q. Model for thermal conductivity of carbon nanotube-based composites. *Physica B: Condensed Matter* **2005**, *368*, 302-307.
98. Einstein, A. Eine neue bestimmung der moleküldimensionen. *Annalen der Physik* **1906**, *19*, 289-306.
99. Batchelor, G. The effect of brownian motion on the bulk stress in a suspension of spherical particles. *Journal of fluid mechanics* **1977**, *83*, 97-117.

100. Brinkman, H. The viscosity of concentrated suspensions and solutions. *The Journal of Chemical Physics* **1952**, *20*, 571-571.
101. Krieger, I.M.; Dougherty, T.J. A mechanism for non-Newtonian flow in suspensions of rigid spheres. *Transactions of the Society of Rheology* **1959**, *3*, 137-152.
102. Maron, S.H.; Pierce, P.E. Application of Ree-Eyring generalized flow theory to suspensions of spherical particles. *Journal of Colloid Science* **1956**, *11*, 80-95.
103. Brenner, H.; Condiff, D.W. Transport mechanics in systems of orientable particles. IV. Convective transport. *Journal of Colloid and Interface Science* **1974**, *47*, 199-264.

Appendix

Resumen Ampliado

Resumen ampliado

El crecimiento industrial de las últimas décadas junto con el rápido desarrollo demográfico y económico han traído consigo un aumento de la dependencia energética. De acuerdo con el Informe sobre el Estado Mundial de la Energía y el CO_2 de 2019 *"Global Energy & CO_2 Status Report 2019",* en 2018 el consumo energético mundial aumentó en un 2.3% respecto al año anterior, doblando así la tasa de crecimiento promedio de la última década. Una parte importante de esta mayor demanda energética está fuertemente ligada a procesos de transferencia de calor y, en especial, a los sistemas de refrigeración y calefacción. En la mayor parte de países esta situación ha derivado en un mayor consumo de recursos energéticos de todo tipo, siendo, los combustibles fósiles la principal fuente de energía, llegando a cubrir aproximadamente hasta el 70% del incremento de la demanda mundial de los últimos dos años. Es bien sabido que esta situación de desarrollo económico y tecnológico, sobre todo en los países industrializados, junto con la dependencia de las fuentes de energía de origen fósil, son el origen de una serie de problemas de carácter medioambiental. Afortunadamente, la sociedad es cada día más consciente de la importancia que la mejora de la eficiencia energética de las instalaciones térmicas tiene para disminuir su impacto sobre el entorno. En este sentido, el almacenamiento energético, es decir, la acumulación de energía cuando ésta se encuentra en exceso o disponible a un bajo coste para utilizarla posteriormente en los momentos de escasez o demanda, se espera que juegue un papel clave en los próximos años. Este tipo de tecnologías no sólo consiguen mejorar la flexibilidad de las instalaciones térmicas, corrigiendo posibles desajustes no previstos entre la oferta y el consumo, sino que también permiten mejorar la eficiencia de las mismas optimizando su utilización.

En las últimas décadas, diferentes compuestos orgánicos, inorgánicos, o mezclas de éstos han sido propuestos como potenciales materiales de cambio de fase (PCMs) sólido-líquido, la transición más prometedora tanto desde un punto de vista tecnológico como económico. Dentro de los materiales de cambio de fase orgánicos, las parafinas, los azúcares, los ácidos grasos y diferentes polímeros como los glicoles polietilénicos reúnen la mayor parte de las características necesarias para la implementación práctica de los mismos en sistemas de almacenamiento energético. En particular, los glicoles polietilénicos presentan cambios de fase congruentes en un amplio rango de temperaturas, que son dependientes de las masas moleculares del polímero en cuestión, con entalpías apropiadas, no son tóxicos, tienen una baja presión de vapor y pueden adquirirse a un precio competitivo. Sin embargo, al igual que la mayor parte de los PCM orgánicos, los materiales poliméricos presentan una baja conductividad térmica. Esto último puede suponer una limitación para la aplicabilidad de estos materiales dado que dificulta la

transferencia de calor, alargando los procesos de captación y entrega de energía almacenada. Con el objetivo de mejorar las capacidades de los PCMs para la transferencia de calor, la dispersión de materiales de tamaño nanométrico y de alta conductividad térmica ha adquirido una especial relevancia en los últimos años, dando lugar a lo que se conoce como nano-PCMs o materiales de cambio de fase nano-mejorados, NePCMs. En los últimos años diferentes nanomateriales han sido considerandos como aditivos en la preparación de NePCMs, siendo las estructuras alotrópicas del carbono y las nanopartículas metálicas aquellas potencialmente más prometedoras. Pero la dispersión de nanoaditivos no sólo permite mejorar el proceso de transferencia de calor de los sistemas de acumulación basados en el calor latente de cambio de fase, sino que también puede ayudar a superar el subenfriamiento, otra limitación de los PCMs comentados. El subenfriamiento es el fenómeno por el cual ciertos materiales necesitan ser enfriados por debajo de su punto de fusión para que comience el proceso de solidificación. En el caso de los PCMs este comportamiento es indeseable dado que la energía almacenada se libera a una temperatura menor o en un rango de temperatura mayor del esperado, lo que a su vez puede disuadir o limitar el uso de este tipo de materiales.

El objeto de esta Tesis Doctoral ha sido el de mejorar las propiedades termofísicas de materiales de cambio de fase, glicoles polietilénicos con diferentes masas moleculares, mediante la dispersión de diferentes nanoestructuras y proponer así materiales de cambio de fase para su possible uso en sistemas de almacenamiento térmico a baja temperatura. Para ello, se han seleccionado diferentes nanoestructuras de carbono, como los nanotubos de carbono de paredes múltiples (MWCNT) o las nanoplaquetas de grafeno funcionalizadas (fGnP), que no sólo tienen altas conductividades térmicas sino también extraordinarias propiedades mecánicas y electroquímicas. También se ha optado por un tipo de nanopartículas metálicas como la plata (Ag), ya que es un material muy importante en los campos de la física o la química, por sus propiedades eléctricas, térmicas u ópticas. Además, todos ellos poseen alta resistencia a la corrosión, lo cual es muy importante para obtener buenos comportamientos en intercambiadores de calor.

Esta Tesis Doctoral se ha desarrollado como compendio de artículos en los que se han diseñado, caracterizado y analizado las propiedades termofísicas de nuevos materiales de cambio de fase nano-mejorados. Las investigaciones se han llevado a cabo en el marco de dos Proyectos de Investigación *"Diseño y desarrollo de nanofluidos para la producción y almacenamiento de energía (ENE2014-55489-C2-1/2-R)"* y *"Desarrollo de nanofluidos híbridos, nanolubricantes y materiales de cambio de fase nano mejorados para la transferencia, almacenamiento y producción de energía (ENE2017-86425-C2-1/2-R)"* concedidos dentro del Programa Nacional de Investigación *"Innovación, Desarrollo e Investigación Orientada a los Retos de la Sociedad"*.

Estos Proyectos se han coordinado entre el Laboratorio de Propiedades Termofísicas (Grupo NaFoMat, Universidade de Santiago de Compostela) y el grupo FA2 (Universidade de Vigo). Además, el doctorando ha desarrollado parte del trabajo durante estancias de investigación en dos instituciones internacionales, la Rzeszow University of Technology (Rzeszow, Polonia) y el Istituto per le Tecnologie della Costruzione of the Italian National Research Council (ITC-CNR, Padua, Italia). Parte de la formación como investigador y de las colaboraciones o estancias en otros centros de investigación europeos, se ha llevado a cabo en el marco de la acción COST Nanouptake - Overcoming Barriers to Nanofluids Market Uptake (COST Action CA15119).

La metodología que se ha seguido en el diseño y caracterización termofísica de los nuevos NePCMs es la que se presenta en la Figura 1.

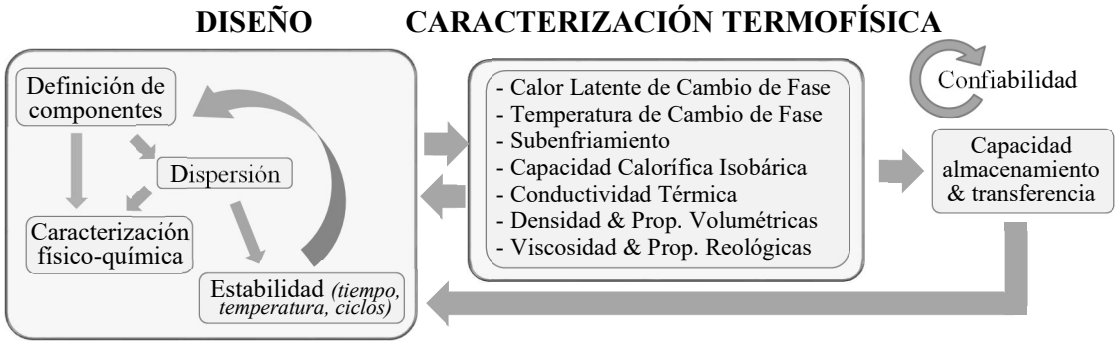

Figura 1. Metodología seguida en el diseño y caracterización termofísica de los nuevos NePCMs.

Como fluidos base de partida se han empleado varios glicoles polietilénicos con masas moleculares comprendidas en el rango de 200 a 400 $g \cdot mol^{-1}$ (comercialmente disponibles como PEG200, PEG300 y PEG400). Como nanoaditivos para la mejora de las propiedades térmicas se han seleccionado cuatro nanopolvos, nanotubos de carbono multicapa comerciales suministrados por el fabricante Baytubes® (c-MWCNT) y nanotubos de carbono multicapa sintetizados (s-MWCNT) en el marco de esta tesis doctoral en colaboración con el grupo del profesor Konstantin N. Semenov del *"Institute of Chemistry"* de la *"Saint-Petersburg State University"* (San Petersburgo, Rusia), nanoplaquetas de grafeno funcionalizadas (fGnP) del fabricante Iolitec, nanopartículas de Ag recubiertas de polivinilpirrolidona (PVP-Ag) y preparadas con la ayuda de la start-up NANOGAP (Santiago de Compostela, España). Así, se han diseñado cinco conjuntos de nanofluidos que se corresponden con un total de veinticuatro dispersiones con concentraciones de nanopartículas entre el 0.025 y el 1.1% en masa.

Una vez definidas las combinaciones de nanoaditivos y materiales de cambio de fase más apropiadas, se ha procedido a su caracterización físico-química mediante diferentes técnicas. Así, con la ayuda del Centro de Apoyo Científico y Tecnológico a la Investigación (CACTI) de la

Universidade de Vigo se ha estudiado la morfología, naturaleza y la presencia de impurezas en los nanoaditivos mediante microscopía de transmisión electrónica (TEM), microscopía de barrido electrónico (SEM), microscopía electrónica de transmisión de barrido (S-TEM), espectroscopia de energía dispersiva de rayos X (EDS), Raman Espectroscopía y/o porosimetría de intrusión de mercurio; mientras que la estructura molecular, la composición y/o pureza de los PCMs base se ha determinado mediante espectrometría de masas de ionización por electroespray (ESI-MS). En cuanto a los nanomateriales en base carbono, las estructuras de grafeno exhibieron una morfología en forma de plaqueta con espesores promedio ~11-15 nm (según análisis SEM), los MWCNT sintetizados en el marco de esta tesis doctoral presentaron diámetros promedio ~7 nm y longitudes ~80 nm (TEM), mientras que el MWCNT comercial mostró longitudes promedio ~10-20 μm y diámetros ~20-30 nm (TEM y SEM). Los microanálisis de EDS evidenciaron la presencia esperada de carbono y oxígeno en el nanopolvo de grafeno funcionalizado con algunos contenidos marginales de otros elementos, que pueden ser trazas de los reactivos usados en la síntesis del nanomaterial. Los espectros Raman realizados a las muestras de MWCNT presentaron las bandas D y G características de los materiales en base carbono. En el caso del MWCNT sintetizado, la intensidad de la banda G es significativamente mayor que la de la banda D, lo que corrobora la calidad de la nanostructura de carbón obtenida. Además, las bandas a 180 cm^{-1} y 260 cm^{-1} también indican la presencia de nanotubos de carbono de una sola capa. En cuanto a las muestras de Ag con recubrimiento de PVP, las nanopartículas presentaron una morfología cuasi esférica con diámetros ~22±7 nm (S-TEM). En cuanto a los glicoles polietilénicos utilizados como materiales base para preparar los NePCM, los análisis de espectrometría de masas ESI confirmaron la elevada pureza, así como su cuasi-monodispersidad de los polímeros (con índices de polidispersidad en el rango de 1.02-1.05). La disposición de esta información ha sido de gran ayuda durante la interpretación de los resultados de las propiedades térmicas y físicas de los nuevos NePCMs.

En el caso de los sistemas basados en nanoplaquetas de grafeno y nanotubos de carbono multicapa, la preparación de los nuevos materiales de cambio de fase nano-mejorados se ha llevado a cabo mediante el método conocido como de dos pasos. Así, el polvo de nanopartículas se ha dispersado en los PCMs empleando agitación mecánica y/o ultrasonicación. En concreto se ha empleado un baño de ultrasonicos Ultrasounds (JP Selecta S.A.) y/o un disruptor Sonoplus HD 2200 (Bandelin). En el caso de los nanofluidos PVP-Ag/PEG400, las nanopartículas de plata se han sintetizado directamente en el fluido base (preparación en un solo paso).

La estabilidad temporal de las dispersiones se ha evaluado en base a un estudio de las distribuciones de tamaños aparentes de nanoaditivos en dispersión, obtenidas con un Zetasizer Nano ZS (Malvern) basado en la técnica de dispersión de luz dinámica (que se corresponde con

las siglas en inglés DLS) mientras que la estabilidad térmica se ha analizado mediante análisis termogravimétrico con un equipo de TGA/DSC1 (Mettler Toledo). La técnica DLS se ha utilizado en el análisis de la evolución temporal del tamaño hidrodinámico de nanopartículas de Ag cubiertas con PVP y dispersiones diluidas de s-MWCNT en PEG400 (0.01% en peso) en condiciones de agitación y estáticas. Los resultados de DLS mostraron que, si la dispersión de s-MWCNT en PEG400 se mantiene en condiciones estáticas (como las que tendrían lugar durante el almacenamiento con el PCM en fase líquida), se puede observar un aumento en el tamaño hidrodinámico aparente de las partículas dispersas. Este comportamiento indica una posible aglomeración de los s-MWCNT en condiciones de reposo. Sin embargo, después de agitar manualmente las muestras durante algunos segundos, los tamaños de DLS aparentes promedio se reducen hasta ~150 nm, lo que indica que la aglomeración puede solventarse con la simple circulación de los fluidos en dispositivos o instalaciones térmicas. En el caso del sistema PVP-Ag/PEG400, las muestras presentaron tamaños promedio ~50 nm durante el período analizado de 4 semanas (tanto en condiciones estáticas como en agitación), lo que prueba la buena estabilidad de los NePCMs diseñados. Por otro lado, los termogramas TGA mostraron pequeñas reducciones en la temperatura de inicio de descomposición térmica de menos de 17 K para todos los sistemas analizados, lo que evidencia que la estabilidad térmica de los glicoles polietilénicos no se ve afectada significativamente por la dispersión de nanopartículas.

Para cumplir con los objetivos que se desean alcanzar con esta Tesis Doctoral, el estudio de las propiedades termofísicas es un paso fundamental en el desarrollo de NePCMs con propiedades mejoradas, ya que proporciona la información necesaria para evaluar las mejoras en las capacidades térmicas obtenidas gracias a la dispersión de partículas de tamaño nanométrico. Las propiedades termofísicas que se han analizado en el marco de esta Tesis Doctoral son aquellas con una mayor influencia en la singularización de los NePCMs no sólo como materiales de almacenamiento energético sino también como fluidos de transferencia de calor:

- Características de cambio de fase sólido-líquido (calor latente, temperatura de fusión y temperatura de recristalización)
- Capacidad calorífica isobárica
- Conductividad térmica
- Densidad y comportamiento volumétrico
- Viscosidad dinámica
- Tensión superficial

En primer lugar, se han determinado las temperaturas y entalpías de cambio de fase sólido-líquido de los sistemas fGnP/PEG400 y PVP-Ag/PEG400 con el objetivo de evaluar la influencia que la dispersión de los nanoaditivos tiene sobre la reducción del subenfriamiento y el calor

latente de fusión de las muestras. Estos análisis se han llevado con un calorímetro diferencial de barrido DSC Q2000 (TA Instruments, New Castle, DE, EE. UU.) empleando velocidades de enfriamiento y calentamiento en el rango de 1-5 $K \cdot min^{-1}$. A modo de ejemplo, en el caso del NePCM basado en fGnP/PEG400 con una concentración de nanoplaquetas de grafeno al 0.5 wt.%, la temperatura de cristalización se redujo en 4 K (en comparación con el PEG400 empleado como fluido base) y el intervalo en el que se produce la fusión se redujo en 2.5 K, sin una reducción significativa en la capacidad de calor latente del glicol polietilénico. Para poder asegurar un correcto funcionamiento en servicio de los NePCMs es necesario que sus características de cambio de fase permanezcan inalteradas con el paso de los ciclos de fusión-solidificación. Por ello, durante el desarrollo de la Tesis Doctoral se han llevado a cabo estudios en los que se han descartado posibles reducciones en el calor latente de fusión (punto clave en el diseño de este tipo de sistemas) con la sucesión de los ciclos de enfriamiento-calentamiento.

Este mismo calorímetro diferencial de barrido también se utilizó para obtener la capacidad calorífica isobárica (C_p), trabajando con un método cuasi-isotérmico de calorimetría diferencial de barrido modulado por temperatura (TMDSC por sus siglas en inglés). Dicha capacidad calorífica isobárica se determinó experimentalmente, en un amplio rango de temperaturas para los fluidos base, las nanopartículas y/o los NePCMs. Se han observado pequeñas reducciones en esta propiedad (con respecto al fluido base correspondiente) de 3%, 0.34%, 0.9% para las muestras de s-MWCNT(1 wt.%)/PEG400, fGnP(0.5 wt.%)/PEG400 y PVP-Ag(1.1 wt.%)/PEG400, respectivamente.

El estudio de las conductividades térmicas (k) de los NePCM basados en PEG400 se ha realizado con un Analizador de Propiedades Térmicas KD2 Pro (Decagon Devices, Inc., Pullman, WA, EE. UU.), para las dispersiones de s-MWCNT y fGnP en PEG400, mientras que un Hot Disk Thermal Constants (Hot Disk AB, Göteborg, Suecia) se ha utilizado para investigar las dispersiones de nanopartículas de Ag recubiertas con PVP en PEG400. Los resultados mostraron que la conductividad térmica mejora con la adición de nanopartículas para todos los sistemas de NePCM investigados, alcanzando mejoras de hasta el 23%, 12.7% y 3.9% para fGnP(0.5 wt.%)/PEG400, s-MWCNT(1.0 wt.%)/PEG400 y PVP-Ag (1.1 wt.%)/PEG400, respectivamente.

Las densidades (ρ) de los NePCMs y fluidos base se midieron para los sistemas fGnP/PEG400, s-MWCNT/PEG400 y PVP-Ag/PEG400. La densidad de los NePCMs aumenta (con respecto al PEG400 utilizado como fluido base) con la adición de nanopartículas sólidas. Esos incrementos en densidad fueron del 0.33% para fGnP(0.5 wt.%)/PEG400, 0.42% para s-MWCNT(1.0 wt.%)/PEG400 y 2.2% para PVP-Ag(1.1 wt.%)/PEG400. Como era de esperar, las densidades de los PEGs utilizados como fluidos base y de los NePCMs se redujo con el aumento de temperatura. La dependencia de la densidad con la temperatura también se investigó a través de la expansividad

térmica isobárica (α_p) obteniéndose reducciones máximas en esta última propiedad (con respecto al fluido base) de 2.6% y 1.8% para muestras de fGnP(0.5 wt.%)/PEG400 y s-MWCNT(1.0 wt.%)/PEG400, respectivamente.

La viscosidad dinámica (η) se estudió para los cinco sistemas de NePCM diseñados. Para las dispersiones fGnP/PEG400, los estudios se realizaron en el rango de temperatura 283-373 K con un viscosímetro-densímetro Stabinger rotatorio SVM 3000 (Anton Paar, Graz, Austria). Para los sistemas c-MWCNT/PEG200, c-MWCNT/PEG300 y s-MWCNT/PEG400, las curvas de flujo se determinaron mediante un reómetro rotacional Physica MCR 101 (Anton Paar, Austria), mientras que en el caso de las muestras de PVP-Ag/PEG400 los estudios de flujo se realizaron un reómetro rotacional AR-G2 (TA Instruments, New Castle, DE, EE.UU.). Como se esperaba, la viscosidad dinámica aumentó con la adición de nanoaditivos. Los aumentos máximos en la viscosidad dinámica (en comparación con el fluido base correspondiente) fueron 24% y 29.6% para las dispersiones fGnP(0.5 wt.%)/PEG400 y s-MWCNT(1.0 wt.%)/PEG400, respectivamente. Estos resultados son mucho más bajos que los aumentos en la viscosidad dinámica (con respecto al fluido base) de 102% y 71% obtenidos para concentraciones de 0.70 wt.% de MWCNT comerciales en PEG200 y PEG300, respectivamente. Finalmente, se obtuvo un aumento del 5.4% para la dispersión de Ag con recubrimiento de PVP (1.1 wt.%), en comparación con PEG400 puro. También se ha observado que las muestras c-MWCNT/PEG200 y c-MWCNT/PEG300 presentaban un adelgazamiento pseudoplástico más intenso que las dispersiones de s-MWCNT/PEG400. Así, mientras que los NePCMs basados en PEG400 mostraron un comportamiento no-Newtoniano para concentraciones de s-MWCNTs superiores al 0.05 wt.%, las dispersiones de c-MWCNTs en PEG200 y PEG300 mostraron un comportamiento pseudoplástico incluso a la concentración de nanopartículas del 0.025 wt.% (la más baja de las estudiadas). La dependencia de la viscosidad dinámica con la temperatura se describió mediante la ecuación de Vogel-Fulcher-Tammann, con desviaciones máximas (entre datos experimentales y correlacionados) que oscilan entre 1.2% y 3.8% para fGnP/PEG400 y c-MWCNT/PEG200, respectivamente. Finalmente, también se llevaron a cabo experimentos reológicos oscilatorios para los sistemas c-MWCNT/PEG200 y c-MWCNT/PEG300 con el fin de identificar la región viscoelástica lineal e investigar el comportamiento viscoelástico de las dispersiones diseñadas.

La tensión superficial se determinó para el PEG400 puro y para los NePCMs de PVP-Ag/PEG400 mediante un analizador de forma de gota DSA30 (Krüss GmBH, Hamburgo, Alemania) con una cámara que permite controlar la humedad y la temperatura de la muestra y el aire que la rodea. Los ensayos realizados en el rango de temperaturas entre 288.15 y 328.15 K mostraron que la tensión superficial del fluido base y los NePCMs disminuye con el aumento de temperatura en ~(0.21–0.22)% cada 10 K. También se observó una reducción en la tensión

superficial para este sistema de NePCMs con la concentración de nanopartículas de plata. Estas disminuciones, que alcanzaron el 2.2% para la muestra de PVP-Ag(1.1 wt.%)/PEG400, pueden atribuirse a la presencia de surfactante PVP en las dispersiones.

Los resultados obtenidos para los NePCM diseñados, se compararon con otros materiales de la bibliografía y con los glicoles polietilénicos utilizados como fluidos base. En general, se han logrado aumentos interesantes en propiedades como la conductividad térmica, sin penalizar demasiado otras propiedades como la viscosidad. Por tanto, los nanofluidos estudiados pueden ser potencialmente útiles, por ejemplo, como materiales de transferencia de calor o medios de almacenamiento para su aplicación en sistemas de refrigeración domésticos o comerciales.